SOLID STATE NMR STUDIES OF METAL HYDRIDES

Thesis by

Ann Tryon Nicol

In Partial Fulfillment of the Requirements for the
Degree of
Doctor of Philosophy

California Institute of Technology
Pasadena, California 91125

1979

(Submitted 27 July 1978)

To Malcolm

ACKNOWLEDGMENTS

During my years at the California Institute of Technology many people have touched my life, and I would like to name just a few.

First, let me thank my research advisor, Professor Robert W. Vaughan, who is both a creative scientist and a kind human being. He has always encouraged me in my work by his positive outlook on life and his enthusiasm for science.

I am very grateful for the friendship of Dr. Cecil R. Dybowski who found the time to discuss many aspects of science and of life with me when I first joined Professor Vaughan's group. His aid in the early stages of my work is much appreciated, as is the aid of Dr. J. Piott, and the intellectual stimulation provided by Dr. Michael E. Stoll.

Thanks are due to Dr. Marie-Jeanne Peltre for helpful scientific discussions, for advice and for friendship. Also, I very much appreciate having had the opportunity to interact with Mr. Douglas G. Carson, both as scientist and friend. I am, indeed, indebted in one way or another to every member of the Vaughan group, and I thank them all.

I would like to express my appreciation to Professor G. W. Robinson and the members of his group who welcomed me during my first year at Caltech.

Also, my thanks go to Sharon ViGario who typed most of my manuscripts and to Lenore Kerner and to Kathy Lewis who also typed parts of the manuscripts and the thesis.

Special thanks and great appreciation for my time spent at Caltech go to the members of my family. My husband, Malcolm, and our daughters,

Barbara, Katherine, and Virginia, gave me time and space in which to work and a great deal of love and support.

Finally, I would like to acknowledge a Teaching Assistantship provided by Caltech and support for my work from the Department of Energy and from an IBM Fellowship.

ABSTRACT

Both conventional and multiple pulse proton NMR studies of the compounds $H_2Os_3(CO)_{10}$, $H_4Ru_4(CO)_{12}$, and $H_4Os_4(CO)_{12}$ as well as multiple pulse studies of CaH_2, SrH_2, and BaH_2 are reported.

Chemical shift tensors for protons directly bonded to heavy metal atoms in the metal carbonyl compounds are found to have an isotropic value close to that observed in solution and are found to have an anisotropy of less than 30 ppm. The temperature dependent spectra of $H_4Ru_4(CO)_{12}$ indicates the presence of anisotropic proton reorientation at room temperature. The isotropic proton chemical shift for the ionic solids CaH_2, SrH_2, and BaH_2 are found in the range $\bar{\sigma}$ = 0 ppm to $\bar{\sigma}$ = - 10 ppm, and a trend in the isotropic value to shift toward higher field as a function of cation electronegativity is noted.

Structured proton NMR lineshapes, observed by conventional pulse NMR, are reported for the metal cluster carbonyl compounds; and the results are interpreted in terms of four dipolar coupled spin $\frac{1}{2}$ nuclei. Contributions to the lineshapes from heteronuclear dipolar interaction with a Zeeman perturbed quadrupolar nucleus, indirect nuclear coupling, and restricted motion are discussed.

Two analytical calculations which were developed for interpreting the results of the conventional pulsed NMR experiments, but which are more generally applicable, are presented. The first is an analytical solution to the dipolar coupled four spin $\frac{1}{2}$ problem for a parallelogram configuration of spins, and the second is a calculation of the heteronuclear dipolar energy for a spin $\frac{3}{2}$ nucleus in a Zeeman perturbed quadrupolar state interacting with spin $\frac{1}{2}$ nuclei.

Table of Contents

Chapter 1

General Introduction

Metal cluster compounds composed of three or more metal atoms bonded together in a cluster with carbonyls or other ligands bonded to the metal atoms have been the subject of many studies recently (see a review by Kaesz [1]). There is interest in characterizing both structure and motional properties of such compounds; and, in particular, for metal cluster hydrides it would be useful to know the location of the hydrogens within the molecule and to be able to describe any hydrogen motion which takes place. Cluster compounds of the type described in this thesis, namely $H_2Os_3(CO)_{10}$, $H_4Ru_4(CO)_{12}$ and $H_4Os_4(CO)_{12}$, which do not crystallize well can be studied by means of solid state NMR so such studies can provide structural and motional information even for polycrystalline materials in contrast to, for example, neutron diffraction studies which require single crystals. Thus, solid state NMR studies of the polycrystalline metal cluster hydrides $H_2Os_3(CO)_{10}$, $H_4Ru_4(CO)_{12}$ and $H_4Os_4(CO)_{12}$, which have hydrogens participating in covalent bonds to metals, were undertaken. In addition, for contrast, the binary metal hydrides CaH_2, SrH_2, and BaH_2 which are ionic solids were also studied. Such solid state studies as presented in this thesis were not done in the past because techniques and equipment were not available. However, in recent years a new class of experiments has been developed for the study of high resolution NMR in solids.[2,3] These multiple pulse techniques have the effect of supressing the homonuclear dipolar interaction which is often the dominant one in conventional solid state NMR. Thus it is possible to observe other smaller interactions such as the chemical shift. Furthermore, the development of technology for performing the multiple pulse experiments has resulted in improved equipment making it possible to

obtain more detailed and accurate lineshapes from the Fourier transform of the free induction decay than has usually been obtained by conventional pulsed NMR.

Both the dipolar spectra obtained by the Fourier transform of the free induction decay and the chemical shift spectra obtained by multiple pulse studies can yield valuable information about compounds containing spin ½ nuclei. Studies of chemical shift tensor powder patterns yielding information on isotropic shifts and chemical shift anisotropies can be interpreted in terms of the kind of bonding in which the atom containing the spin ½ nucleus is involved. Temperature dependent chemical shift powder pattern studies can provide information on motional processes that the spin ½ nucleus may be undergoing,[2] while dipolar lineshape studies can provide both structural and motional information. Both kinds of proton NMR studies have been employed in extracting information about the metal carbonyl hydrides $H_2Os_3(CO)_{10}$, $H_4Ru_4(CO)_{12}$, and $H_4Os_4(CO)_{12}$ and the alkaline earth hydrides CaH_2, SrH_2, and BaH_2.

The impact of these studies is twofold. On one hand, the interpretation of the experimental results provides information not readily available by other means on structure, bonding, and proton motion in the compounds studied. On the other hand, these are a new class of compounds for high resolution solid state NMR studies which also provide model systems for dipolar lineshape calculations.

These are a new class of compounds for high resolution solid state NMR studies in that the hydrogens are directly bonded to metals. To my knowledge, only one other multiple pulse study has been carried out on a metal hydride, Th_4H_{15},[4] and that particular hydride is metallic whereas the compounds reported on here are either covalently bonded molecular solids (metal carbonyl hydrides) or ionic solids (alkaline earth hydrides). Furthermore, most other high resolution proton NMR studies have confined themselves to cases where hydrogens are bonded to elements in the first row of the periodic table.[2,3] (There is one reported case of a measurement of a chemical shift tensor for a hydrogen bonded to sulfur in H_2S.[4])

In order to understand how these metal hydrides fit into the scheme of things, it is necessary to consider what kind of information is available at the present time about chemical shift tensors for hydrogen in solids. To date, chemical shift tensor information is largely correlative and a number of tensors have been measured which can be classified according to the type of bonding in the compound studied. Ultimately, it is hoped that accurate experimental chemical shift tensor results will aid in theoretical interpretations of bonding. For example, it has been suggested theoretically that proton magnetic shielding anisotropies may be more sensitive measures of features of hydrogen bonding than are isotropic proton shielding constants.[6] Another theoretical study suggested that the up field chemical shift noted for protons directly

bonded to transition metals might be accompanied by an unusually large chemical shift anisotropy (500 ppm).[7] However, if such theories are to be tested and developed, it is necessary to have some experimental results with which to compare.

At the present time, published proton chemical shift tensors include studies of protons in hydrogen bonds,[2,3,5] protons in methylene groups ($-CH_2$),[2,3] protons in alkenes (-CH=CH-)[2,3] and protons on aromatic rings.[2,3,8] Some general trends have been noted.[2,3] For protons in hydrogen bonds the shielding tensor is close to axially symmetric with the most shielded component approximately along the hydrogen bond. The tensor anisotropy is typically about 20 ppm but has been seen to be as large as 34 ppm for ice[5] and 44 ppm for KHF_2.[3] The isotropic value of the tensor is usually in the range σ = - 10 ppm to - 20 ppm. For methylene protons the shielding tensors are reported to be axially symmetric with an anisotropy of 5 - 6 ppm, and the most shielded direction is found to be along the C-H bond. Although both methylene protons and protons in alkenes have their isotropic chemical shift in the range σ = 0 ppm to - 10 ppm and exhibit a similar chemical shift anisotropy, the olefinic protons are observed to have a completely nonaxially symmetric tensor with the least shielded direction perpendicular to the molecular plane. The in plane direction of the tensor components are not necessarily correlated with C-H bond directions, but one component is sometimes found along the carbon-carbon double bond. Aromatic protons also have their isotropic chemical shift in the range σ = 0 ppm to - 10 ppm and show a chemical shift anisotropy of about 5 to 6 ppm.[2,3,8] A more thorough listing and discussion of most of these data and correlations can

be found in the books by Mehring[2] and Haeberlen.[3] With the exception of the studies of thorium hydride[4] no reported multiple pulse studies have involved systems in which the hydrogen was directly bonded to a metal. (Effects other than chemical shift were taken into account in interpreting the thorium hydride multiple pulse data, and no chemical shift tensor is reported for that compound.[4]) As a result of the studies presented in this thesis it is possible to say that the ionic alkaline earth binary hydrides CaH_2, SrH_2, and BaH_2 have their isotropic chemical shift in the range σ = 0 ppm to - 10 ppm and that any chemical shift anisotropy which may be present must be very small. The details are given in Chapter 7 of this thesis. For the metal carbonyl hydrides (Chapter 5) anisotropies of less than 30 ppm are found, and the chemical shift tensor has its isotropic value approximately at the same point in the NMR spectrum as is observed for these compounds in solution. That is, isotropic values are in the range σ = + 10 ppm to + 20 ppm for these compounds. These are important results for they show that the cause of the up field shift observed for such compounds cannot be attributed to an unusually large chemical shift anisotropy. Also, these are the first reported solid state chemical shift tensor data for hydrogens covalently bound to metal atoms and participating in metal-metal bonds. Thus a basis in experiment is provided for the development of theoretical models to explain chemical shift tensors in such molecules.

The results for the dipolar lineshape studies also present a new departure for solid state NMR in that the metal cluster compounds provide idealized isolated four proton systems arranged in the geometry of a parallelogram. A full analytical solution to the problem of four dipolar

coupled spin ½ nuclei in a parallelogram configuration is presented in Chapter 2 of this thesis. The structured lineshapes obtained experimentally (Chapter 4) compare well with the results of the calculation thereby providing an example of a system of a small number of isolated spins not previously studied.

These calculations have value in interpreting further NMR studies of this type since they point to the fact that structured dipolar lineshapes observed for polycrystalline samples may well be interpreted in terms of homonuclear dipolar coupling of up to four isolated spin ½ nuclei just as in the past structured lineshapes have been interpreted in terms of two and three dipolar coupled spins.[9] However, care has been taken to consider other possible sources of the experimentally observed lineshapes, and the results of a perturbation calculation of the effect of a nearby nucleus of spin 3/2 on a spin ½ pair powder spectrum (Chapter 3) shows that, in the limit where the spin 3/2 nucleus is in a non-Zeeman quantized state, the heteronuclear dipolar interaction between ^{189}Os and a proton pair will not produce a structured spin ½ pair lineshape.

In addition to providing a contribution to solid state NMR studies of small numbers of spins and in addition to furnishing some experimental results for compounds of a type not previously studied by means of high resolution solid state NMR, these studies provide some specific and useful information about the particular compounds studied.

For the carbonyl hydrides there is interest in knowing both where the hydrogens are located structurally relative to each other and what motional processes they may be undergoing. As previously mentioned, solid state NMR studies can

address these questions and can provide answers not so readily available by other means. For example, until recently x-ray diffraction studies of $H_4Ru_4(CO)_{12}$ were not available, but were done on compounds analogous to $H_4Ru_4(CO)_{12}$ but with one carbonyl replaced by a large ligand.[10] This has the effect of facilitating crystallization for an otherwise globular molecule. By contrast, $H_4Ru_4(CO)_{12}$ is essentially globular and so the energy to sit down in one orientation is not greatly different from the energy to sit down in some other orientation. The result is that it is difficult to obtain single crystals of these cluster carbonyl compounds. Thus, only recently has an x-ray diffraction study of $H_4Ru_4(CO)_{12}$ been published;[10] and, to my knowledge, no neutron diffraction results are available for this compound. On the other hand, there are several advantages of proton NMR studies. The pure compound can be studied in the solid state thus eliminating solvent effect. Polycrystalline samples can be studied so the simple carbonyl hydride without a large ligand attached can be investigated. Indeed, for solid state NMR studies the simpler compound having chemically one kind of hydrogen is preferred. Because the carbonyls serve to isolate the protons somewhat from neighboring molecules, chemical shift spectra and dipolar spectra can yield even more details of structure and motion than is usually obtained from the study of such spectra in solids. For example, when small numbers of symmetrically located isolated spins are involved, such as the protons in $H_4Ru_4(CO)_{12}$, anisotropic reorientations of the spins will result in unusual chemical shift powder patterns.[2] Although evidence has been given for anisotropic reorientation of protons in tetraruthenium compounds in solution (the protons move from one site to another in apparently coherent jumps),[12] the results in Chapter 5 provide the first reported

evidence for such reorientation in the solid state.

Studies of dipolar lineshapes can yield information on internuclear distances thus aiding in understanding the structure of compounds containing spin ½ nuclei. Usually for compounds such as $H_4Ru_4(CO)_{12}$ the proton positions have been inferred from a consideration of the bonding and the disposition of the carbonyls in the molecule. For example, as the carbonyls are directed over the faces of the near tetrahedron formed by the metal atoms[11] and as a model for bonding in such compounds has a near octrahedral coordination of the metal atom[13] it is believed that the protons will be edge budging four of the six sides of the near tetrahedron in the form of a square. For the compound $H_2Os_3(CO)_{10}$ recently available neutron diffraction data indicate that molecular packing results in one short intermolecular proton-proton contact with the two close pairs forming a nearly linear configuration of four spins.[14] Both the square and the line of four spins are special cases of the parallelogram. Computer simulated lineshapes using the results of the calculation given in Chapter 2 when compared with the experimental lineshapes given in Chapter 4 are consistent with the geometry of a square of protons for the tetrametal compounds.[15] Similarly, the computer simulated lineshapes for a line of four spins formed by two close pairs exhibit the features seen in the experimental results for $H_2Os_3(CO)_{10}$[15] and are in good agreement with the internuclear distances provided by Sheldrich.[14]

Finally, the temperature dependence of the dipolar lineshapes observed for the cluster compounds indicates that there is proton motion in solid state $H_4Ru_4(CO)_{12}$ over the temperature range 300 K to 220 K in agreement with the chemical shift data. For the two osmium compounds, on the other

hand, the dipolar lineshapes were not seen to change from 300 K to 100 K and this is taken as evidence for no proton motion sufficient to average the dipolar interaction differently over that temperature range. The chemical shift spectra for $H_2Os_3(CO)_{10}$ were not seen to change as a function of temperature and substantiate the dipolar lineshape results.

To summarize, two kinds of metal hydrides have been studied by both conventional pulsed NMR and the newer techniques of high resolution solid state NMR. The chemical shift results presented here represent the first reported studies of that type for compound where hydrogens are directly bonded to metal atoms and participating in ionic bonds (alkaline earth hydrides) or covalent bonds (metal cluster compounds). The dipolar lineshape results have been interpreted in terms of structure, and both chemical shift and dipolar spectra have provided evidence for proton motion in solid $H_4Ru_4(CO)_{12}$. Furthermore, analytical calculations were developed for extracting structural information from dipolar spectra which can be applied to other systems containing small numbers of dipolar coupled spins.

References

1. H. D. Kaesz, Chem. in Britain 9, 344 (1973).

2. M. Mehring, "High Resolution NMR Spectroscopy in Solids," NMR Basic Principles and Progress, P. Kiehl, E. Fluck, R. Kosfeld, eds., Vol. 11, Springer-Verlag, New York, 1976.

3. U. Haeberlen, "High Resolution NMR in Solids, Selective Arranging," Advances in Magnetic Resonance, J. S. Waugh, ed., Suppl. 1, Academic, New York, 1976.

4. K. F. Lau and R. W. Vaughan, Phys. Rev. B15, 2449 (1977).

5. L. M. Ryan, R. C. Wilson, and B. C. Gerstein, Chem. Phys. Lett. 52, 341 (1977).

6. R. Ditchfield and R. E. McKinney, Jr., Chem. Phys. 13, 187 (1976).

7. A. D. Buckingham and P. J. Stephens, J. Chem. Soc., Part III, 2747 (1964).

8. L. M. Ryan, R. C. Wilson, and B. C. Gerstein, J. Chem. Phys. 67, 4310 (1977).

9. A. Abragram, The Principles of Nuclear Magnetism, Oxford University Press, London, 1961.

10. R. D. Wilson and R. Bau, J. Am. Chem. Soc. 98, 4687 (1976).

11. R. D. Wilson, S. M. Wu, R. A. Love, and R. Bau, Inorg. Chem. 17, 1271 (1978).

12. J. R. Shapley, S. I. Richter, M. R. Churchill and R. A. Lashewycz, J. Am. Chem. Soc. 99, 7384 (1977).

13. M. Elian, M. M. L. Chen, D. M. P. Mingos, and R. Hoffmann, Inorg. Chem. 15, 1148 (1976).

14. G. M. Sheldrick, private communication.

15. A. T. Nicol and R. W. Vaughan, Proceedings of the XXth Congress Ampre, Tallinn, 1978, to be published.

Chapter 2

Analytical Solution for a Planar Configuration of Four Dipolar Coupled Spin $\frac{1}{2}$ Nuclei

(Chapter 2 is a manuscript of A. T. Nicol and R. W. Vaughan which is being prepared for publication.)

I. Introduction

This paper details the analytical solution of the dipolar coupled four spin ½ problem for a parallelogram configuration of spins. Both eigenfunctions and eigenvalues for this problem are presented, and predicted NMR dipolar spectra for squares and linear chains of four spin ½ nuclei are given. Such results are of interest in explaining unusual spectra observed in metal carbonyl cluster hydrides[1] and are essential for extracting accurate structural information from the data.

The problem of the magnetic resonance spectra of a small number of isolated spin ½ nuclei has been considered by many people. Two and three spin ½ problems have found their way into standard works on magnetic resonance[2]. The general formulation of the four spin ½ problem was treated early by Itah, et al.[3] and by Bersohn and Gutowsky[4], who provide the matrix elements for the general case and then specialize to solve for particular geometries. Bersohn and Gutowsky specialized to a tetrahedral configuration, and Itoh, et al. specialized to a rectangular configuration of spins where two parallel sides of the rectangle are much shorter than the other two sides. Later, Eichoff and Zachmann[5], starting with the results of Bersohn and Gutowsky, treated the rectangle in greater detail and, more recently, Boden and Levine treated the rectangle from another point of view[6]. Unfortunately, there are disagreements between Bersohn and Gutowsky and Itoh, et al. over some of the matrix elements of the dipolar Hamiltonian. Our matrix elements agree with those of Itoh, et al. and thus solutions obtained for particular geometries[5] which used the Bersoh and Gutowsky matrix elements will not agree with results reported here. Therefore, in addition to presenting an analytical solution for a parallogram configuration of spins, we present a detailed development of the general four spin ½ problem so that sources of disagreement can be indicated.

II. Formulation of the Problem

The total spin Hamiltonian for the four spin ½ system can be written as

$$H = H_Z + H_D + H_A \tag{1}$$

H_Z is the Zeeman Hamiltonian given by $-\gamma h \underset{\sim}{H_0} \cdot \underset{\sim}{I}$ where $\underset{\sim}{I} = \sum_{i=1}^{4} \underset{\sim}{I}_i$. H_A represents any other Hamiltonians such as chemical shift indirect nuclear coupling or heteronuclear dipolar coupling which can be considered to be much smaller than the homonuclear dipolar Hamiltonian. H_D represents the homonuclear dipolar Hamiltonian, and since the dipole-dipole energy is small compared with the Zeeman energy, the dipolar interaction is treated as a perturbation.

The secular part of the dipolar Hamiltonian (that which commutes with the Zeeman Hamiltonian) can be written in the form

$$H_D = \sum_{i<j} A_{ij}(\underset{\sim}{I}_i \cdot \underset{\sim}{I}_j - 3I_{z_i} I_{z_j}) \tag{2}$$

where

$$A_{ij} = \frac{\gamma^2 h^2}{2r_{ij}^3} (3\cos^2\theta_{ij} - 1) \tag{3}$$

and where γ is the gyromagnetic ratio for the spin ½ nucleus, r_{ij} is the distance between nucleus i and j; and θ_{ij} is the angle that r_{ij} makes with the magnetic field.

For the four spin ½ problem, the Zeeman quantized eigenstates can be designated by $|m_1 m_2 m_3 m_4\rangle$ and could also be labeled by M such that $M = \sum_i m_i$. Since there are no matrix elements of H_D between states of different M, it remains to calculate the matrix elements of H_D within

a given M manifold in order to obtain eigenvalues and eigenfunctions under the prescription of degenerate perturbation theory. Then, to predict spectra, transition matrix elements must be calculated using the resulting eigenfunctions.

III. Matrix Elements of the Dipolar Hamiltonian

Using Equations (2) and (3) and the $|m_1 m_2 m_3 m_4>$ basis set, the matrix elements of $\mathcal{H}_D$ are summarized in Table 1. Note that, in this representation, the problem of a 16 x 16 matrix is reduced to one 6 x 6 matrix, two 4 x 4 matrices, and two 1 x 1 matrices. The matrix can be further block-diagonalized by choice of an LSIM representation. The representation has $\underset{\sim}{L} = \underset{\sim}{I}_1 + \underset{\sim}{I}_2$, $\underset{\sim}{S} = \underset{\sim}{I}_3 + \underset{\sim}{I}_4$, and $\underset{\sim}{I} = \underset{\sim}{L} + \underset{\sim}{S}$. The transformation is shown in Table 2. The notation is chosen for ease of comparison with the works of both Bersohn and Gutowsky[4] and Itoh, et al.[3]. Our ψ_i's correspond to those of Bersohn and Gutowsky and the alternative |LSIM> notation is used by both sets of authors. Matrix elements of $\mathcal{H}_D$ in the LSIM represntation are given in Table 3. Note that in both choices of basis sets the two 4 x 4 matrices are identical as are the two 1 x 1 matrices. However, the 6 x 6 matrix obtained in the $m_1 m_2 m_3 m_4$ representation breaks down into two unlike 3 x 3 matrices in the LSIM representation.

It is at this point that comparisons can be made among the various works[3,4]. We note a disagreement in the matrix elements $<0000|\mathcal{H}_D|1100>$, $<1121|\mathcal{H}_D|1011>$ and $<1111|\mathcal{H}_D|1011>$. Both our work and that of Itoh, et al.[3] find the $<0000|\mathcal{H}_D|1100>$ matrix element to be zero, contrary to the results of Bersohn and Gutowsky[4]. This matrix

element occurs in one of the 3 x 3 matrices, the one we designate the ψ_{11}, ψ_6, ψ_{10} matrix. Also, there is a disagreement in sign of elements in the 4 x 4 matrix. Using a particular choice of phase, we have been able to get agreement with Itoh, et al. Specifically, we get a different sign for the two matrix elements $\langle 1121|\mathcal{H}_D|1011\rangle$ and $\langle 1111|\mathcal{H}_D|1011\rangle$ from Bersohn and Gutowsky. This results in a different general form of the 4 x 4 secular equation and, of course, different eigenvalues. All other discrepancies between our results and that of Bersohn and Gutowsky or Itoh, et al. can be attributed to an overall change of sign of the wavefunction. Since Eichoff and Zachmann[5] used the results of Bersohn and Gutowsky for their treatment of a rectangular configuration of four spin ½ nuclei their results disagree with ours for the 4 x 4 matrix and for one of the 3 x 3 matrices.

Returning to the problem of interest, consider the case of a parallogram configuration of four spin ½ nuclei. Such a configuration will have

$$\begin{aligned} A_{12} &= A_{34} \\ A_{13} &= A_{24} \end{aligned} \tag{4}$$

and is illustrated in Figure 1. The matrix elements of the dipolar Hamiltonian under the constraint of Equation (4) are given in Table 4. The transition matrix elements, $\langle\psi_n|I_x|\psi_m\rangle$, needed for simulation of spectra are given in Table 5. By solving the secular equations, obtaining the new eigenfunctions, and using the proper intensities from Table 5,

we can simulate spectra for single crystals or polycrystalline samples.

IV. Solution of the Secular Equation

From Table 4, provides the eigenfunctions

$$\psi_{1'} = \psi_1 \text{ and } \psi_{16'} = \psi_{16} \tag{5}$$

with eigenvalues

$$E_{1'} = E_{16'} = -(A_{12}+A_{13}) - \frac{(A_{23}+A_{14})}{2} \tag{6}$$

where the ψ_i's are defined in Table 2.

From Table 4 the ψ_{11}, ψ_6, ψ_{10} 3x3 matrix provides a secular determinant of the general form

$$\begin{vmatrix} 0-\lambda & A & 0 \\ A & B-\lambda & C \\ 0 & C & 0-\lambda \end{vmatrix} = 0 \tag{7}$$

which has roots

$$\lambda_1 = 0$$
$$\lambda_{\pm} = \frac{B \pm \sqrt{B^2+4(A^2+C^2)}}{2} \tag{8}$$

Using these results, one can obtain the eigenfunctions and they are given in Table 6. The appropriate values of A,B,C obtained using Table 4 in comparison with Equation (7) are also given in Table 6.

From Table 4, the secular equation for the ψ_8, ψ_9, ψ_7 3 x 3 matrix is seen to be of the form

$$\begin{vmatrix} A'-\lambda & C' & D' \\ C' & A'-\lambda & D' \\ D' & D' & B'-\lambda \end{vmatrix} = 0 \qquad (9)$$

which has roots

$$\lambda_o = A' - C' \qquad (10)$$

$$\lambda_{\pm} = \frac{(A'+B'+C') \pm \{(A'-B'-C')^2 + 8(D')^2\}^{\frac{1}{2}}}{2} \qquad (11)$$

and leads to eigenfunctions which are, again, summarized in Table 6 along with the appropriate expressions for A', B', C', and D'.

The results for both 3 x 3 matrices are sufficiently general to be applied to any parallelogram of spin ½ particles. We note that the eigenvalues of the second, more complicated 3 x 3 matrix agree with those of Eichoff and Zachmann[5] who started with the same secular equation for that case, and the eigenvalues for the simpler 3 x 3 matrix agrees with the results of Itoh, et al.[3]. Neither of those authors included eigenfunctions in their papers.

The secular equation obtained from the 4 x 4 matrices of Table 4 is of the form

$$\begin{vmatrix} E''-\lambda & 0 & 3D'' & -3D'' \\ 0 & B''-\lambda & D'' & D'' \\ 3D'' & D'' & A''-\lambda & C'' \\ -3D'' & D'' & C'' & A''-\lambda \end{vmatrix} = 0 \qquad (12)$$

This is the general form for a parallelogram of spins. Note that choosing a square or even a line of four spin ½ particles does not

simplify this secular equation.

The expansion of the determinant[12] conveniently factors, providing

$$(E''-\lambda)\,(A''-\lambda-C'') - 18D''^2 = 0$$
$$(B''-\lambda)\,(A''-\lambda+C'') - 2D''^2 = 0 \qquad (13)$$

whence

$$\lambda_{\pm} = \frac{(A''+E''-C'') \pm \{(-A''+E''+C'')^2 + 4(18)\,(D'')^2\}^{\frac{1}{2}}}{2}$$
$$\lambda'_{\pm} = \frac{(A''+B''+C'') \pm \{(A''-B''-C'')^2 + 8(D'')^2\}^{\frac{1}{2}}}{2} \qquad (14)$$

As in previous cases, the secular equation provides the set of linear equations leading to the eigenfunctions. The results are summarized in Table 6 where the appropriate values for A", B", C", D" and E" are also given. Note that the new eigenfunctions are designated ψ_i'. These were chosen for convenience in that the ψ_i' eigenfunctions specialize to the ψ_i eigenfunctions given in Table 2 for certain special cases. For example, for certain orientation of a square, ψ_9 is the largest admixture in $\psi_{9'}$. This will not be the case for all parallelogram configurations in all orientations; however, it does provide a convenient notation. The eigenvalues are denoted by E_i, so that which eigenvalue belongs to which eigenfunction is clear.

V. Summary and Discussion

The eigenfunctions and eigenvalues given in Table 6 are a general

result for a parallelogram configuration of spin ½ nuclei. These results, along with the transition matrix elements given in Table 5 can be used to predict dipolar spectra for solids containing such configurations of spins. In the most complicated cases the results predict up to 24 lines and even what might seem to be a less complicated case, that of a straight-line of spins, can produce 24 lines. In the following section we treat some special cases showing theoretical results for squares of spins in specific orientations and for linear chains for which all the internuclear distances may or may not be equal. In a companion paper[7] the theory is applied to cases of carbonyl cluster hydrides which are believed to have parallelogram configurations of spins and for which unusual dipolar spectra have been observed[1].

VI. Special Cases

Figure 1 illustrates the two specific configurations considered for this problem, a square and a straight line of four spin ½ nuclei. Both geometries are of more than theoretical interest as they can correspond to configurations of spins observed experimentally[1].

A. The Square of Spin ½ Nuclei in Specific Orientations

Table 7 summarizes the matrix elements for a square of spin ½ nuclei. In that case $r_{12} = r_{13}$, $r_{14} = r_{23}$, and $r_{23} = \sqrt{2}\, r_{12}$. Comparison of Table 7 and Table 4 shows no mathematical simplification of the general form of the matrices for the square as compared with the general parallelogram. However, for specific orientations of a square, those for which $A_{14} = A_{23}$, the problem is considerably simplified.

Two such cases are considered, each of which was initially solved independently as a test.

1. Case of a Square of Spin - ½ Nuclei where All $\theta_{ij} = \pi/2$

Consider the orientation of a square in the x-y plane, where, in general $\theta_{ij} = \frac{\pi}{2}$ and $P_2(\cos\theta_{ij}) = -\frac{1}{2}$. The simplifications of the matrix elements for this particular case are summarized in Table 8. Note that the 4 x 4 matrices and one of the 3 x 3 matrices block-diagonalize to no greater than 2 x 2. For the matrices given in Table 8 it is straightforward to prepare an energy-level diagram; the left side of Figure 2 shows just such a diagram labeled with energies. The upper spectrum in Figure 3 illustrates the result. The dashed lines correspond to the spectrum of an isolated spin ½ pair.
Note that the case of a square where all $\theta_{ij} = \frac{\pi}{2}$ produces eight lines.

2. Case of a Square of Spin ½ Nucleus Where $\theta_{12} = \frac{\pi}{2}$, $\theta_{13} = 0$, and $\theta_{23} = \theta_{14} = \frac{\pi}{4}$

In this case $P_{12}(\cos\theta) = -\frac{1}{2}$, $P_{13}(\cos\theta) = +1$, and $P_{23}(\cos\theta) = +\frac{1}{4}$. Using this information and the fact that $r_{12} = r_{13} = \sqrt{2}\, r_{14}$, Table 9 is obtained. Note that there are no matrices larger than 2 x 2. (If we had not chosen $\theta_{23} = \theta_{14}$, the situation would be different.) The results are used to prepare an energy-level diagram and predicted spectra. The energy levels are indicated on the right side of Figure 2 for convenient comparison with the results of the last section, and the lower

part of Figure 3 illustrates the resulting spectrum which has split into ten lines. Again, the dashed line corresponds to the case of an isolated spin pair. Note that for general orientations, in which $A_{14} \neq A_{23}$, we cannot expect such simple spectra consisting of only eight or ten lines. In particular, examination of form of the eigenfunctions given in Table 6 shows that the degree to which predicted spectra will deviate from the simple cases considered depends on the size of $(A_{23}-A_{14})$, which, when large, can mix states strongly.

B. Straight Line of Four Spin ½ Nuclei

The geometry in which all four spins lie along the same vector would appear to offer some simplification. However, as previous authors[8-10] have indicated, and as we will show explicitly for the four spin problems, almost no simplification occurs. Even if one makes the rough approximation that all $A_{ij} = 0$ for $j \neq i+1$, inspection of the mathematical form of the resulting secular equations, given in Table 10, shows almost no improvement over the general case. From the point of view of synthesizing powder spectra, however, there is the decided advantage for the problem of a linear chain in that one can factor $(3 \cos^2\theta_{ij} - 1)$ from every A_{ij} since all internuclear vectors make the same angle with the field. Using Tables 5 and 6, it is possible to simulate spectra for the linear chain, and it is not necessary to neglect A_{ij} for which $j \neq i+1$.

It is instructive to consider the relative magnitudes of A_{12} and

and A_{23} since those quantities, reflect the degree to which a linear chain can be thought of as a four spin ½ problem or as a problem of two proton pairs.

Case Where $A_{12} = A_{23}$

In this case $r_{12} = r_{23} = r_{34}$. Since, then, $r_{13} = 2r_{12}$ we have $A_{13} = \left(\frac{1}{8}\right)A_{12}$ and similarly $A_{14} = \left(\frac{1}{27}\right) A_{12}$. Letting $A = A_{12}$ and $A_{13} = \left(\frac{1}{8}\right) A$ but neglecting A_{14}, and using Table 6 we prepare Figure 4 which shows the energy level splittings and the expected spectra for the case where the four spin ½ particles are equidistant and in a straight line. (Figure 4 also shows cases yet to be discussed.) The lower spectrum in Figure 5 show the 24 symmetrically split lines obtained. The dashed lines drawn for comparison correspond to the splitting for an isolated proton pair. One can infer from the form of Figure 4b that powder spectra of four spin ½ chains will show structure more complex than that observed for spin ½ pairs.

2. Case Where $A_{12} = 2A_{23}$

For this case, the internuclear distance $r_{23} = (2)^{1/3} r_{12}$. In the same way as the previous case, under the assumption that $A_{23} = 2A_{23} = A$ and that we can neglect all other A_{ij}, we obtain the energy level diagram given in Figure 4 and the upper spectrum of Figure 5. This case produces 23 lines that are not spread out over such a wide range, and more importantly, note the grouping of intense lines in the region of the ideal isolated pair spectra (dashed lines). Making the further specialization that A_{12} is much larger than other A_{ij} we obtain results indicated in Figure 4, which are the results for isolated spin ½ pairs.

Although only stick spectra are presented here, one notes that for linear configurations as all splittings will have a $(3\cos^2\theta-1)$ dependence (axially symmetric second rank tensor) it is possible to visualize powder spectra showing more structure than is usually seen for proton NMR dipolar spectra. Such isolated linear configurations will give rise to a "dip" in the center of the spectrum, a situation usually attributed to isolated pairs. Thus, it would be easy to misinterpret experimental results for a four spin ½ case in terms of isolated proton pairs. Truly isolated spin ½ pairs powder spectra, for example, are expected to exhibit sharp inner peaks with a spacing half that of the outer peaks (shoulders)[2], and this has been observed experimentally[11]. On the other hand, features such as broadened inner peaks and high outer shoulders at less than twice the inner peak spacing are characteristic of linear chains of four spin ½ particles. It is necessary to take such factors into consideration when trying to extract useful structural information from NMR data.

References

1. A. T. Nicol and R. W. Vaughan, "Solid State Nuclear Magnetic Resonance Study of Heavy Metal Hydrides," Transition Metal Hydrides, Advances in Chemistry Series, Volume 167, July 1978.
2. A. Abragam, The Principles of Nuclear Magnetism, Oxford University Press, 1961. Chapter four.
3. J. Itoh, R. Kusaka, Y. Yamagata, R. Kiriyama, and H. Ibamoto, J. Phys. Soc. Japan 8, 293 (1953).
4. R. Bersohn and H. S. Gutowsky, J. Chem. Phys. 33, 651 (1954).
5. V. U. Eichoff and H. G. Zachmann, Kolloid-z.w.z. Polymere 241, 928 (1970).
6. N. Boden and Y.-K. Levine, Mol. Phys. 29, 1221 (1975).
7. A. T. Nicol and R. W. Vaughan, to be published.
8. A. Sur and I. J. Lowe, Phys. Rev. B12, 4597 (1975).
9. A. Sur, D. Jasnow, and I. J. Lowe, Phys. Rev. B12, 3845 (1975).
10. M. Engelsberg, I. J. Lowe, and F. L. Carolan, Phys. Rev. B7, 924 (1973).
11. M. E. Stoll, Ph.D. Thesis, California Institute of Technology (1972).

TABLE 1

	$\beta\beta\beta\beta$ or $\lvert\alpha_1\alpha_2\alpha_3\alpha_4\rangle$	$\lvert\beta_1\beta_2\beta_3\beta_4\rangle$
$(\alpha\alpha\alpha\alpha)$ or $(\beta\beta\beta\beta)$	$(-\frac{1}{2}\sum_{j<k} A_{jk})$	0
	0	$(-\frac{1}{2}\sum A_{jk})$

	$\alpha\beta\beta\beta$ or $\beta\alpha\alpha\alpha$	$\beta\alpha\beta\beta$ or $\alpha\beta\alpha\alpha$	$\beta\beta\alpha\beta$ or $\alpha\alpha\beta\alpha$	$\beta\beta\beta\alpha$ or $\alpha\alpha\alpha\beta$
$\beta\alpha\alpha\alpha$ or $\beta\alpha\alpha\alpha$	$-\frac{1}{2}\{-A_{12}-A_{13}-A_{14}+A_{23}+A_{24}+A_{34}\}$	$\frac{1}{2}A_{12}$	$\frac{1}{2}A_{13}$	$\frac{1}{2}A_{14}$
$\alpha\beta\alpha\alpha$ or $\beta\alpha\beta\beta$	$\frac{1}{2}A_{12}$	$-\frac{1}{2}\{-A_{12}+A_{13}+A_{14}-A_{23}-A_{24}+A_{34}\}$	$\frac{1}{2}A_{23}$	$\frac{1}{2}A_{24}$
$\alpha\alpha\beta\alpha$ or $\beta\beta\alpha\beta$	$\frac{1}{2}A_{13}$	$\frac{1}{2}A_{23}$	$-\frac{1}{2}\{A_{12}-A_{13}+A_{14}-A_{23}+A_{24}-A_{34}\}$	$\frac{1}{2}A_{34}$
$\alpha\alpha\alpha\beta$ or $\beta\beta\beta\alpha$	$\frac{1}{2}A_{14}$	$\frac{1}{2}A_{24}$	$\frac{1}{2}A_{34}$	$-\frac{1}{2}\{A_{12}+A_{13}-A_{14}+A_{23}-A_{24}-A_{34}\}$

TABLE 1 (cont)

	$\beta\beta\alpha\alpha$	$\alpha\beta\beta\alpha$	$\beta\alpha\beta\alpha$	$\beta\alpha\alpha\beta$	$\alpha\beta\alpha\beta$	$\alpha\alpha\beta\beta$
$\beta\beta\alpha\alpha$	$-\frac{1}{2}\{A_{12}-A_{13}-A_{14}-A_{23}-A_{24}+A_{34}\}$	$\frac{1}{2}A_{13}$	$\frac{1}{2}A_{23}$	$\frac{1}{2}A_{24}$	$\frac{1}{2}A_{14}$	0
$\alpha\beta\beta\alpha$	$\frac{1}{2}A_{13}$	$-\frac{1}{2}\{-A_{12}-A_{13}+A_{14}+A_{23}-A_{24}-A_{34}\}$	$\frac{1}{2}A_{12}$	0	$\frac{1}{2}A_{34}$	$\frac{1}{2}A_{24}$
$\beta\alpha\beta\alpha$	$\frac{1}{2}A_{23}$	$\frac{1}{2}A_{12}$	$-\frac{1}{2}\{-A_{12}+A_{13}-A_{14}-A_{23}+A_{24}-A_{34}\}$	$\frac{1}{2}A_{34}$	0	$\frac{1}{2}A_{14}$
$\beta\alpha\alpha\beta$	$\frac{1}{2}A_{24}$	0	$\frac{1}{2}A_{34}$	$-\frac{1}{2}\{-A_{12}-A_{13}+A_{14}+A_{23}-A_{24}-A_{34}\}$	$\frac{1}{2}A_{12}$	$\frac{1}{2}A_{13}$
$\alpha\beta\alpha\beta$	$\frac{1}{2}A_{14}$	$\frac{1}{2}A_{34}$	0	$\frac{1}{2}A_{12}$	$-\frac{1}{2}\{-A_{12}+A_{13}-A_{14}-A_{23}+A_{24}-A_{34}\}$	$\frac{1}{2}A_{23}$
$\alpha\alpha\beta\beta$	0	$\frac{1}{2}A_{24}$	$\frac{1}{2}A_{14}$	$\frac{1}{2}A_{13}$	$\frac{1}{2}A_{23}$	$-\frac{1}{2}\{A_{12}-A_{13}-A_{14}-A_{23}-A_{24}+A_{34}\}$

TABLE 2. Transformation between LSIM Representation and $m_1m_2m_3m_4$ Representation.

	L	S	I	M														
ψ_1	1	1	2	2	1													$\alpha_1\alpha_2\alpha_3\alpha_4$
$2\psi_2$	1	1	2	1		1	1	1	1									$\beta_1\alpha_2\alpha_3\alpha_4$
$2\psi_3$	1	1	1	1		-1	-1	1	1									$\alpha_1\beta_2\alpha_3\alpha_4$
$\sqrt{2}\psi_4$	1	0	1	1		0	0	-1	1									$\alpha_1\alpha_2\beta_3\alpha_4$
$\sqrt{2}\psi_5$	0	1	1	1		-1	1	0	0									$\alpha_1\alpha_2\alpha_3\beta_4$
$\sqrt{6}\psi_6$	1	1	2	0						1	1	1	1	1	1			$\beta_1\beta_2\alpha_3\alpha_4$
$\sqrt{2}\psi_7$	1	1	1	0						1	0	0	0	0	-1			$\alpha_1\beta_2\beta_3\alpha_4$
$2\psi_8$	1	0	1	0	=					0	-1	-1	1	1	0			$\beta_1\alpha_2\beta_3\alpha_4$
$2\psi_9$	0	1	1	0						0	1	-1	-1	1	0			$\beta_1\alpha_2\alpha_3\beta_4$
$2\psi_{10}$	0	0	0	0						0	-1	1	-1	1	0			$\alpha_1\beta_2\alpha_3\beta_4$
$2\sqrt{3}\psi_{11}$	1	1	0	0						-2	1	1	1	1	-2			$\alpha_1\alpha_2\beta_3\beta_4$
$2\psi_{12}$	1	1	2	-1												1	1	$\alpha_1\beta_2\beta_3\beta_4$
$2\psi_{13}$	1	1	1	-1												-1	-1	$\beta_1\alpha_2\beta_3\beta_4$
$\sqrt{2}\psi_{14}$	1	0	1	-1												0	0	$\beta_1\beta_2\alpha_3\beta_4$
$\sqrt{2}\psi_{15}$	0	1	1	-1												-1	1	$\beta_1\beta_2\beta_3\alpha_4$
ψ_{16}	1	1	2	-2													1	$\beta_1\beta_2\beta_3\beta_4$

TABLE 3

	$\psi_1 =$ aaaa
ψ_1	$-\frac{1}{2}\sum_{i<j} A_{ij}$

	ψ_2 or ψ_{12}	ψ_3 or ψ_{13}	ψ_4 or ψ_{14}	ψ_5 or ψ_{15}
ψ_2 or ψ_{12}	$\frac{1}{4}\sum_{i<j} A_{ij}$	$-\frac{3}{4}(A_{12} - A_{34})$	$\frac{-3}{4\sqrt{2}}\{A_{13}+A_{23} -A_{14}-A_{24}\}$	$\frac{-3}{4\sqrt{2}}\{A_{13}+A_{14} -A_{23}-A_{24}\}$
ψ_3 or ψ_{13}		$-\frac{1}{4}\{-A_{12}-A_{34} +A_{14}+A_{24} +A_{13}+A_{23}\}$	$\frac{-1}{4\sqrt{2}}\{A_{13}+A_{23} -A_{14}-A_{24}\}$	$\frac{-1}{4\sqrt{2}}\{-A_{13}-A_{24} +A_{23}+A_{14}\}$
ψ_4 or ψ_{14}			$-\frac{1}{2}A_{12}$	$-\frac{1}{4}\{A_{13}-A_{24} +A_{23}+A_{14}\}$
ψ_5 or ψ_{15}				$-\frac{1}{2}A_{34}$

TABLE 3 (cont)

	ψ_{11}	ψ_6	ψ_{10}
ψ_{11}	0	$\frac{-1}{2\sqrt{2}}\{-2A_{12}-2A_{34}+A_{13}+A_{14}+A_{23}+A_{24}\}$	0
ψ_6		$\frac{1}{2}\sum_{i<j} A_{ij}$	$\frac{-\sqrt{6}}{4}\{A_{13}+A_{24}-A_{14}-A_{23}\}$
ψ_{10}			0

	ψ_8	ψ_9	ψ_7
ψ_8	A_{12}	$-\frac{1}{2}\{A_{13}+A_{24}-A_{14}-A_{23}\}$	$\frac{-1}{2\sqrt{2}}\{A_{13}+A_{23}-A_{14}-A_{24}\}$
ψ_9		A_{34}	$\frac{-1}{2\sqrt{2}}\{A_{23}+A_{24}-A_{13}-A_{14}\}$
ψ_7			$-\frac{1}{2}\{A_{12}+A_{34}-A_{13}-A_{14}-A_{23}-A_{24}\}$

TABLE 4

Matrix Elements for H_D for the Case of a Parallogram

$\psi_{16} = |112\text{-}2\rangle$
or
$\psi_1 = |1122\rangle$

ψ_1 or ψ_{16}	$-\frac{1}{2}\{2A_{12}+2A_{13}+A_{23}+A_{14}\}$

	$\psi_{12}=\|112\text{-}1\rangle$ $\psi_2=\|1121\rangle$	$\psi_{13}=\|111\text{-}1\rangle$ $\psi_3=\|1111\rangle$	$\psi_{14}=\|101\text{-}1\rangle$ $\psi_4=\|1011\rangle$	$\psi_{15}=\|011\text{-}1\rangle$ $\psi_5=\|0111\rangle$
ψ_{12} or ψ_2	$\frac{1}{4}\{2A_{12}+2A_{13}+A_{23}+A_{14}\}$	0	$\frac{-3}{4\sqrt{2}}\{A_{23}-A_{14}\}$	$\frac{-3}{4\sqrt{2}}\{A_{14}-A_{23}\}$
ψ_{13} or ψ_3		$-\frac{1}{4}\{-2A_{12}+2A_{13}+A_{23}+A_{14}\}$	$\frac{-1}{4\sqrt{2}}\{A_{23}-A_{14}\}$	$\frac{-1}{4\sqrt{2}}\{A_{23}-A_{14}\}$
ψ_{14} or ψ_4			$-\frac{1}{2}A_{12}$	$-\frac{1}{4}\{-2A_{13}+A_{23}+A_{14}\}$
ψ_{15} or ψ_5				$-\frac{1}{2}A_{12}$

TABLE 4 (cont)

	$\psi_{11} = \|1100\rangle$	$\psi_6 = \|1120\rangle$	$\psi_{10} = \|0000\rangle$
ψ_{11}	0	$\frac{-1}{2\sqrt{2}}\{-4A_{12}+2A_{13}+A_{14}+A_{23}\}$	0
ψ_{16}		$\frac{1}{2}\{2A_{12}+2A_{13}+A_{14}+A_{23}\}$	$\frac{-\sqrt{6}}{4}\{2A_{13}-A_{14}-A_{23}\}$
ψ_{10}			0

	$\psi_8 = \|1010\rangle$	$\psi_9 = \|0110\rangle$	$\psi_7 = \|1110\rangle$
ψ_8	$+A_{12}$	$-\frac{1}{2}\{2A_{13}-A_{14}-A_{23}\}$	$\frac{-1}{2\sqrt{2}}\{A_{23}-A_{14}\}$
ψ_9		$+A_{12}$	$\frac{-1}{2\sqrt{2}}\{A_{23}-A_{14}\}$
ψ_7			$-\frac{1}{2}\{2A_{12}-2A_{13}-A_{14}-A_{23}\}$

TABLE 5

Transition Matrix Elements

$\lvert\langle\psi_n\lvert I_x\rvert\psi_m\rangle\rvert^2$	Relative Intensity
$\lvert\langle\psi_1\lvert I_x\rvert\psi_2\rangle\rvert^2 = \lvert\langle\psi_{16}\lvert I_x\rvert\psi_{12}\rangle\rvert^2$	1
$\lvert\langle\psi_6\lvert I_x\rvert\psi_2\rangle\rvert^2 = \lvert\langle\psi_6\lvert I_x\rvert\psi_{12}\rangle\rvert^2$	3/2
$\lvert\langle\psi_3\lvert I_x\rvert\psi_7\rangle\rvert^2 = \lvert\langle\psi_7\lvert I_x\rvert\psi_{13}\rangle\rvert^2$	1/2
$\lvert\langle\psi_4\lvert I_x\rvert\psi_8\rangle\rvert^2 = \lvert\langle\psi_8\lvert I_x\rvert\psi_{14}\rangle\rvert^2$	1/2
$\lvert\langle\psi_5\lvert I_x\rvert\psi_9\rangle\rvert^2 = \lvert\langle\psi_9\lvert I_x\rvert\psi_{15}\rangle\rvert^2$	1/2

All other transition matrix elements = 0.

Note that these transition matrix elements obey the selection rules $\Delta L = 0$, $\Delta S = 0$, $\Delta I = 0$, $\Delta M = \pm 1$.

TABLE 6

Eigenfunction	Eigenvalue
$\psi_{1'} = \psi_1$	$E_{1'} = E_{16'} = -(A_{12}+A_{13}) - \frac{(A_{23}+A_{14})}{2}$
$\psi_{16'} = \psi_{16}$	

$$\psi_{2',12'} = \left\{\frac{(E''-\lambda_+)^2}{36D^2 + 2(E-\lambda_+)^2}\right\}^{\frac{1}{2}} \left\{\frac{-6D''}{(E''-\lambda_+)}\ \psi_2 + \psi_4 - \psi_5\right\} \qquad \lambda_+ = E_{2'} = \frac{A_{23}+A_{14}}{4} + \left\{\left(\frac{A_{12}+A_{13}}{2}\right)^2 + \frac{9}{16}(A_{23}-A_{14})^2\right\}^{\frac{1}{2}}$$

$$\psi_{3',13'} = \left\{\frac{(B''-\lambda'_+)^2}{4D^2 + 2(B''-\lambda'_+)^2}\right\}^{\frac{1}{2}} \left\{\frac{-2D}{(B-\lambda'_+)}\ \psi_3 + \psi_4 + \psi_5\right\} \qquad \lambda'_+ = E_{3'} = -\left(\frac{A_{23}+A_{14}}{4}\right) + \left\{\left(\frac{A_{12}-A_{13}}{2}\right)^2 + \frac{1}{16}(A_{23}-A_{14})^2\right\}^{\frac{1}{2}}$$

$$\psi_{4',14'} = \left\{\frac{(B''-\lambda'_-)^2}{4D^2 + 2(B''-\lambda'_-)^2}\right\}^{\frac{1}{2}} \left\{\frac{-2D''}{(B''-\lambda'_-)}\ \psi_3 + \psi_4 + \psi_5\right\} \qquad \lambda'_- = E_{4'} = -\left(\frac{A_{23}+A_{14}}{4}\right) - \left\{\left(\frac{A_{12}-A_{13}}{2}\right)^2 + \frac{1}{16}(A_{23}-A_{14})^2\right\}^{\frac{1}{2}}$$

$$\psi_{5',15'} = \left\{\frac{(E''-\lambda_-)^2}{36D^2 + 2(E-\lambda_-)^2}\right\}^{\frac{1}{2}} \left\{\frac{-6D''}{(E''-\lambda_-)}\ \psi_2 + \psi_4 - \psi_5\right\} \qquad \lambda_- = E_{5'} = \left(\frac{A_{23}+A_{14}}{4}\right) - \left\{\left(\frac{A_{12}+A_{13}}{2}\right)^2 + \frac{9}{16}(A_{23}-A_{14})^2\right\}^{\frac{1}{2}}$$

where $E'' = \left(\frac{A_{12}+A_{13}}{2}\right) + \left(\frac{A_{23}+A_{14}}{4}\right)$ $\qquad C'' = \frac{A_{13}}{2} - \left(\frac{A_{23}+A_{14}}{4}\right)$

$B'' = \left(\frac{A_{12}-A_{13}}{2}\right) - \left(\frac{A_{23}+A_{14}}{4}\right)$ $\qquad D'' = \frac{-1}{4\sqrt{2}}(A_{23}-A_{14})$

$A'' = -\frac{A_{12}}{2}$

TABLE 6. (cont.)

$$\psi_{9'} = \psi_0 = \frac{1}{\sqrt{2}}\left\{\psi_8 - \psi_9\right\} \qquad E_{9'} = A' - C' = (A_{12}+A_{13}) - \tfrac{1}{2}(A_{14}+A_{23})$$

$$\psi_{8'} = \psi_- = \left\{\frac{(\lambda_- - B')^2}{2(\lambda_- - B')^2 + 4(D')^2}\right\}^{\frac{1}{2}}\left\{\psi_8+\psi_9 + \left(\frac{2D'}{\lambda_- - B'}\right)\psi_7\right\} \qquad E_{8'} = \lambda_- = \frac{(A_{14}+A_{23})}{2} - \tfrac{1}{2}\left\{(A_{14}-A_{23})^2 + 4(A_{12}-A_{13})^2\right\}^{\frac{1}{2}}$$

$$\psi_{7'} = \psi_+ = \left\{\frac{(\lambda_+ - B')^2}{2(\lambda_+ - B')^2 + 4(D')^2}\right\}^{\frac{1}{2}}\left\{\psi_8+\psi_9 + \left(\frac{2D'}{\lambda_+ - B'}\right)\psi_7\right\} \qquad E_{7'} = \lambda_+ = \frac{(A_{14}+A_{23})}{2} + \tfrac{1}{2}\left\{(A_{14}-A_{23})^2 + 4(A_{12}-A_{13})^2\right\}^{\frac{1}{2}}$$

where $A' = A_{12}$

$C' = -A_{13} + \dfrac{(A_{14}+A_{23})}{2}$

$B' = -(A_{12}-A_{13}) + \left(\dfrac{A_{14}+A_{23}}{2}\right)$

$D' = -\dfrac{1}{2\sqrt{2}}(A_{23} - A_{14})$

TABLE 6. (cont.)

$$\psi_{11'} = \psi_{\lambda=0} = \left(\frac{A^2}{C^2+A^2}\right)^{\frac{1}{2}} \left(\frac{-C}{A}\,\psi_{11} + \psi_{10}\right) \qquad \lambda_0 = E_{11'} = 0$$

$$\psi_{10'} = \psi_{\lambda+} = \left(\frac{A^2}{A^2+C^2+\lambda_+^2}\right)^{\frac{1}{2}} \left(\psi_{11} + \frac{\lambda_+}{A}\,\psi_6 + \frac{C}{A}\,\psi_{10}\right) \qquad \lambda_+ = E_{10'} = \frac{B}{2} + \tfrac{1}{2}\left(B^2 + 4(A^2+C^2)\right)^{\frac{1}{2}}$$

$$\psi_{6'} = \psi_{\lambda-} \left(\frac{A^2}{A^2+C^2+\lambda_-^2}\right)^{\frac{1}{2}} \left(\psi_{11} + \frac{\lambda_-}{A}\,\psi_6 + \frac{C}{A}\,\psi_{10}\right) \qquad \lambda_- = E_{6'} = \frac{B}{2} - \tfrac{1}{2}\left(B^2 + 4(A^2+C^2)\right)^{\frac{1}{2}}$$

where $A = -\frac{1}{\sqrt{2}}\left\{(-2A_{12}+A_{13}) + \left(\frac{A_{14}+A_{23}}{2}\right)\right\}$

$$B = (A_{12}+A_{13}) + \left(\frac{A_{14}+A_{23}}{2}\right)$$

$$C = \left(\frac{-\sqrt{6}}{2}\,A_{13}\right) + \sqrt{6}\,\frac{(A_{14}+A_{23})}{4}$$

TABLE 7

Matrix Elements for the Case of a Square of Spin ½ Nuclei

	ψ_1 or ψ_{16}
ψ_1 or ψ_{16}	$-\frac{\gamma^2\hbar^2}{r^3}\left\{(P_{12}+P_{13}) + \frac{(P_{14}+P_{23})}{4\sqrt{2}}\right\}$

$$A_{ij} = \frac{\gamma^2\hbar^2}{2r_{ij}^3}(3\cos^2\theta_{ij}-1)$$

or

$$A_{ij} = \frac{\gamma^2\hbar^2}{r_{ij}^3} P_2(\cos\theta_{ij})$$

Let $P_2(\cos\theta_{ij}) = P_{ij}$

$r = r_{12} = r_{13}$

$r_{14} = r_{23} = \sqrt{2}r_{12} = \sqrt{2}\,r$

	ψ_{12} or ψ_2	ψ_{13} or ψ_3	ψ_{14} or ψ_4	ψ_{13} or ψ_5
ψ_{12} or ψ_2	$\frac{\gamma^2\hbar^2}{2r^3}\left\{(P_{12}+P_{13}) + \frac{(P_{23}+P_{14})}{4\sqrt{2}}\right\}$	0	$\frac{-3}{16}\frac{\gamma^2\hbar^2}{r^3}(P_{23}-P_{14})$	$\frac{3}{16}\frac{\gamma^2\hbar^2}{r^3}(P_{23}-P_{14})$
ψ_{13} or ψ_3		$\frac{\gamma^2\hbar^2}{2r^3}\left\{(P_{12}-P_{13}) - \frac{(P_{23}+P_{14})}{4\sqrt{2}}\right\}$	$-\frac{\gamma^2\hbar^2}{16r^3}(P_{23}-P_{14})$	$\frac{-\gamma^2\hbar^2}{16r^3}(P_{23}-P_{14})$
ψ_{14} or ψ_4			$-\frac{\gamma^2\hbar^2}{2r^3}P_{12}$	$\frac{\gamma^2\hbar^2}{2r^3}\left\{P_{13} - \frac{(P_{23}+P_{14})}{4\sqrt{2}}\right\}$
ψ_{15} or ψ_5				$-\frac{\gamma^2\hbar^2}{2r^3}P_{12}$

TABLE 7 (cont)

	ψ_{11}	ψ_6	ψ_{10}
ψ_{11}	0	$\frac{\gamma^2\hbar^2}{r^3}\left\{\frac{2P_{12}-P_{13}}{\sqrt{2}} - \frac{(P_{23}+P_{14})}{8}\right\}$	0
ψ_6		$\frac{\gamma^2\hbar^2}{r^3}\left\{(P_{12}+P_{13}) + \frac{(P_{23}+P_{14})}{4\sqrt{2}}\right\}$	$\frac{\gamma^2\hbar^2}{r^3}\left(\frac{-\sqrt{6}}{2}\right)\left\{P_{13} - \frac{(P_{23}+P_{14})}{4\sqrt{2}}\right\}$
ψ_{10}			0

	ψ_8	ψ_9	ψ_7
ψ_8	$\frac{\gamma^2\hbar^2}{r^3} P_{12}$	$-\frac{\gamma^2\hbar^2}{r^3}\left\{P_{13} - \frac{(P_{23}+P_{14})}{4\sqrt{2}}\right\}$	$-\frac{\gamma^2\hbar^2}{8r^3}\ (P_{23}-P_{14})$
ψ_9		$\frac{\gamma^2\hbar^2}{r^3}\ P_{12}$	$-\frac{\gamma^2\hbar^2}{8r^3}\ (P_{23}-P_{14})$
ψ_7			$-\frac{\gamma^2\hbar^2}{r^3}\left\{(P_{12}-P_{13}) - \frac{(P_{23}+P_{14})}{4\sqrt{2}}\right\}$

TABLE 8

Simplification of the Problem of the Square of Spin ½ Nuclei.

Special Orientations with Respect to the Field.

All $\theta_{ij} = \pi/2$

$P_{ij}(\cos\theta) = -\frac{1}{2}$

$r = r_{12} = \sqrt{2}\ r_{23}$

	ψ_1 or ψ_{16}
ψ_1 or ψ_{16}	$\frac{\gamma^2\hbar^2}{r^3}\left[1 + \frac{1}{4\sqrt{2}}\right]$

	ψ_2 or ψ_{12}	ψ_3 or ψ_{13}	ψ_4 or ψ_{14}	ψ_5 or ψ_{15}
ψ_2 or ψ_{12}	$-\frac{\gamma^2\hbar^2}{2r^3}\left[1 + \frac{1}{4\sqrt{2}}\right]$	0	0	0
ψ_3 or ψ_{13}		$\frac{\gamma^2\hbar^2}{8\sqrt{2}\ r^3}$	0	0
ψ_4 or ψ_{14}			$\frac{\gamma^2\hbar^2}{4r^3}$	$-\frac{\gamma^2\hbar^2}{4r^3}\left[1 - \frac{1}{2\sqrt{2}}\right]$
ψ_5 or ψ_{15}				$\frac{\gamma^2\hbar^2}{4r^3}$

TABLE 8 (cont)

	ψ_{11}	ψ_6	ψ_{10}
ψ_{11}	0	$-\frac{\gamma^2\hbar^2}{2\sqrt{2}\,r^3}\left[1-\frac{1}{2\sqrt{2}}\right]$	0
ψ_6		$-\frac{\gamma^2\hbar^2}{r^3}\left[1+\frac{1}{4\sqrt{2}}\right]$	$\sqrt{6}\,\frac{\gamma^2\hbar^2}{4r^3}\left[1-\frac{1}{2\sqrt{2}}\right]$
ψ_{10}			0

	ψ_8	ψ_9	ψ_7
ψ_8	$-\frac{\gamma^2\hbar^2}{2r^3}$	$\frac{\gamma^2\hbar^2}{2\,r^3}\left[1-\frac{1}{2\sqrt{2}}\right]$	0
ψ_9		$-\frac{\gamma^2\hbar^2}{2r^3}$	0
ψ_7			$-\frac{\gamma^2\hbar^2}{4\sqrt{2}\,r^3}$

TABLE 9

Simplification of the Problem of the Square of Spin ½ Nuclei.
Special Orientation with Respect to the Field. $\theta_{12}=\frac{\pi}{2}$, $\theta_{13}=0$, $\theta_{23}=\theta_{14}=\frac{\pi}{4}$

	ψ_1 or ψ_{16}
ψ_1 or ψ_{16}	$\frac{-\gamma^2\hbar^2}{2r_{12}^3}\left\{1+\frac{1}{4\sqrt{2}}\right\}$

$P_{12}(\cos\theta) = -\frac{1}{2}$

$P_{13}(\cos\theta) = +1$

$P_{23}(\cos\theta) = +\frac{1}{4}$

$r = r_{12}$

	ψ_2 or ψ_{12}	ψ_3 or ψ_{13}	ψ_4 or ψ_{14}	ψ_5 or ψ_{15}
ψ_2 or ψ_{12}	$\frac{\gamma^2\hbar^2}{4r^3}\left\{1+\frac{1}{4\sqrt{2}}\right\}$	0	0	0
ψ_3 or ψ_{13}		$\frac{-\gamma^2\hbar^2}{4r^3}\left\{3+\frac{1}{4\sqrt{2}}\right\}$	0	0
ψ_4 or ψ_{14}			$\frac{\gamma^2\hbar^2}{4r^3}$	$\frac{\gamma^2\hbar^2}{2r^3}\left\{1-\frac{1}{8\sqrt{2}}\right\}$
ψ_5 or ψ_{15}				$\frac{\gamma^2\hbar^2}{4r^3}$

TABLE 10

Matrix Elements for H_D for the Case of a Line of Four Spin ½ Nuclei

	ψ_1 or ψ_{16}
ψ_1 or ψ_{16}	$-\frac{1}{2}\{2A_{12}+A_{23}\}$

	ψ_2 or ψ_{12}	ψ_3 or ψ_{13}	ψ_4 or ψ_{14}	ψ_5 or ψ_{15}
ψ_2,ψ_{12}	$\frac{1}{4}\{2A_{12}+A_{23}\}$	0.	$\frac{-3}{4\sqrt{2}}A_{23}$	$\frac{3}{4\sqrt{2}}A_{23}$
ψ_3,ψ_{13}		$-\frac{1}{4}\{-2A_{12}+A_{23}\}$	$\frac{-1}{4\sqrt{2}}\{A_{23}\}$	$\frac{-1}{4\sqrt{2}}\{A_{23}\}$
ψ_4,ψ_{14}			$-\frac{1}{2}A_{12}$	$-\frac{1}{4}\{A_{23}\}$
ψ_5,ψ_{15}				$-\frac{1}{2}A_{12}$

TABLE 10 (cont)

	ψ_{11}	ψ_6	ψ_{10}
ψ_{11}	0	$\frac{-1}{2\sqrt{2}}\{-4A_{12}+A_{23}\}$	0
ψ_6		$\frac{1}{2}\{2A_{12}+A_{23}\}$	$\frac{-\sqrt{6}}{4}\{-A_{23}\}$
ψ_{10}			0

	ψ_8	ψ_9	ψ_7
ψ_8	A_{12}	$\frac{1}{2}\{A_{23}\}$	$\frac{-1}{2\sqrt{2}}\{A_{23}\}$
ψ_9		A_{12}	$\frac{-1}{2\sqrt{2}}\{A_{23}\}$
ψ_7			$-\frac{1}{2}\{2A_{12}-A_{23}\}$

Figure Captions

Figure 1. Proton geometries.

Figure 2. Energy level diagrams for a square of four spin 1/2 nuclei at specific orientations (a) All $\theta_{ij} = \pi/2$. (b) $\theta_{12} = \pi/2$, $\theta_{13} = 0$, $\theta_{23} = \theta_{14} = \pi/4$. Levels are labeled with numbers corresponding to subscripts used in text.

Figure 3. Theoretical spectra for a square of four spin 1/2 nuclei at specific orientations. The upper spectrum corresponds to all $\theta_{ij} = \pi/2$ and the lower spectrum corresponds to $\theta_{12} = \pi/2$, $\theta_{13} = 0$ and $\theta_{14} = \theta_{23} = \pi/4$. The lines are labeled by numbers indicating which levels are involved in the transition.

Figure 4. Energy level diagram for a linear configuration of four spin 1/2 nuclei. (a) Zeeman levels unperturbed by dipolar interaction. (b) Dipolar interaction with $A_{12} >>$ other A_{ij} (isolated spin pairs) (c) $A_{12} = 2A_{23}$. (d) $A_{12} = A_{23}$.

Figure 5. Theoretical spectra for a line of four spin 1/2 nuclei corresponding to cases (c) $A_{12} = 2A_{23}$, and (d) $A_{12} = A_{23}$ of Figure 4.

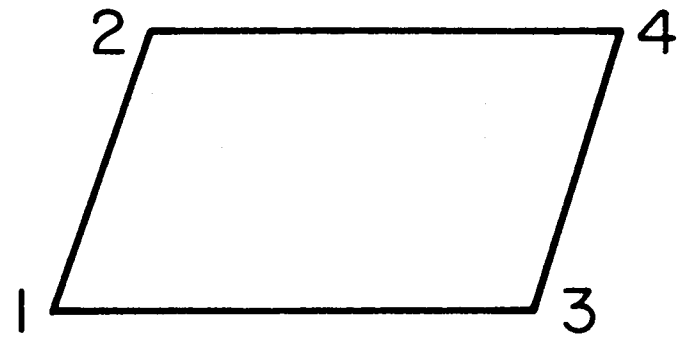

(a)

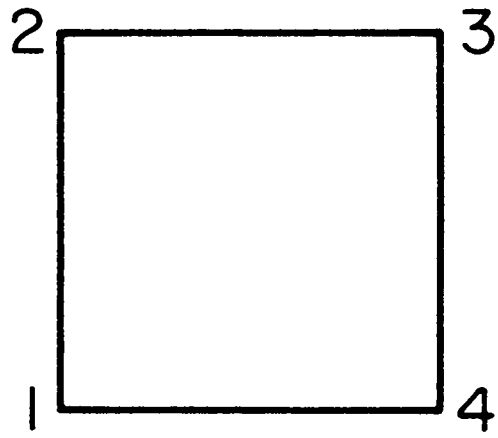

(b)

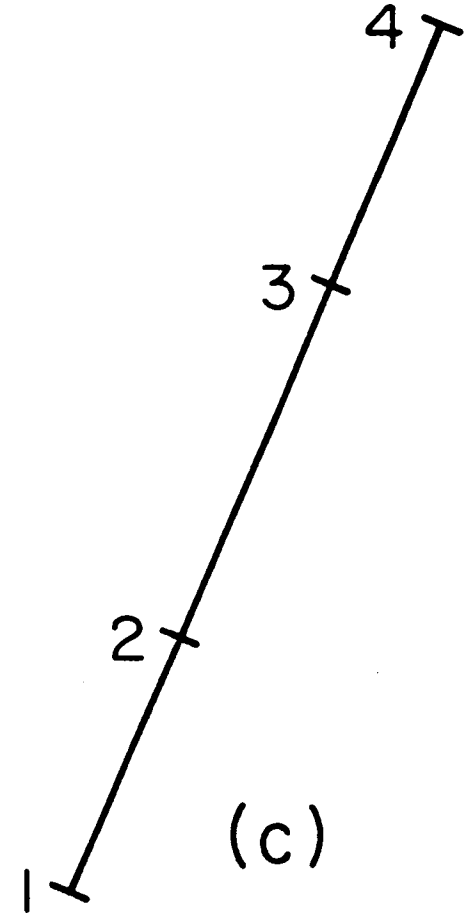

(c)

Figure 1

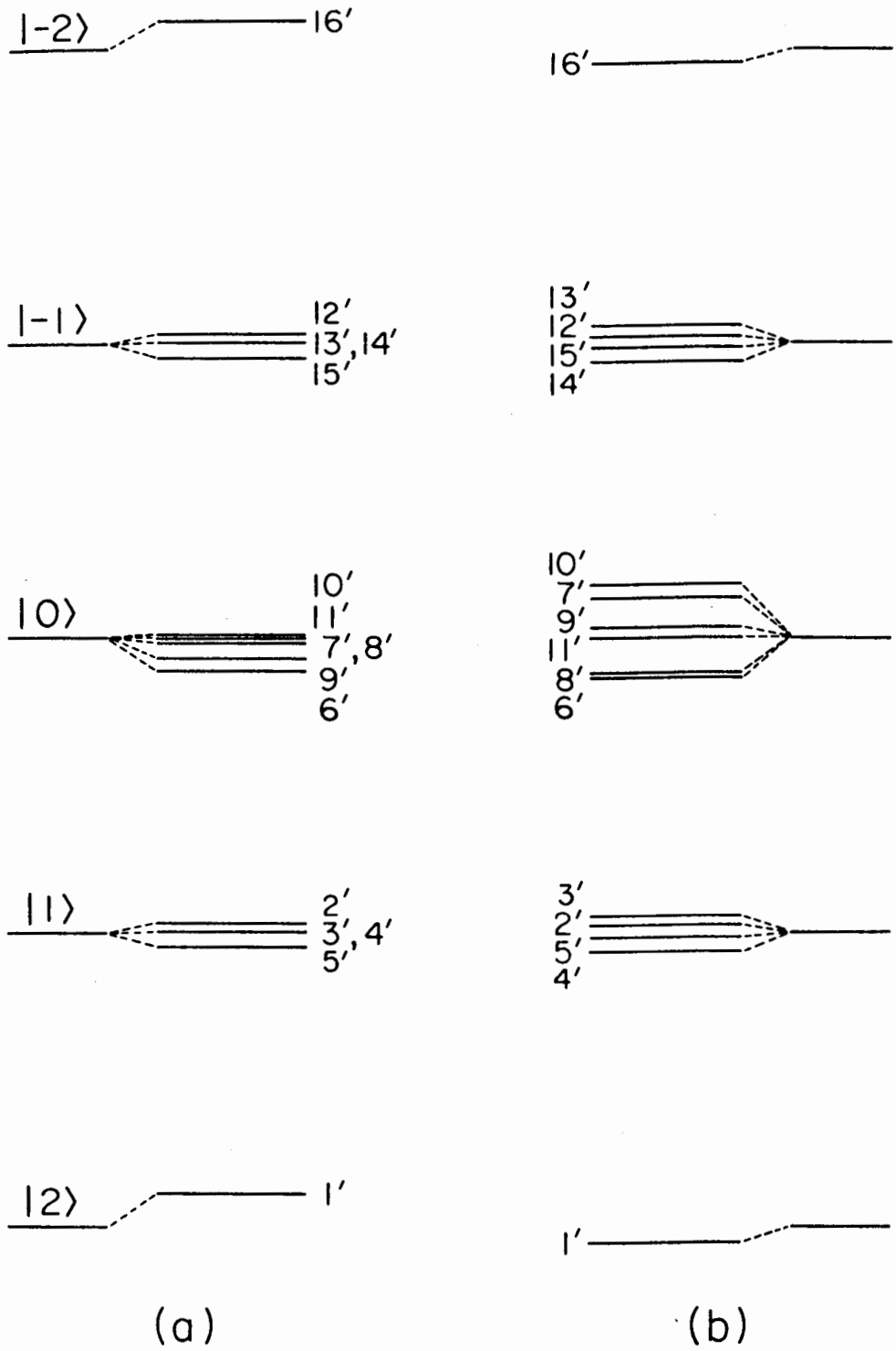
|-2⟩
16′
16′
|-1⟩
12′
13′,14′
15′
13′
12′
15′
14′
|0⟩
10′
11′
7′,8′
9′
6′
10′
7′
9′
11′
8′
6′
|1⟩
2′
3′,4′
5′
3′
2′
5′
4′
|2⟩
1′
1′
(a)
(b)

Figure 2

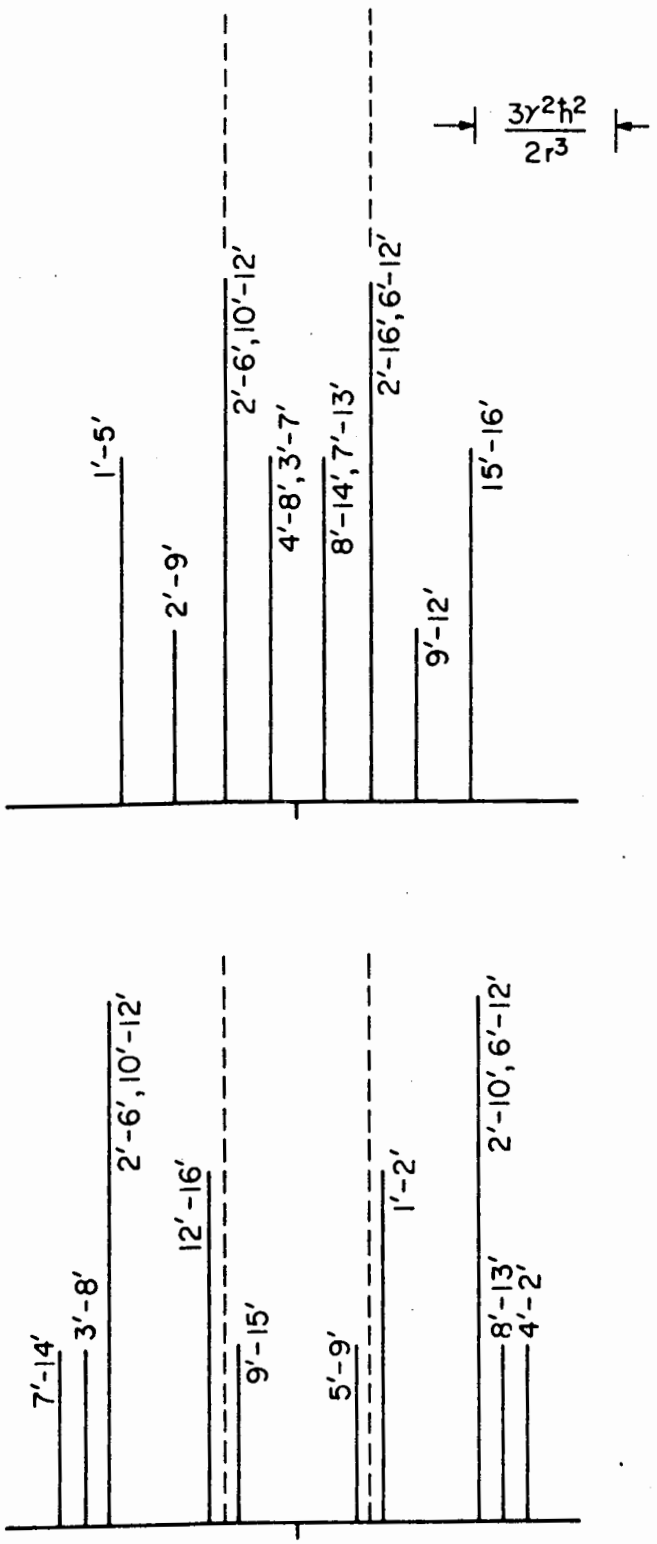
1'-5'
2'-9'
2'-6', 10'-12'
4'-8', 3'-7'
8'-14', 7'-13'
2'-16', 6'-12'
9'-12'
15'-16'
$\frac{3\gamma^2\hbar^2}{2r^3}$
7'-14'
3'-8'
2'-6', 10'-12'
12'-16'
9'-15'
5'-9'
1'-2'
2'-10', 6'-12'
8'-13'
4'-2'

Figure 3

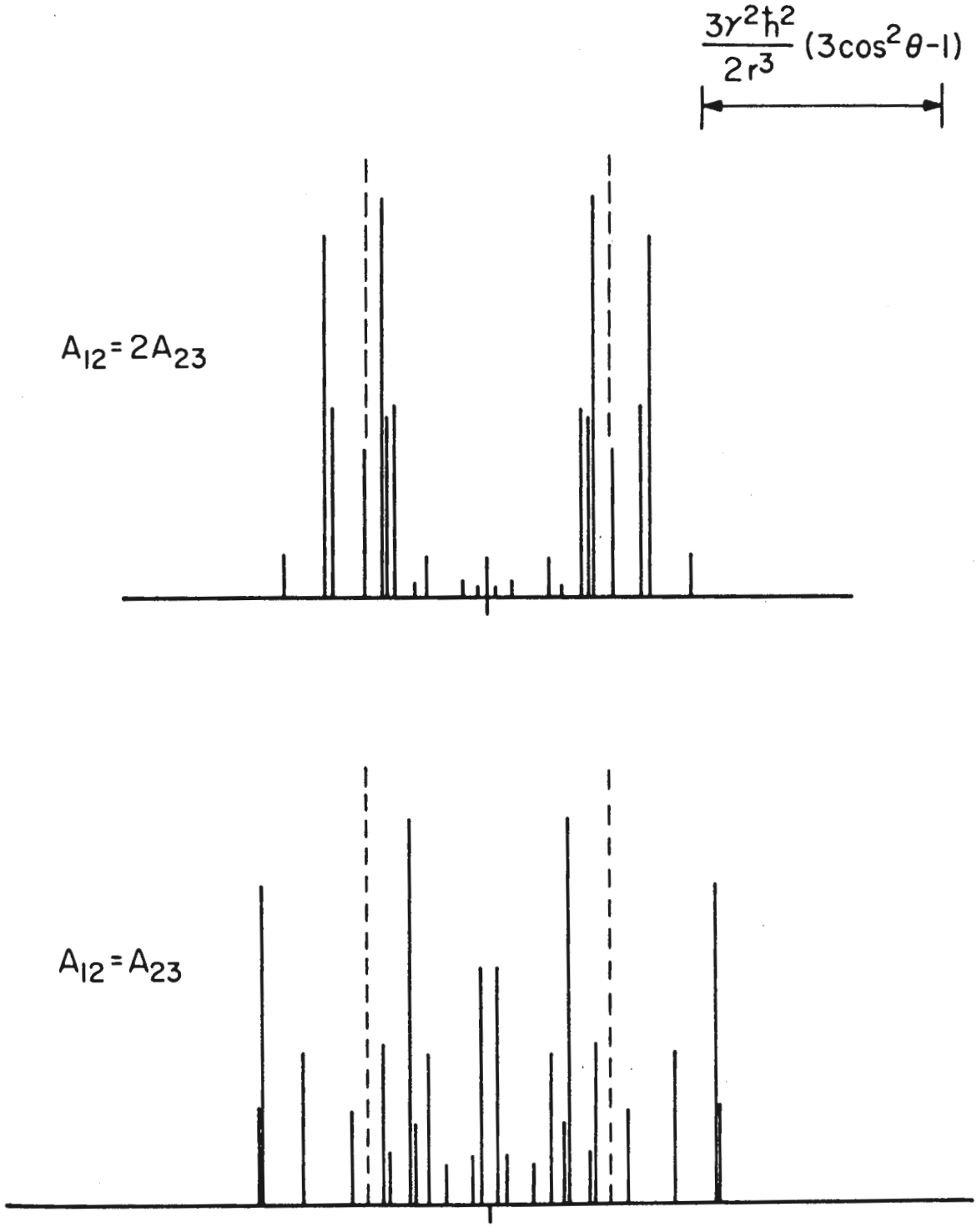

Figure 5

Chapter 3

Dipolar Lineshapes of Spin $\frac{1}{2}$ Nuclei Interacting with a Non-Zeeman Quantized Spin $\frac{3}{2}$ Nucleus

(Chapter 3 is a manuscript by A. T. Nicol and R. W. Vaughan which is being prepared for publication.)

I. Introduction

This paper deals with the dipolar interaction of a quadrupolar nucleus of spin $\frac{3}{2}$ with nearby spin $\frac{1}{2}$ nuclei. The fact that one can observe lineshape changes in the spectra of a spin $\frac{1}{2}$ nucleus produced by the quadrupolar interactions of a second dipolar-coupled nucleus has been discussed previously[1,2], and the purpose of this paper is to calculate explicitly such effects for a spin $\frac{3}{2}$ nucleus on the dipolar lineshape of one or two spin $\frac{1}{2}$ nuclei. A number of heavy metal cluster hydrides have received recent attention in the literature, and solid state NMR in several carbonyl hydrides has been reported[3]. Since the carbonyl ligands isolate the protons in one molecule from those in another, the solid state proton NMR spectra exhibit lineshapes with structural features due to only a small number of coupled spins. In addition to the proton-proton dipolar interaction, however, a number of the heavy metal ions have nuclei with spin and, in most cases, a large quadrupole interaction. Thus, a detailed analysis of such hydride spectra involves not only the calculation of the lineshapes of a small number of interacting spin $\frac{1}{2}$ nuclei, but also the explicit consideration of the effects on such spectra by directly bonded metal nuclei having spin greater than $\frac{1}{2}$ and large quadrupole interaction. The work reported here has been performed with the osmium and ruthenium carbonyl hydrides in mind[3]; however, the results are general for any spin $\frac{3}{2}$ nuclei in a Zeeman perturbed quadrupole state.

The approach used consists, first, of obtaining the correct eigenfunctions for a spin $\frac{3}{2}$ nucleus in a magnetic field where the quadrupolar energy is much greater than the Zeeman energy and the asymmetry parameter

is non-zero. For a spin $\frac{3}{2}$ nucleus Dean[4] provided eigenfunctions for the case of zero asymmetry parameter (η) and also obtained eigenvalues for the case of non-zero asymmetry parameter. We carried the problem further since we needed the eigenfunctions for the case of $\eta \neq 0$ in order to calculate heteronuclear dipole-dipole energies for a case where the spin $\frac{3}{2}$ nucleus is at a site of low symmetry. We then coupled the eigenfunctions with those for a single spin $\frac{1}{2}$ particle and, subsequently, for a spin pair. Using these eigenfunctions, we obtained an expression for the spin $\frac{1}{2}$ pair energies in a Zeeman field of the form:

$$h\omega_{(-1,0)} = \gamma_I h H_o + \frac{3}{4}\frac{\gamma_I^2 h^2}{r_{II}^3}(1-3\cos^2\delta) \pm \frac{\gamma_I \gamma_S}{r_{IS}^3} f(\eta,\theta,\phi,\theta',\phi',\theta'',\phi'') \quad (1)$$

$$h\omega_{(0,1)} = \gamma_I h H_o - \frac{3}{4}\frac{\gamma_I^2 h^2}{r_{II}^3}(1-3\cos^2\delta) \pm \frac{\gamma_I \gamma_S}{r_{IS}^3} f(\eta,\theta,\phi,\theta',\phi',\theta'',\phi'') \quad (2)$$

where δ = the angle the spin $\frac{1}{2}$ internuclear vector makes with the field

γ_I = spin $\frac{1}{2}$ gyromagnetic ratios

γ_S = other nucleus gyromagnetic rations (spin $\frac{3}{2}$)

r_{II} = internuclear distance for spin $\frac{1}{2}$ nuclei

r_{IS} = distance between spin $\frac{1}{2}$ nucleus and spin $\frac{3}{2}$ nucleus

θ,ϕ specify field direction in principal axis system of field gradient tensor

$\theta'\phi'$ specify orientation of first spin $\frac{1}{2}$ nucleus in principal axis system of field gradient tensor

$\theta''\phi''$ specify orientation of second spin $\frac{1}{2}$ nucleus in principal axis system of field gradient tensor

η = the asymmetry parameter .

The following two sections describe the derivation of equations (1) and (2). First (section II), the eigenfunction for a spin $\frac{3}{2}$ nucleus for which $H_Q >> H_z$ and $\eta \neq 0$ are obtained. Then (Section III) the dipole-dipole energies between the spin $\frac{3}{2}$ nucleus and spin $\frac{1}{2}$ nuclei are obtained.

II. Eigenfunctions for a Nucleus of Spin $\frac{3}{2}$

A. Matrix Elements of the Quadrupolar Hamiltonian

Cohen and Reif[5] tabulated the matrix elements of the quadrupolar Hamiltonian

$$\begin{aligned}\langle m'|H_Q|m\rangle = A\langle m'|(3I_Z^2 - \underset{\sim}{I}^2)\, V_0 + (I_+I_Z + I_ZI_+)\, V_{-1} \\ + (I_-I_Z + I_ZI_-)\, V_1 + I_+^2V_{-2} + I_-^2V_2|m\rangle\end{aligned} \tag{3}$$

where

$$A = \frac{eQ}{4I(2I - 1)} \tag{4}$$

and where

$$\begin{aligned}V_0 &= V_{ZZ} \\ V_{\pm1} &= V_{XZ} \pm iV_{YZ} \\ V_{\pm2} &= \tfrac{1}{2}(V_{XX} - V_{YY}) \pm iV_{XY}\end{aligned} \tag{5}$$

Q is the quadrupole moment, e the charge on the nucleus, and I the spin of the nucleus. V_{ij} is an element of the electric field gradient tensor.

Since the field gradient tensor is a symmetric second-rank tensor of zero trace, it has, in general, five independent elements. However, if we transform to the principal axis system of the electric field gradient tensor, x, y, z, the expressions (5) become:

$$\begin{aligned}V_0 &= V_{zz} \\ V_{\pm1} &= 0 \\ V_{\pm2} &= \tfrac{1}{2}(V_{xx} - V_{yy})\end{aligned} \tag{6}$$

By convention, we define two new parameters q and η such that

$$eq = V_{zz} \tag{7}$$

$$\eta = (V_{xx} - V_{yy})/V_{zz} \tag{8}$$

and η is called the asymmetry parameter. The principal axis system is usually chosen such that

$$|V_{zz}| \geq |V_{yy}| \geq |V_{xx}| \tag{9}$$

whence

$$0 \leq \eta \leq 1 \tag{10}$$

We cannot use this convention in our development, and in a more general choice of the orientation of the principal axis system we have

$$-\infty \leq \eta \leq \infty \tag{11}$$

In the principal axis system of the field gradient tensor, and using (6), (7), and (8) along with the properties of raising and lowering operators, (3) yields

$$\langle m|H_Q|m\rangle = Aeq \left[3m^2 - I\ (I + 1)\right] \tag{12}$$

$$\langle m\pm2|H_Q|m\rangle = \frac{Aeq\eta}{2} \left[(I \mp m)(I \mp m-1)(I \pm m+1)(I \pm m+2)\right]^{\frac{1}{2}} \tag{13}$$

The case to be considered here is that for spin $\frac{3}{2}$, for which (12) and (13) specialize to

$$\langle m|H_Q|m\rangle = Aeq \left[3m^2 - 15/4\right] \tag{14}$$

$$\langle m\pm2|H_Q|m\rangle = \frac{Aeq\eta}{2}\left[\left(\frac{3}{2}\mp m\right)\left(\frac{1}{2}\mp m\right)\left(\frac{5}{2}\pm m\right)\left(\frac{7}{2}\pm m\right)\right]^{\frac{1}{2}} \qquad (15)$$

B. Eigenvalues and Eigenfunctions for the Spin $\frac{3}{2}$ System with Large Quadrupolar Interaction and Small Zeeman Interaction

We wish to obtain the eigenfunctions for the case where $\eta \neq 0$ and there is a small Zeeman perturbation present. In order to do this, we will build up from simpler cases which have been discussed thoroughly by Dean[4] and by Das and Hahn[6]. The early development of this section parallels parts of Das and Hahn and, where convenient, uses the same notation. This method of building up insures that one never has to solve a larger than 2 x 2 determinant. Table 1 outlines the development and also summarizes the results we will obtain, and Figure 1 illustrates the results schematically.

1. $\eta = 0, \quad H_z = 0$

We start with the $|I,m\rangle$ eigenfunctions of $\underset{\sim}{I}^2$ and I_z, which for a spin $\frac{3}{2}$ will be designated by $|\frac{3}{2}\rangle$, $|-\frac{3}{2}\rangle$, $|\frac{1}{2}\rangle$, $|-\frac{1}{2}\rangle$ from which, using (14) and (15) we obtain the well-known quadrupolar energies for this case[6].

$$\langle\tfrac{3}{2}|H_Q|\tfrac{3}{2}\rangle = \langle-\tfrac{3}{2}|H_Q|-\tfrac{3}{2}\rangle = 3Aeq \qquad (16)$$

$$\langle\tfrac{1}{2}|H_Q|\tfrac{1}{2}\rangle = \langle-\tfrac{1}{2}|H_Q|-\tfrac{1}{2}\rangle = -3Aeq \qquad (17)$$

There are two doubly degenerate levels separated by $6Aeq = e^2aQ/2$. Note that the definition of "A" used here is that of Cohen and Reif[5] and not that of Das and Hahn[6]. However, we simplify intermediate

calculations by defining

$$a = 3Aeq \tag{18}$$

2. $\underline{\eta \neq 0,\ H_z = 0}$

Again starting with the basis states $|\frac{3}{2}\rangle$, $|\frac{1}{2}\rangle$, $|-\frac{1}{2}\rangle$, $|-\frac{3}{2}\rangle$ we obtain the same results from (14), namely equations (16) and (17); however, now (15) yields the following non-zero matrix elements:

$$\begin{aligned}
&\langle\tfrac{3}{2}|H_Q|-\tfrac{1}{2}\rangle = 2A\sqrt{3}\ V_2 \\
&\langle-\tfrac{3}{2}|H_Q|\tfrac{1}{2}\rangle = 2A\sqrt{3}\ V_2 \\
&\langle\tfrac{1}{2}|H_Q|-\tfrac{3}{2}\rangle = 2A\sqrt{3}\ V_2 \\
&\langle-\tfrac{1}{2}|H_Q|\tfrac{3}{2}\rangle = 2A\sqrt{3}\ V_2
\end{aligned} \tag{19}$$

Each of the matrix elements of (19) can be expressed in terms of $\frac{\sqrt{3}}{3}a\eta$ by using equations (6),(7), and (18). Table 2 shows the 4 x 4 matrix to be solved in order to obtain the eigenfunctions for this case. The conveniently block diagonal matrix of Table 2 yields two identical secular equations leading to the eigenvalues for the case of finite asymmetry parameter but no Zeeman perturbation:

$$\lambda = \pm a\,(1 + \eta^2/3)^{\frac{1}{2}} \tag{20}$$

To obtain the eigenfunctions we use an orthonormal form for solution for 2 x 2 symmetric real matrices. We obtain

$$\psi_a = \cos\beta|\tfrac{3}{2}\rangle + \sin\beta|-\tfrac{1}{2}\rangle = A_{3/2}$$

$$\psi_b = -\sin\beta|\tfrac{3}{2}\rangle + \cos\beta|-\tfrac{1}{2}\rangle = B_{-1/2} \qquad (21)$$

$$\psi_c = \cos\beta|-\tfrac{3}{2}\rangle + \sin\beta|\tfrac{1}{2}\rangle = B_{-3/2}$$

$$\psi_d = -\sin\beta|-\tfrac{3}{2}\rangle + \cos\beta|\tfrac{1}{2}\rangle = A_{1/2}$$

where

$$\tan 2\beta = \frac{\sqrt{3}\,\eta}{3} \qquad (22)$$

and A_m, B_m are the notations of Das and Hahn[6] for these states. The subscript indicates what state is obtained in the absence of an asymmetry parameter. Dean[4] has written (21) in a slightly different, but entirely equivalent, form.

Algebraic manipulations yield

$$\cos\beta = \frac{1}{\sqrt{2}}\left\{\frac{1 + (1 + \eta^2/3)^{1/2}}{(1 + \eta^2/3)^{1/2}}\right\}^{1/2}$$

$$\sin\beta = \frac{1}{\sqrt{2}}\left\{\frac{(1 + \eta^2/3)^{1/2} - 1}{(1 + \eta^2/3)^{1/2}}\right\}^{1/2} \qquad (23)$$

clearly revealing the η dependency of (21). Note that for $\eta \to 0$ we get $\cos\beta = 1$, $\sin\beta = 0$, and for $\eta \to \pm\infty$, we get $\cos\beta = \sin\beta = \frac{1}{\sqrt{2}}$.

3. $\underline{\eta = 0,\ H_z \ll H_Q}$

Consider the Hamiltonian

$$\mathcal{H} = \frac{e^2qQ}{4I(2I-1)}\ (3I_z^2 - \underset{\sim}{I}^2) - \gamma\hbar H_o I_{z'} \tag{24}$$

Here the quadrupolar Hamiltonian with zero asymmetry parameter is written in the principal axis frame of the field gradient tensor, but the Zeeman part of the Hamiltonian is written in the Zeeman frame. As it will be convenient to work in the principal axis frame of the field gradient tensor, the Zeeman term is rewritten in that frame, giving

$$-\gamma\hbar H_o I_{z'} = -\gamma\hbar H_o\ (I_z \cos\theta + I_x \sin\theta \cos\phi + I_y \sin\theta \sin\phi) \tag{25}$$

and is treated as a perturbation on the quadrupolar interaction ($\mathcal{H}_z \ll \mathcal{H}_Q$). Considering the basis states $|\frac{3}{2}\rangle$, $|-\frac{3}{2}\rangle$, $|\frac{1}{2}\rangle$, $|-\frac{1}{2}\rangle$ and the perturbation Hamiltonian (25), we see that only the $I_z \cos\theta$ term of (25) produces a first-order energy shift. However, since the $\pm\frac{1}{2}$ states are degenerate under the quadrupolar Hamiltonian, it is necessary to apply degenerate perturbation theory in that case. Thus, the states $|+\frac{3}{2}\rangle$ and $|-\frac{3}{2}\rangle$ are split so that they have energies

$$E_{\pm m} = \frac{a}{3}\left[3m^2 - I(I+1)\right] \mp \gamma\hbar H_o\, m \cos\theta \tag{26}$$

or, explicitly,

$$E_{\pm 3/2} = a \mp \frac{3}{2}\gamma\hbar H_o \cos\theta \tag{27}$$

For the states $|\frac{1}{2}\rangle$, $|-\frac{1}{2}\rangle$ the matrix of the Hamiltonian $\mathcal{H}_Q + \mathcal{H}_z$ is given in Table 3. The off-diagonal elements were obtained using the properties of raising and lowering operators. Note that this matrix is Hermitian rather than real symmetric in contrast with the case for non-zero asymmetry parameter and no Zeeman interaction. If we choose $\phi = 0$,

the matrix becomes real symmetric and we obtain the eigenfunctions of Das and Hahn[6]. This is an oversimplification since we want to be able to calculate expectation values of I_x and I_y for the spin $\frac{3}{2}$ nucleus. To do this, we would like to have the magnetic field at an arbitrary orientation in the frame of the electric field gradient tensor rather than along one particular axis. Dean[4] gives such a more general case and we will give still another.

The secular equation which is obtained from Table 3 has the solution

$$\lambda_{\pm} = \frac{a}{3}\left[\frac{3}{4} - I(I+1)\right] \mp \frac{\gamma\hbar H_0}{2}\cos\theta\,(1 + (I+\tfrac{1}{2})^2\tan^2\theta)^{\frac{1}{2}} \qquad (28)$$

which, for $I = \frac{3}{2}$, becomes

$$\lambda_{\pm} = -a \mp \frac{\gamma\hbar H_0}{2}\cos\theta\,(1 + 4\tan^2\theta)^{\frac{1}{2}} \qquad (29)$$

The eigenvectors can be written in the form

$$\begin{aligned}\psi_+ &= e^{-i\phi}\cos\theta'|\tfrac{1}{2}\rangle + \sin\theta'|-\tfrac{1}{2}\rangle \\ \psi_- &= \cos\theta'|-\tfrac{1}{2}\rangle - e^{-i\phi}\sin\theta'|\tfrac{1}{2}\rangle\end{aligned} \qquad (30)$$

where

$$\tan 2\theta' = +(I+\tfrac{1}{2})\tan\theta \qquad (31)$$

The wavefunctions (30) differ in form from those of Dan and Hahn[6], and the phase factor chosen here differs from that of Dean[4], but either ours or Dean's can be shown to be correct. It is not, at first, obvious that one requires phase factors (both Abragam[7] and Das and Hahn[6] omit a phase factor) since we are considering a case of axially symmetric field gradient. It would appear that the ϕ dependence

of H_0 in the principal axis system of the field gradient tensor could be chosen arbitrarily. However, if one wishes to calculate the expectation values $\langle I_x \rangle$ and $\langle I_y \rangle$, as we ultimately will, neglecting the phase factor leads to confusion. Omitting the phase factor amounts to choosing the field orientation along x, and calculation of $\langle I_x \rangle$ and $\langle I_y \rangle$ then leads to static terms in the expectation value for I_x but not I_y. Although this may be reasonable physically since we cannot choose in an axially symmetric case where x or y should be located, it gives the artificial appearance that x and y are distinguishable. Therefore, we choose to be more general.

Equation (31), which will provide the coefficients in (30) in terms of θ, is obtained from the simple requirement that

$$\langle \psi_+ | H_Q + H_z | \psi_- \rangle = 0 \tag{32}$$

If we expand (32) using (30), we obtain

$$0 = \langle \psi_+ | H_Q + H_z | \psi_- \rangle = e^{+i\phi} \cos^2\theta' \langle \tfrac{1}{2} | H_Q | -\tfrac{1}{2} \rangle - e^{-i\phi} \sin^2\theta' \langle -\tfrac{1}{2} | H_Q | \tfrac{1}{2} \rangle$$
$$+ \sin\theta' \cos\theta' \left(\langle -\tfrac{1}{2} | H_Q | -\tfrac{1}{2} \rangle - \langle \tfrac{1}{2} | H_Q | \tfrac{1}{2} \rangle \right)$$

or from Table 2

$$0 = (\cos^2\theta' - \sin^2\theta')(-\gamma\hbar H_0(\tfrac{1}{2}))(I + \tfrac{1}{2}) \sin\theta + \sin\theta' \cos\theta' \left(\gamma\hbar H_0 \cos\theta \right)$$

or

$$(I + \tfrac{1}{2}) \cos 2\theta' \sin\theta = \sin 2\theta' \cos\theta$$

which gives (31). The results given in (30) and (31) can be shown to reduce to those of Das and Hahn if we choose $\alpha = \frac{\pi}{2} - \theta$ and let $\phi = 0$.

The results for the axially symmetric case can be used as a check on the general case which we will discuss in detail.

If one lets

$$f = \left\{1 + (I + \tfrac{1}{2}) \tan^2\theta\right\}^{\frac{1}{2}} \tag{33}$$

algebraic and trigonometric manipulation yield

$$\tan\Theta' = \left(\frac{f - 1}{f + 1}\right)^{\frac{1}{2}} \tag{34}$$

which is a well-known result[4].

4. $\underline{\eta \neq 0}$, $H_z \ll H_Q$

So far, we have discussed results for a special case of the spin $\frac{3}{2}$ problem. Now we will consider the most general case and obtain the eigenfunctions needed for calculating expectation values of I_x, I_y, and I_z.

Consider the Hamiltonian

$$H = H_Q + H_z \tag{35}$$

where

$$H_Q = \frac{e^2qQ}{4I(2I - 1)}\left\{(3I_z^2 - \underset{\sim}{I}^2) + \tfrac{1}{2}\eta(I_+^2 + I_-^2)\right\} \tag{36}$$

is the quadrupolar Hamiltonian, and where

$$H_z = -\gamma\hbar H_o\left[I_x \sin\theta\cos\phi + I_y \sin\theta \sin\phi + I_z \cos\theta\right] \tag{37}$$

is the Zeeman Hamiltonian. Both Hamiltonians are written in the frame of the principal axis systems of the field gradient tensor. We use as a basis set the eigenfunctions of H_Q given by (21) which, for convenience

of notation, are rewritten as

$$\begin{aligned} A_{3/2} &= x_1|\tfrac{3}{2}\rangle + y_1|-\tfrac{1}{2}\rangle \\ B_{-3/2} &= x_1|-\tfrac{3}{2}\rangle + y_1|\tfrac{1}{2}\rangle \\ A_{1/2} &= x_2|-\tfrac{3}{2}\rangle + y_2|\tfrac{1}{2}\rangle \\ B_{-1/2} &= x_2|\tfrac{3}{2}\rangle + y_2|-\tfrac{1}{2}\rangle \end{aligned} \tag{38}$$

where clearly

$$\begin{aligned} x_1 &= \cos\beta = y_2 \\ y_1 &= \sin\beta = -x_2 \end{aligned} \tag{39}$$

These coefficients are given in terms of η by (23). Since the functions (38) represent two sets of doubly degenerate states under $H_Q(\eta \neq 0)$, we expect that the addition of the Zeeman perturbation will result in two 2 x 2 secular determinants. To write them down we require matrix elements of the type

$$\langle A_{3/2}|H_z|A_{3/2}\rangle = (x_1\langle\tfrac{3}{2}| + y_1\langle-\tfrac{1}{2}|)\, H_z\, (x_1|\tfrac{3}{2}\rangle + y_1|-\tfrac{1}{2}\rangle) \tag{40}$$

Inspection of (37) shows that only states $|m\rangle$ where $\Delta m = 0, \pm 1$ are connected by H_z. For matrix elements of the type $\langle A_m|H_z|A_m\rangle$ and $\langle B_m|H_z|B_m\rangle$ we obtain

$$\begin{aligned} \langle A_{3/2}|H_z|A_{3/2}\rangle &= -\gamma\hbar H_0 \cos\theta \left[\tfrac{3}{2}x_1^2 - \tfrac{1}{2}y_1^2\right] = -\langle B_{-3/2}|H_z|B_{-3/2}\rangle \\ \langle A_{1/2}|H_z|A_{1/2}\rangle &= -\gamma\hbar H_0 \cos\theta \left[-\tfrac{3}{2}x_2^2 + \tfrac{1}{2}y_2^2\right] = -\langle B_{-1/2}|H_z|B_{-1/2}\rangle \end{aligned} \tag{41}$$

Similarly, equations (38) and (37) yield

$$\begin{aligned} \langle A_{3/2}|H_z|B_{-3/2}\rangle &= -\gamma\hbar H_0 \sin\theta \left\{ x_1 y_1 \sqrt{3}\ e^{-i\phi} + y_1^2 e^{i\phi} \right\} \\ &= (\langle B_{-3/2}|H_z|A_{3/2}\rangle)^* \\ \langle A_{1/2}|H_z|B_{-1/2}\rangle &= \langle B_{-1/2}|H_z|A_{1/2}\rangle^* \\ &= -\gamma\hbar H_0 \sin\theta \left[\sqrt{3}\ x_2 y_2 e^{i\phi} + y_2^2 e^{-i\phi} \right] \end{aligned} \tag{42}$$

Recalling that under the pure quadrupolar Hamiltonian the eigenvalues for $A_{3/2}$ and $B_{3/2}$ were $+ a(1 + \eta^2/3)^{\frac{1}{2}}$ and for $A_{1/2}$ and $B_{-1/2}$ were $-a(1 + \eta^2/3)^{\frac{1}{2}}$, these results, given in Table 4, show that the general form of both secular equations is

$$\begin{vmatrix} A-B-\lambda_{\pm} & C \\ C^* & A+B-\lambda_{\pm} \end{vmatrix} = 0 \tag{43}$$

which has the solution

$$\lambda_{\pm} = A \pm (B^2 + |C|^2)^{\frac{1}{2}} \tag{44}$$

For the $A_{3/2}$, $B_{-3/2}$ case we now have, using Table 4

$$E_{\pm 3/2} = a(1 + \frac{\eta^2}{3})^{\frac{1}{2}} \pm \gamma\hbar H_0 \left((\tfrac{3}{2} x_1^2 - \tfrac{1}{2} y_1^2)^2 \cos^2\theta + \sin^2\theta \left[3 x_1^2 y_1^2 + y_1^4 + 2\sqrt{3}\, x_1 y_1^3 \cos 2\phi \right] \right)^{\frac{1}{2}} \tag{45}$$

Similarly, for the $A_{1/2}$, $B_{1/2}$ case, Table 4 yields

$$E_{\pm 1/2} = -a(1 + \frac{\eta^2}{3})^{\frac{1}{2}} \pm \gamma\hbar H_0 \left((-\tfrac{3}{2} x_2^2 + \tfrac{1}{2} y_2^2)^2 \cos^2\theta + \sin^2\theta \left[3 x_2^2 y_2^2 + 2\sqrt{3}\, x_2 y_2^3 \cos 2\phi \right] \right)^{\frac{1}{2}} \tag{46}$$

These eigenvalues are in agreement with published results[4,6] although there appears to be an omission of the exponent in the last terms of equation (46) in the paper of Das and Hahn[6]. We now obtain the analytic eigenfunctions for this case which have not been published.

The secular equation of the general form (43) can be solved to yield a new basis set of the form

$$\psi_A = C' \sin\alpha|A'> + \cos\alpha|B'>$$
$$\psi_B = C' \cos\alpha|A'> - \sin\alpha|B'> \tag{47}$$

where C' is a complex coefficient. The requirement $<\psi_A|H|\psi_B> = 0$ provides the required parametrization. Specifically,

$$<\psi_A|H|\psi_B> + (C'^{*} \sin\alpha <A'| + \cos<B'|)H\,(C' \cos\alpha|A'> - \sin\alpha|B'>)$$

or

$$<\psi_A|H|\psi_B> = C'^{*}C' \sin\alpha\cos\alpha <A'|H|A'> + C' \cos^2\alpha <B'|H|A'>$$
$$- C'^{*} \sin^2\alpha <A'|H|B'> - \sin\alpha\cos\alpha <B'|H|B'> \tag{48}$$

With the aid of Table 4 and letting $A' = A_{3/2}$, $B' = B_{-3/2}$, we find (49)

$$\begin{aligned}<\psi_A|H|\psi_B> = \sin\alpha\cos\alpha &\left\{C'^{*} C' \left[-\gamma\hbar H_o \cos\theta \left(\tfrac{3}{2} x_1^2 - \tfrac{1}{2} y_1^2\right)\right]\right. \\ &\left. -\gamma\hbar H_o \cos\theta \left[\tfrac{3}{2} x_1^2 - \tfrac{1}{2} y_1^2\right]\right\} \\ &+ C' \cos^2\alpha \left\{-\gamma\hbar H_o \sin\theta \left[x_1 y_1 \sqrt{3}\ e^{i\phi} + y_1^2 e^{i\phi}\right]\right\} \\ &-C^{*} \sin^2\alpha \left\{-\gamma\hbar H_o \sin\theta \left[x_1 y_1 \sqrt{3}\, e^{i\phi} + y_1^2 e^{i\phi}\right]\right\}\end{aligned} \tag{50}$$

Requiring that (50) be real and that equations (47) are normalized, we obtain

$$C' = \frac{x_1 y_1 \sqrt{3}\, e^{-i\phi} + y_1^2 e^{i\phi}}{\left[3x_1^2 y_1^2 + y_1^4 + 2\sqrt{3}\, x_1 y_1^3 \cos 2\phi\right]^{\frac{1}{2}}} \tag{51}$$

Substitution of (51) into (50) yields

$$-(2 \sin\alpha \cos\alpha)(\cos\theta)\left[\frac{3}{2} x_1^2 - \frac{1}{2} y_1^2\right] = (\cos^2\alpha - \sin^2\alpha) \sin\theta \left(3x_1^2 y_1^2 + y_1^4 + 2\sqrt{3}\, x_1 y_1^3 \cos 2\phi\right)^{\frac{1}{2}}$$

or

$$\tan 2\alpha = \frac{-\tan\theta \left[3x_1^2 y_1^2 + y_1^4 + 2\sqrt{3}\, x_1 y_1^3 \cos 2\phi\right]^{\frac{1}{2}}}{\left[\frac{3}{2} x_1^2 - \frac{1}{1} y_1^2\right]} \tag{52}$$

Equations (52), (51), and (47) specify the general form of the ψ_A and ψ_B wavefunctions in terms of θ, ϕ, and the asymmetry parameter, η. Specifically, as we will show, these are the wavefunctions which specialize to $|\frac{3}{2}>$ and $|-\frac{3}{2}>$ in the case $\eta = 0$.

In an entirely analogous manner we can write down the wavefunctions for the states that specialize to ψ_+, ψ_- if $\eta = 0$ by making use of Table 4, normalization conditions, and the requirement that the new representation be diagonal.

We get

$$\begin{aligned} \psi_C &= C'' \sin\gamma |A_{1/2}> + \cos\gamma |B_{-1/2}> \\ \psi_D &= C'' \cos\gamma |A_{1/2}> - \sin\gamma |B_{-1/2}> \end{aligned} \tag{53}$$

where

$$C'' = \frac{x_2\, y_2 \sqrt{3}\, e^{i\phi} + y_2^2\, e^{-i\phi}}{\left[3\, x_2^2\, y_2^2 + y_2^4 + 2\sqrt{3}\, x_2\, y_2^3 \cos^2\phi\right]^{\frac{1}{2}}} \tag{54}$$

and where

$$\tan 2\gamma = \frac{-\tan\theta\left[3\, x_2^2\, y_2^2 + y_2^4 + 2\sqrt{3}\, x_2\, y_2^3 \cos\phi\right]^{\frac{1}{2}}}{\left[-\frac{3}{2} x_2^2 + \frac{1}{2} y_2^2\right]} \tag{55}$$

We note that equations (55) and (52) for the general case are analogous to equation (31) obtained in the axially symmetric case. We can define

$$g = (1 + \tan^2 2\alpha)^{\frac{1}{2}} \tag{56}$$

where $\tan 2\alpha$ is given by (52) and

$$h = (1 + \tan^2 2\gamma)^{\frac{1}{2}} \tag{57}$$

where $\tan 2\gamma$ is given by (55).

These definition lead to expressions analogous to the result in the axially symmetric case.

$$\tan\alpha = \left\{\frac{g + 1}{g - 1}\right\}^{\frac{1}{2}} \tag{58}$$

$$\tan\gamma = \left\{\frac{h + 1}{h - 1}\right\}^{\frac{1}{2}} \tag{59}$$

The wavefunctions for the general case of a spin $\frac{3}{2}$ nucleus where the quadrupolar interaction is much larger than the Zeeman interaction and where the asymmetry parameter is not zero are given by equations (53) and (47). All the parametrization required to express these functions in

terms of η, the asymmetry parameter, and θ and ϕ, the angles that the Zeeman field makes within the principal axis system of the field gradient tensor are contained in equations (55), (54), (52), (51), (38), (39) and (23). We will now tabulate and discuss the eigenfunctions and eigenvalues.

C. Discussion of the Eigenfunctions and Eigenvalues

1. Summary of Eigenfunctions

In order to understand the relationships among the eigenfunctions for the various cases, we start with the most generalized. Equations (53) and (47) are rewritten with slightly different notation.

$$\begin{aligned}
\psi_{I}^{3/2} &= C' \sin\alpha|A_{3/2}> + \cos\alpha|B_{-3/2}> \\
\psi_{II}^{-3/2} &= C' \cos\alpha|A_{3/2}> - \sin\alpha|B_{-3/2}> \\
\psi_{III}^{+1/2} &= C'' \sin\gamma|A_{1/2}> + \cos\gamma|B_{-1/2}> \\
\psi_{IV}^{-1/2} &= C'' \cos\gamma|A_{1/2}> - \sin\gamma|B_{-1/2}>
\end{aligned} \tag{60}$$

The superscripts indicate what states are obtained in the limit that $\eta = 0$ or the Zeeman field is removed.

Also, recall equations (38) and (39)

$$\begin{aligned}
A_{3/2} &= x_1|\tfrac{3}{2}> + y_1|-\tfrac{1}{2}> \\
B_{-3/2} &= x_1|-\tfrac{3}{2}> + y_1|\tfrac{1}{2}> \\
A_{1/2} &= x_2|-\tfrac{3}{2}> + y_2|\tfrac{1}{2}> \\
B_{-1/2} &= x_2|\tfrac{3}{2}> + y_2|-\tfrac{1}{2}>
\end{aligned} \tag{38}$$

$$x_1 = y_1 = \cos\beta$$

$$y_1 = \sin\beta \tag{39}$$

$$x_2 = -\sin\beta$$

where $\sin\beta$ and $\cos\beta$ are given by (23)

$$\cos\beta = \frac{1}{\sqrt{2}}\left\{\frac{1 + (1 + \eta^2/3)^{\frac{1}{2}}}{(1 + \eta^2/3)^{\frac{1}{2}}}\right\}^{\frac{1}{2}}$$

$$\sin\beta = \frac{1}{\sqrt{2}}\left\{\frac{(1 + \eta^2/3)^{\frac{1}{2}} - 1}{(a + \eta^2/3)^{\frac{1}{2}}}\right\}^{\frac{1}{2}} \tag{23}$$

and where C' and C" are given by (51) and (54).

$$C' = \frac{x_1 y_1 \sqrt{3}\, e^{-i\phi} + y_1^2\, e^{i\phi}}{\left(3\, x_1^2\, y_1^2 + y_1^4 + 2\sqrt{3}\, x_1\, y_1^3 \cos 2\phi\right)^{\frac{1}{2}}} \tag{51}$$

$$C'' = \frac{x_2 y_2 \sqrt{3}\, e^{i\phi} + y_2^2\, e^{-i\phi}}{\left(3\, x_2^2\, y_2^2 + y_2^4 + 2\sqrt{3}\, x_2\, y_2^3 \cos 2\phi\right)^{\frac{1}{2}}} \tag{54}$$

2. Specialization for Zero Asymmetry Parameter

We see from (23) that when $\eta = 0$ we get $\sin\beta = 0$, $\cos\beta = 1$ so that equations (38) reduce to the eigenfunctions labeled by the subscript. For example, $A_{3/2} \to |\frac{3}{2}\rangle$. Also note that for $\eta = 0$, we obtain $C' \to e^{-i\phi}$ and $C'' \to e^{-i\phi}$. Thus, the general case when specialized to $\eta = 0$ results in

$$\psi_I^{3/2} = e^{-i\phi} \sin\alpha |\tfrac{3}{2}\rangle + \cos\alpha |-\tfrac{3}{2}\rangle$$

$$\psi_{II}^{-3/2} = e^{-i\phi} \cos\alpha |\tfrac{3}{2}\rangle - \sin\alpha |-\tfrac{3}{2}\rangle$$

$$\psi_{III}^{+1/2} = e^{-i\phi} \sin\gamma |\tfrac{1}{2}\rangle + \cos\gamma |-\tfrac{1}{2}\rangle \tag{61}$$

$$\psi_{IV}^{-1/2} = e^{-i\phi}\cos\gamma|\tfrac{1}{2}\rangle - \sin\gamma|-\tfrac{1}{2}\rangle$$

However, equations (52), (54), and (58) readily show for $\eta = 0$ and θ finite that

$$\begin{aligned} \psi_{I}^{3/2} &= e^{-i\phi}|\tfrac{3}{2}\rangle \\ \psi_{II}^{-3/2} &= -\,|-\tfrac{3}{2}\rangle \end{aligned} \tag{62}$$

An analogous discussion of equations (55), (57), and (59) shows that $\psi_{III}^{1/2}$ and $\psi_{IV}^{-1/2}$ reduce to ψ^{+} and ψ^{-}. Specifically, equation (55) shows $\tan 2\gamma = -2\tan\theta$ for $\eta = 0$ and equation (57) then provides

$$h = (1 + 4\tan^2\theta)^{\frac{1}{2}} \tag{63}$$

where

$$\tan\gamma = \left(\frac{h+1}{h-1}\right)^{\frac{1}{2}} \tag{64}$$

Expressions ψ_{III} and ψ_{IV} of (61) then become

$$\begin{aligned} \psi_{III}^{1/2} &= e^{-i\phi}\sin\gamma|\tfrac{1}{2}\rangle + \cos\gamma|-\tfrac{1}{2}\rangle = \psi_{+} \\ \psi_{IV}^{-1/2} &= e^{-i\phi}\cos\gamma|\tfrac{1}{2}\rangle - \sin\gamma|-\tfrac{1}{2}\rangle = \psi_{-} \end{aligned} \tag{65}$$

if we make the identification $\gamma = \frac{\pi}{2} - \theta$. (This provides $\tan 2\theta' = -\tan 2\gamma$ as well as $\sin\gamma = \cos\theta'$, $\tan\theta = \mathrm{ctn}\gamma$, et cetera for direct comparison with (30) and (31). Further, note that the relationships $\sin\gamma = (\frac{h+1}{2})^{\frac{1}{2}}$ and $\cos\gamma = (\frac{h-1}{2})^{\frac{1}{2}}$ provide that $\psi_{III}^{1/2}$ and $\psi_{IV}^{-1/2}$ specialize to $|\frac{1}{2}\rangle$ and $|-\frac{1}{2}\rangle$, respectively, when $h = 1$, i.e., when the θ dependence is removed.

3. Specialization for No Zeeman Interaction

If we remove the θ and ϕ dependence from the general results, we see that equations (51) and (54) provide $C' = C'' = 1$. Furthermore, the elimination of θ dependence results in $\sin\gamma = 1$, $\cos\gamma = 0$ through the relationships (59), (57), and (55). Thus, $\psi_{III}^{1/2}$ reduces to $A_{1/2}$ and $\psi_{IV}^{-1/2}$ reduces to $-B_{-1/2}$. By an analogous argument $\psi_{I}^{3/2}$ reduces to $A_{3/2}$ and $\psi_{II}^{-3/2}$ to $-B_{-3/2}$.

4. Comments on Eigenfunctions

In Table 5 we illustrate how the wave functions are related in the various degrees of perturbation. We do not worry about the overall change of sign of a wavefunction in any case. The phase factor in $\psi_A \rightarrow e^{i\phi}|\frac{3}{2}\rangle$ is rather artificial since, in first order, the $|\frac{3}{2}\rangle$ states are not perturbed by a magnetic field. More importantly, it does not affect the results of our calculations. We will be calculating expectation values $\langle I_x\rangle$, $\langle I_y\rangle$ and $\langle I_z\rangle$ using the wavefunctions we have obtained. When doing that we obtain both static and oscillatory terms. We neglect the latter. Because $|\frac{3}{2}\rangle$ and $|-\frac{3}{2}\rangle$ are not connected by I_x, I_y, or I_z, the effects of a phase factor on one of those states are irrelevant (i.e., $\langle\frac{3}{2}|I_z|\frac{3}{2}\rangle \equiv \langle e^{-i\phi}\frac{3}{2}|I_z|e^{i\phi}\frac{3}{2}\rangle$ but $\langle e^{i\phi}\frac{3}{2}|I_x|-\frac{3}{2}\rangle = 0$). This is to be contrasted with the result for the states ψ_+ and ψ_- which are linear combinations of $|\frac{1}{2}\rangle$ and $|-\frac{1}{2}\rangle$ and so are connected by all three operators. The inclusion of phase factors in that case does not change the static term in $\langle I_z\rangle$; however, it results in a factor of $\cos\phi$ in the static part of $\langle I_x\rangle$ and a factor of $\sin\phi$ in the static part of $\langle I_y\rangle$ thus reflecting the orientation of the field within the frame of the field gradient tensor.

D. The Calculation of Expectation Values of I_x, I_y, I_z for a Spin in Zeeman Perturbed Quadrupolar States

If m denotes eigenfunctions of the time-independent Schrodinger equation, we can write the general time-dependent solution as

$$\Psi(\tau) = \sum_m C_m e^{-iE_m\tau/\hbar} |m\rangle \tag{66}$$

Then the expectation values of the angular momentum operators will be given by

$$\langle I_i(\tau)\rangle = \sum_{mm'} C_{m'}^* C_m \langle m'|I_i|m\rangle e^{i(E_{m'}-E_m)\tau/\hbar} \tag{67}$$

where i = x, y, z.

For our case, using equations (60), we write down the explicit form

$$\langle I_i(\tau)\rangle = C_I^* C_I \langle\psi_I|I_i|\psi_I\rangle + C_I^* C_{II}\langle\psi_I|I_i|\psi_{II}\rangle e^{i(E_I-E_{II})\tau/\hbar}$$

$$+ C_I^* C_{III}\langle\psi_I|I_i|\psi_{III}\rangle e^{i(E_I-E_{III})\tau/\hbar} + C_I^* C_{IV}\langle\psi_I|I_i|\psi_{IV}\rangle e^{i(E_I-E_{IV})\tau/\hbar}$$

$$+ C_{II}^* C_I\langle\psi_{II}|I_i|\psi_I\rangle e^{i(E_{II}-E_I)\tau/\hbar} + C_{II}^* C_{II}\langle\psi_{II}|I_i|\psi_{II}\rangle$$

$$+ C_{II}^* C_{III}\langle\psi_{II}|I_i|\psi_{III}\rangle e^{i(E_{II}-E_{III})\tau/\hbar} + C_{II}^* C_{IV}\langle\psi_{II}|I_i|\psi_{IV}\rangle e^{i(E_{II}-E_{IV})\tau/\hbar}$$

$$+ C_{III}^* C_I \langle\psi_{III}|I_i|\psi_I\rangle e^{i(E_{III}-E_I)\tau/\hbar} + C_{III}^* C_{II}\langle\psi_{III}|I_i|\psi_{II}\rangle e^{i(E_{III}-E_{II})\tau/\hbar}$$

$$+ C^*_{III}C_{III}\langle\psi_{III}|I_i|\psi_{III}\rangle + C^*_{III}C_{IV}\langle\psi_{III}|I_i|\psi_{IV}\rangle\, e^{i(E_{III}-E_{IV})\tau/\hbar}$$

$$+ C^*_{IV}C_{I}\langle\psi_{IV}|I_i|\psi_{I}\rangle\, e^{i(E_{IV}-E_{I})\tau/\hbar} + C^*_{IV}C_{II}\langle\psi_{IV}|I_i|\psi_{II}\rangle\, e^{i(E_{IV}-E_{II})\tau/\hbar}$$

$$+ C^*_{IV}C_{III}\langle\psi_{IV}|I_i|\psi_{III}\rangle\, e^{i(E_{IV}-E_{III})\tau/\hbar} + C^*_{IV}C_{IV}\langle\psi_{IV}|I_i|\psi_{IV}\rangle \qquad (68)$$

Figure 1, a schematic representation of the evolution of the energy levels and wavefunctions, clearly shows the forms of the exponentials. We have

$$\begin{aligned} E_{II} - E_I &= 2\lambda_{3/2} \\ E_{IV} - E_{III} &= 2\lambda_{1/2} \end{aligned} \qquad (69)$$

and

$$\begin{aligned} E_I - E_{IV} &= 2a(1 + \eta^2/3)^{\frac{1}{2}} - \lambda_{3/2} - \lambda_{1/2} \\ E_{II} - E_{III} &= 2a(1 + \eta^2/3)^{\frac{1}{2}} + \lambda_{3/2} + \lambda_{1/2} \\ E_I - E_{III} &= 2a(1 + \eta^2/e)^{\frac{1}{2}} - \lambda_{3/2} + \lambda_{1/2} \\ E_{II} - E_{IV} &= 2a(1 + \eta^2/3)^{\frac{1}{2}} + \lambda_{3/2} - \lambda_{1/2} \end{aligned} \qquad (70)$$

Equations (69) and (70) show that most of the terms of (68) will be oscillating at a rate which effectively eliminates the terms in $\langle I_i(\tau)\rangle$ containing exponentials of (70). The remaining terms in $\langle I_i(\tau)\rangle$ are the static terms and the terms arising from exponential of $2\lambda_{3/2}$ and $2\lambda_{1/2}$ given in (69). One might ask whether the terms in $\lambda_{3/2}$ and $\lambda_{1/2}$ should be considered since they can be zero for certain orientations of the

field. However, when the Zeeman splittings are zero, the wavefunctions revert to the pure quadrupole limit. In that limit explicit calculation shows no static terms in $\langle I_x \rangle$, $\langle I_y \rangle$, or $\langle I_z \rangle$. Restricting (68) to static terms only results in

$$\begin{aligned}\langle I_i(\tau) \rangle = {} & C_I^* C_I \langle \psi_I | I_i | \psi_I \rangle \\ & + C_{II}^* C_{II} \langle \psi_{II} | I_i | \psi_{II} \rangle + C_{III}^* C_{III} \langle \psi_{III} | I_i | \psi_{III} \rangle \\ & + C_{IV}^* C_{IV} \langle \psi_{IV} | I_i | \psi_{IV} \rangle \end{aligned} \tag{71}$$

Equations (60) yield

$$\begin{aligned}\langle \psi_I | I_z | \psi_I \rangle &= -\langle \psi_{II} | I_z | \psi_{II} \rangle \\ &= (\sin^2\alpha - \cos^2\alpha)\left(\tfrac{3}{2} x_1^2 - \tfrac{1}{2} y_1^2\right)\end{aligned} \tag{72}$$

$$\begin{aligned}\langle \psi_{III} | I_z | \psi_{III} \rangle &= -\langle \psi_{IV} | I_z | \psi_{IV} \rangle \\ &= (\cos^2\gamma - \sin^2\gamma)\left(\tfrac{3}{2} x_2^2 - \tfrac{1}{2} y_2^2\right)\end{aligned} \tag{73}$$

Letting

$$C_I = a_1 e^{i\alpha_1}, \quad C_{II} = a_2 e^{i\alpha_2}, \quad C_{III} = a_3 e^{i\alpha_3}, \quad C_{IV} = a_4 e^{i\alpha_4} \tag{74}$$

then (71), (72), and (73) yield, for the static expectation value of $\langle I_z(\tau) \rangle$

$$\begin{aligned}\langle I_z \rangle = {} & \left(\tfrac{3}{2} x_1^2 - \tfrac{1}{2} y_1^2\right)(\sin^2\alpha - \cos^2\alpha)(a_1^2 - a_2^2) \\ & + \left(\tfrac{1}{2} y_2^2 - \tfrac{3}{2} x_2^2\right)(\sin^2\gamma - \cos^2\gamma)(a_3^2 - a_4^2)\end{aligned} \tag{75}$$

In the same way, we calculate the static terms in $\langle I_x \rangle$ and $\langle I_y \rangle$.

$$\langle I_x \rangle = (a_1^2 - a_2^2)\left[\frac{2\cos\phi(\sqrt{3}\,x_1y_1 + y_1^2)^2 \sin\alpha\cos\alpha}{\left(3\,x_1^2\,y_1^2 + y_1^4 + 2\sqrt{3}\,x_1\,y_2^3\cos 2\phi\right)^{\frac{1}{2}}}\right] + (a_3^2 - a_4^2)\left[\frac{2\cos\phi(\sqrt{3}\,x_2\,y_2 + y_2^2)^2 \sin\gamma\cos\gamma}{\left(3\,x_2^2\,y_2^2 + y_2^4 + 2\sqrt{3}\,x_2\,y_2^3\cos 2\phi\right)^{\frac{1}{2}}}\right] \tag{76}$$

$$\langle I_y \rangle = (a_1^2 - a_2^2)\left[\frac{2\sin\phi(\sqrt{3}\,x_1\,y_1 - y_1^2)^2 \sin\alpha\cos\alpha}{\left(3\,x_1^2\,y_1^2 + y_1^4 + 2\sqrt{3}\,x_1y_1^3\cos 2\phi\right)^{\frac{1}{2}}}\right] + (a_3^2 - a_4^2)\left[\frac{2\sin\phi(\sqrt{3}\,x_2y_2 - y_2^2)^2 \sin\gamma\cos\gamma}{\left(3\,x_2^2\,y_2^2 + y_2^4 + 2\sqrt{3}\,x_2\,y_2^3\cos 2\phi\right)^{\frac{1}{2}}}\right] \tag{77}$$

These results will be employed in the calculation of the dipole-dipole energies between a spin $\frac{3}{2}$ nucleus and spin $\frac{1}{2}$ nuclei.

III. Dipolar Interactions

A. The Interaction of a Spin $\frac{3}{2}$ Nucleus with a Single Spin $\frac{1}{2}$ Nucleus

So far, we have been discussing the wavefunctions for a spin $\frac{3}{2}$ nucleus for which the quadrupolar energy is much larger than the Zeeman energy. We now turn our attention to the question of what effect such a quadrupolar nucleus will have on a spin $\frac{1}{2}$ nucleus in a Zeeman field. The Hamiltonian for the spin $\frac{1}{2}$ nucleus can be written as

$$H = H_Z + H_D \tag{78}$$

where

$$H_Z = -\underset{\sim}{\mu} \cdot \underset{\sim}{B} = -\gamma \underset{\sim}{H} \cdot \underset{\sim}{I} \tag{79}$$

and

$$H_D = \frac{\underset{\sim}{\mu}_1 \cdot \underset{\sim}{\mu}_2}{r^2} - \frac{3(\underset{\sim}{\mu}_1 \cdot \underset{\sim}{r})\,(\underset{\sim}{\mu}_2 \cdot \underset{\sim}{r})}{r^5} \tag{80}$$

where H_Z is the Zeeman Hamiltonian and H_D is the dipolar Hamiltonian.

Suppose we have eigenfunctions for the spin $\frac{3}{2}$ nucleus. Calling those eigenfunctions ψ_i ($i = 1,2,3,4$) and treating the dipolar interaction as a perturbation, we can form product functions with the states α and β of the spin $\frac{1}{2}$ nucleus such that $\Psi_i^{\alpha} = \alpha\psi$; and $\Psi_i^{\beta} = \beta\psi_i$. Using these, we calculate the energy of transition for the spin $\frac{1}{2}$ particle

$$E_\beta - E_\alpha = \langle\Psi_i^{\beta}|H|\Psi_i^{\beta}\rangle - \langle\Psi_i^{\alpha}|H|\Psi_i^{\alpha}\rangle \tag{81}$$

Since energies are expectation values of the Hamiltonian, they are independent of the frame of reference chosen for the calculation, and we can choose different frames for components of (81). Terms in (81) look like

$$\begin{aligned}\langle\Psi^{\beta}|H|\Psi^{\beta}\rangle &= \langle\beta\psi_i|H_Z + H_D|\beta\psi_i\rangle \\ &= \langle\beta\Psi_i|-\gamma\hbar H_0 I_z|\beta\psi_i\rangle + \langle\beta\psi_i|H_D|\beta\psi_i\rangle \\ &= +\tfrac{1}{2}\gamma\hbar H_0\langle\psi_i|\psi_i\rangle + \langle\beta\psi_i|H_D|\beta\psi_i\rangle\end{aligned} \tag{82}$$

The first term in (82) arises because I_z is operating only on states of the spin $\frac{1}{2}$ nucleus, henceforth denoted as nucleus I. The spin $\frac{3}{2}$ nucleus will be denoted by S. Inspection of (81) and (82) shows that

$$E_\beta = E_\alpha = \gamma\hbar H_o + \left[\langle\psi_i^\beta|\mathcal{H}_D|\psi_i^\beta\rangle - \langle\psi_i^\alpha|\mathcal{H}_D|\psi_i^\alpha\rangle\right] \tag{83}$$

where we have evaluated the first term in the Zeeman frame, and we will calculate the matrix elements of $\mathcal{H}_D$ in the principal axis system (PAS) of the field gradient tensor. We already have the ψ_i's written in that frame. From Figure 2 we would then have

$$\underset{\sim}{H}_o = H_o\left[\hat{\underset{\sim}{x}}\sin\theta\cos\phi + \hat{\underset{\sim}{y}}\sin\theta\sin\phi + \hat{\underset{\sim}{z}}\cos\theta\right] \tag{84}$$

and since only the component of the I spin along the Zeeman field is effective, we need only the I_z component transformed to the PAS frame

$$\underset{\sim}{I} = I_z\left[\hat{\underset{\sim}{x}}\sin\theta\cos\phi + \hat{\underset{\sim}{y}}\sin\theta\sin\phi + \hat{\underset{\sim}{z}}\cos\theta\right] \tag{85}$$

Equation (80) can be expressed as

$$\mathcal{H}_D = \frac{\gamma_I\gamma_S\hbar^2}{r_{IS}^3}\left\{\underset{\sim}{I}\cdot\underset{\sim}{S} - \frac{3(\underset{\sim}{I}\cdot\underset{\sim}{r})(\underset{\sim}{S}\cdot\underset{\sim}{r})}{r^2}\right\} \tag{86}$$

and matrix elements of the type $\langle\psi_i^\beta|\mathcal{H}_D|\psi_i^\beta\rangle$ can be written as

$$E_{D_i}^\beta = \frac{\gamma_I\gamma_S\hbar^2}{r_{IS}^3}\langle\psi_i\beta|\underset{\sim}{I}\cdot\underset{\sim}{S} - \frac{3(\underset{\sim}{I}\cdot\underset{\sim}{r})(\underset{\sim}{S}\cdot\underset{\sim}{r})}{r^3}|\psi_i\beta\rangle \tag{87}$$

where now ψ_i and β are understood to be in the same frame and in whatever frame we choose for $\mathcal{H}_D$.

Making use of the coordinate system shown in Figure 2, we can write

$$\begin{aligned} E_{D_i}^\alpha &= \frac{\gamma_I\gamma_S\hbar^2}{r_{IS}^3}\langle\psi_i\alpha|\underset{\sim}{I}\cdot\underset{\sim}{S} - \frac{3(\underset{\sim}{I}\cdot\underset{\sim}{r})(\underset{\sim}{S}\cdot\underset{\sim}{r})}{r^2}|\psi_i\alpha\rangle \\ &= \frac{\gamma_I\gamma_S\hbar^2}{r_{IS}^3}\left\{\langle\alpha|\underset{\sim}{I}|\alpha\rangle\cdot\langle\psi_i|\underset{\sim}{S}|\psi_i\rangle - \frac{3\langle\alpha|\underset{\sim}{I}\cdot\underset{\sim}{r}\rangle\langle\psi_i|\underset{\sim}{S}\cdot\underset{\sim}{r}|\psi_i\rangle}{r^2}\right\} \end{aligned} \tag{88}$$

Since the I spin is quantized along the field with eigenvalues $\pm\frac{1}{2}$ we get

$$E^{\alpha}_{D_i} = \frac{\gamma_I\gamma_S h^2}{r^3_{IS}}\left\{\frac{1}{2}\,(\hat{x}\sin\theta\cos\phi + \hat{y}\sin\theta\sin\phi + \hat{z}\cos\theta)\cdot (\langle S_x\rangle_i\,\hat{x} + \langle S_y\rangle_i\,\hat{y} + \langle S_z\rangle_i\,\hat{z}) - \frac{3}{2}\frac{\left[(\hat{x}\sin\theta\cos\phi + \hat{y}\sin\theta\sin\phi + \hat{z}\cos\theta)\cdot r\right]}{r^2}\frac{\left[(\langle S_x\rangle_i\,\hat{x} + \langle S_y\rangle_i\,\hat{y} + \langle S_z\rangle_i\,\hat{z})\cdot r\right]}{r^2}\right\} \tag{89}$$

Making use of $r = |r|\left[\hat{x}\sin\theta'\cos\phi' + \hat{y}\sin\theta'\sin\phi' + \hat{z}\cos\theta'\right]$ (90)

and denoting the angle between H and r by γ we have

$$\cos\gamma = \cos\theta\cos\theta' + \sin\theta\sin\theta'\cos(\phi' - \phi) \tag{91}$$

then (89) becomes

$$E^{\alpha}_{D_i} = \frac{\gamma_I\gamma_S h^2}{r^3}\left(\frac{1}{2}\right)\left\{\langle S_x\rangle_i\sin\theta\cos\phi + \langle S_y\rangle_i\sin\theta\sin\phi + \langle S_z\rangle_i\cos\theta - 3\cos\gamma\left[\langle S_x\rangle_i\sin\theta'\cos\phi' + \langle S_y\rangle_i\sin\theta'\sin\phi' + \langle S_z\rangle_i\cos\theta'\right]\right\} \tag{92}$$

Equation (92) is general for the heteronuclear dipolar energy between a spin $\frac{1}{2}$ nucleus, I, and nucleus of spin greater than $\frac{1}{2}$, S, however written in the principal axis frame of the field gradient tensor. For example, we can see that it reduces to a familar form for the case where the S nucleus is in a pure Zeeman state. Then in the coordinate system which we are using, we would have

$$\langle S_x \rangle_i = m_{S_i} \sin\theta \cos\phi$$

$$\langle S_y \rangle_i = m_{S_i} \sin\theta \sin\phi \tag{93}$$

$$\langle S_z \rangle_i = m_{S_i} \cos\theta$$

and, applying equations (91) and (92), we get

$$E_{D_i}^{\alpha} = \frac{\gamma_I \gamma_S \hbar^2}{r^3} \left(\frac{1}{2}\right) (m_{S_i}) (1 - 3\cos^2\gamma) \tag{94}$$

which is exactly what we expect for a heteronuclear dipolar energy when both nuclei are in Zeeman states. Similarly,

$$E_{D_i}^{\beta} = \frac{\gamma_I \gamma_S \hbar^2}{r^3} \left(-\frac{1}{2}\right) (m_{S_i}) (1 - 3\cos^2\gamma) \tag{95}$$

and we have, from (83), for the case where S is in Zeeman states

$$(E_\beta - E_\alpha)_i = \gamma\hbar H_0 - \frac{\gamma_I \gamma_S \hbar^2}{r_{IS}^3} (1 - 3\cos^2\gamma)\, m_{S_i} \tag{96}$$

Since m_{S_i} has values $-\frac{3}{2}, -\frac{1}{2}, \frac{1}{2}, \frac{3}{2}$, we get the familiar result that the NMR line of a spin $\frac{1}{2}$ nucleus is symmetrically split by the heteronuclear dipolar interaction with a spin $\frac{3}{2}$ nucleus in the limit $H_z >> H_Q$ for the quadrupolar nucleus.

Returning to the case of interest, namely that where $H_Q >> H_z$ for the spin $\frac{3}{2}$ nucleus we write, using (81) and (92)

$$(E_\beta - E_\alpha)_i = \gamma\hbar H_0 + \frac{\gamma_I \gamma_S \hbar^2}{r^3} \Big\{ \langle S_x \rangle_i \sin\theta \cos\phi + \langle S_y \rangle_i \sin\theta \sin\phi$$

$$+ \langle S_z \rangle_i \cos\theta - 3\cos\gamma (\langle S_x \rangle_i \sin\theta' \cos\phi' + \langle S_y \rangle_i \sin\theta' \sin\phi'$$

$$+ \langle S_z \rangle_i \cos\theta') \Big\} \tag{97}$$

Expressions for $\langle S_x \rangle_i$, $\langle S_y \rangle_i$, and $\langle S_z \rangle_i$ for the case $H_Q >> H_z$ were given in the last section. Referring to that section, one sees that

$$\langle S_j \rangle_I = -\langle S_j \rangle_{II}$$
$$\langle S_j \rangle_{III} = -\langle S_j \rangle_{IV} \tag{98}$$

where j = x, y, z. Thus, in the limit $H_Q >> H_z$ for the spin $\frac{3}{2}$ nucleus, it is expected that the heteronuclear dipolar interaction will split the line symmetrically. This is a point of interest since the splitting need not be symmetrical in general[1,2].

B. The Interaction of a Spin $\frac{3}{2}$ Nucleus with an Isolated Spin $\frac{1}{2}$ Pair

The development here parallels that for the previous case, but here we want to consider a spin $\frac{1}{2}$ pair. In the case where the Zeeman energy is much larger than the dipolar energy for a spin $\frac{1}{2}$ pair, the spin-spin dipolar interaction is taken as a perturbation. In that case the eigenfunction of the Hamiltonian for the spin pair can be written in the form

$$|1\rangle = |\alpha\alpha\rangle$$
$$|0\rangle = \frac{1}{\sqrt{2}} \left(|\alpha\beta\rangle + |\beta\alpha\rangle \right) \tag{99}$$
$$|-1\rangle = |\beta\beta\rangle$$

Again, we can form product functions of the type $\Psi_i^{(1)} = \psi_i |1\rangle$ where the ψ_i's are eigenfunctions for the S nucleus. Note that this implicitly assumes that the IS dipolar interaction is small compared to the II dipolar interaction. This will be a good assumption for the

applications considered here where the I spins are strongly interacting protons and the S spin is a nucleus with a small gyromagnetic ratio such as ^{189}Os. Only at special orientations where the angular dependence makes the II dipolar interaction small will this assumption be invalid. The Hamiltonian for the spin pair, written in the Zeeman frame, is

$$H = -\gamma\hbar H_o(I_{z_1} + I_{z_2}) + H_D \tag{100}$$

It is easy to see that

$$\begin{aligned} E_{-1} &= \langle\psi_i^{(-1)}|H|\psi_i^{(-1)}\rangle = \gamma\hbar H_o + \langle\psi_i^{(-1)}|H_D|\psi_i^{(-1)}\rangle \\ E_0 &= \langle\psi_i^{(0)}|H|\psi_i^{(0)}\rangle = 0 + \langle\psi_i^{(0)}|H_D|\psi_i^{(0)}\rangle \\ E_{+1} &= \langle\psi_i^{(1)}|H|\psi_i^{(1)}\rangle = -\gamma\hbar H_o + \langle\psi_i^{(1)}|H_D|\psi_i^{(1)}\rangle \end{aligned} \tag{101}$$

and thus we expect

$$\hbar\omega_{(-1,0)} = E_{-1} - E_0 = \gamma\hbar H_o + \langle\psi_i^{(-1)}|H_D|\psi_i^{(-1)}\rangle - \langle\psi_i^{(0)}|H_D|\psi_i^{(0)}\rangle \tag{102}$$

and

$$\hbar\omega_{(0,1)} = E_0 - E_1 = \gamma\hbar H_o + \langle\psi_i^{(0)}|H_D|\psi_i^{(0)}\rangle - \langle\psi_i^{(1)}|H_D|\psi_i^{(1)}\rangle \tag{103}$$

We need only to calculate the three types of matrix elements of H_D in (102) to characterize our system. To do that H_D must be written in the proper form.

$$H_D = \sum_{i<j} \frac{\underset{\sim}{\mu}_i \cdot \underset{\sim}{\mu}_j}{r_{ij}^2} - 3\frac{(\underset{\sim}{\mu}_i \cdot \underset{\sim}{r}_{ij})(\underset{\sim}{\mu}_j \cdot \underset{\sim}{r}_{ij})}{r_{ij}^5} \tag{104}$$

or, for three nuclei

32

$$H_D = \frac{\underset{\sim}{\mu}_1 \cdot \underset{\sim}{\mu}_2}{r_{12}^2} - \frac{3(\underset{\sim}{\mu}_1 \cdot \underset{\sim}{r}_{12})(\underset{\sim}{\mu}_2 \cdot \underset{\sim}{r}_{12})}{r_{12}^5} + \frac{\underset{\sim}{\mu}_1 \cdot \underset{\sim}{\mu}_3}{r_{13}^2} - \frac{3(\underset{\sim}{\mu}_1 \cdot \underset{\sim}{r}_{13})(\underset{\sim}{\mu}_3 \cdot \underset{\sim}{r}_{13})}{r_{13}^5}$$

$$+ \frac{\underset{\sim}{\mu}_2 \cdot \underset{\sim}{\mu}_3}{r_{23}^2} - \frac{3(\underset{\sim}{\mu}_2 \cdot \underset{\sim}{r}_{23})(\underset{\sim}{\mu}_3 \cdot \underset{\sim}{r}_{23})}{r_{23}^5} \qquad (105)$$

The matrix element of the first term of (105), if we take that to be the like spin term, will yield the familiar result[7] for the dipolar splitting

$$\pm \frac{3}{4} \frac{\gamma^2 \hbar^2}{r_{12}^3} (1 - 3\cos^2\delta)$$

where δ is the angle the internuclear vector r_{12} makes with the field. Specifically,

$$\langle \psi_i^{(-1)} | H_D | \psi_i^{(-1)} \rangle = \langle \psi_i^{(1)} | H_D | \psi_i^{(1)} \rangle$$

$$= \langle \psi_i \alpha\alpha | H_D | \psi \alpha\alpha \rangle$$

$$= \langle \psi_i | \psi_i \rangle \langle \alpha\alpha | H_D | \alpha\alpha \rangle$$

$$= \frac{\gamma_I^2 \hbar^2}{4\gamma_{II}^3} (1 - 3\cos^2\delta) \qquad (106)$$

and

$$\langle \psi_i^{(0)} | H_D | \psi_i^{(0)} \rangle = \frac{\gamma_I^2 \hbar^2}{2r_{II}^3} (1 - 3\cos^2\delta) \; . \qquad (107)$$

It remains to calculate the dipolar matrix elements for the unlike spins. By analogy to (88) we may write

$$\langle\psi_i^{(n)}|H_{D_{13}}|\psi_i^{(n)}\rangle = \frac{\gamma_I\gamma_S\hbar^2}{r_{I_1S}^3}\left\{\langle n|\underset{\sim}{I}_1|n\rangle\cdot\langle\psi_i|\underset{\sim}{S}|\psi_i\rangle - \frac{3\langle n|\underset{\sim}{I}_1\cdot\underset{\sim}{r}_{13}|n\rangle\langle\psi_i|\underset{\sim}{S}\cdot\underset{\sim}{r}_{13}|\psi_i\rangle}{r_{I_1S}^2}\right\} \tag{108}$$

and

$$\langle\psi_i^{(n)}|H_{D_{23}}|\psi_i^{(n)}\rangle = \frac{\gamma_I\gamma_S\hbar^2}{r_{I_2S}^3}\left\{\langle n|\underset{\sim}{I}_2|n\rangle\cdot\langle\psi_i|\underset{\sim}{S}|\psi_i\rangle - \frac{3\langle n|\underset{\sim}{I}_2\cdot\underset{\sim}{r}_{23}|n\rangle\langle\psi_i|\underset{\sim}{S}\cdot\underset{\sim}{r}_{23}|\psi_i\rangle}{r_{I_2S}^2}\right\} \tag{109}$$

where (n) denotes 1, 0, -1. Now since a dipolar interaction term like (108) connects only two nuclei at a time, we have the result that factors like

$$\langle 1|I_z|1\rangle = \langle\alpha\,\alpha\,|I_{z_1}|\alpha\,\alpha\rangle = \tfrac{1}{2}$$

Similarly, $\langle +1|I_{z_2}|+1\rangle = \frac{1}{2}$ while (110)

$$\langle -1|I_{z_1}|-1\rangle = \langle -1|I_{z_2}|-1\rangle = -\tfrac{1}{2}$$

and $\langle 0|I_{z_1}|0\rangle = \frac{1}{2}\langle\alpha\,\beta + \beta\,\alpha\,|I_z|\alpha\beta + \beta\alpha\rangle = 0 = \langle 0|I_{z_2}|0\rangle$

Referring to Figure 3 for clarification of notation and recalling the results of the single proton case contained in equation (92), we obtain

$$\langle\psi_i^{(-1)}|H_{D_{13}}|\psi_i^{(-1)}\rangle = \frac{\gamma_I\gamma_S\hbar^2}{r_{13}^3}\left(-\frac{1}{2}\right)\left\{\langle S_x\rangle_i\sin\theta\cos\phi + \langle S_y\rangle_i\sin\theta\sin\theta + \langle S_z\rangle_i\cos\theta\right.$$

(equation continues)

$$- 3\cos\gamma\,(\langle S_x\rangle_i \sin\theta' \sin\phi' + \langle S_y\rangle_i \sin\theta' \cos\phi' + \langle S_z\rangle_i \cos\theta')\Big\} \tag{111}$$

where $\cos\gamma = \sin\theta \cos\phi \sin\theta' \cos\phi' + \sin\theta \sin\phi \sin\theta' \sin\phi' + \cos\theta \cos\theta'$ (112)

Similarly,

$$\langle\psi_i^{(-1)}|\mathcal{H}_{D_{23}}|\psi_i^{(-1)}\rangle = \frac{\gamma_I\gamma_S h^2}{r_{23}^3}\left(-\frac{1}{2}\right)\Big\{\langle S_x\rangle_i \sin\theta \cos\phi + \langle S_y\rangle_i \sin\theta \sin\phi + \langle S_z\rangle_i \cos\theta - 3\cos^2\gamma'\,(\langle S_x\rangle_i \sin\theta'' \cos\phi'' + \langle S_y\rangle_i \sin\theta'' \sin\phi'' + \langle S_z\rangle_i \cos\theta'')\Big\} \tag{113}$$

where

$$\cos\gamma' = \sin\theta \cos\phi \sin\theta'' \cos\phi'' + \sin\theta \sin\phi \sin\theta'' \sin\phi'' + \cos\theta \cos\theta'' \tag{114}$$

Similarly, we can obtain

$$\langle\psi_i^{(1)}|\mathcal{H}_{D_{13}}|\psi_i^{(1)}\rangle = -\langle\psi_i^{(-1)}|\mathcal{H}_{D_{13}}|\psi_i^{(-1)}\rangle \tag{115}$$

and

$$\langle\psi_i^{(1)}|\mathcal{H}_{D_{23}}|\psi_i^{(1)}\rangle = -\langle\psi_i^{(-1)}|\mathcal{H}_{D_{23}}|\psi_i^{(-1)}\rangle\,. \tag{116}$$

Also

$$\langle\psi_i^{(0)}|\mathcal{H}_{D_{13}}|\psi_i^{(0)}\rangle = \langle\psi_i^{(0)}|\mathcal{H}_{D_{23}}|\psi_i^{(0)}\rangle = 0 \tag{117}$$

Now using equation (106), (107), and (111) - (117), we can write the general expressions for the resonant energies given by (102) and (103). Collecting terms we get

$$\hbar\omega^{i}_{(-1,0)} = \gamma\hbar H_0 + \frac{3}{4}\frac{\gamma_I^2\hbar^2}{r_{II}^3}(1 - 3\cos^2\delta) + \frac{\gamma_I\gamma_S\hbar^2}{r_1^3}\Big\{\langle S_x\rangle_i \Big[\sin\theta\cos\phi - \frac{3}{2}(\cos\gamma\sin\theta'\cos\phi' + \cos\gamma'\sin\theta''\cos\phi'')\Big] + \langle S_y\rangle_i \Big[\sin\theta\sin\phi - \frac{3}{2}(\cos\gamma\sin\theta'\sin\phi' + \cos\gamma'\sin\theta''\sin\phi'')\Big] + \langle S_z\rangle_i \Big[\cos\theta - \frac{3}{2}(\cos\gamma\cos\theta' + \cos\gamma'\cos\theta'')\Big]\Big\} \quad (118)$$

Calling the last term in (118) $f^i(\eta, \theta, \phi, \theta', \phi', \theta'', \phi'')$ we write

$$\hbar\omega^{i}_{(0,1)} = \gamma\hbar H_0 - \frac{3}{4}\frac{\gamma_I^2\hbar^2}{r_{II}^3}(1 - 3\cos^2\delta) + f^i(\eta,\theta,\phi,\theta',\phi',\theta'',\phi'') \quad (119)$$

Equations (98) together with (118) and (119) reveal the result for the case where a coupled spin $\frac{1}{2}$ pair is perturbed by a nearby spin $\frac{3}{2}$ nucleus in a Zeeman perturbed quadrupolar state ($H_Q >> H_z$). The spin $\frac{1}{2}$ pair dipolar split lines are symmetrically split by the heteronuclear dipolar interaction. Figure 4 shows a schematic representation of the splitting. Note that this result and the similar result of the last section imply that the effect on the NMR spectra of spin $\frac{1}{2}$ nuclei of the heteronuclear dipolar interaction with a spin $\frac{3}{2}$ nucleus will be a symmetric contribution to the lineshape. This useful result may permit the separation of chemical shift information from heteronuclear dipolar broadening systems where the chemical shift causes an asymmetric lineshape as is often the case.

The results given by equations (118) and (119) are general for any orientation of the spin $\frac{1}{2}$ pair within the principal axis system of the field gradient tensor of the spin $\frac{3}{2}$ nucleus.

References

1. D. L. VanderHart, H. S. Gutowsky, and T. C. Farrar, J. Am. Chem. Soc. 89, 5056 (1967).

2. M. E. Stoll, R. W. Vaughan, R. B. Saillant, and T. Cole, J. Chem. Phys. 61, 2896 (1974).

3. A. T. Nicol and R. W. Vaughan, "Solid State Nuclear Magnetic Resonace Study of Heavy Metal Hydrides," Transition Metal Hydrides, Advances in Chemistry Symposium Series Volume 167, July 1978.

4. C. Dean, Phys. Rev. 96, 1053 (1954).

5. M. H. Cohen and F. Reif, Solid State Physics, Vol. 5, 321-438, F. Seitz and D. Turnbull, ed., Academic Press, New York, 1957.

6. T. P. Das and E. L. Hahn, Solid State Physics, Suppl. 1, F. Seitz and D. Turnbull, ed., Academic Press, New York, 1958.

7. A. Abragam, The Principles of Nuclear Magnetism, Oxford University Press, London, 1961.

TABLE 1

Schematic Representation of the Development of Eigenvalues and Eigenfunctions

	Eigenvalues	Eigenfunction
Case 1 $H_z = 0$ $\eta = 0$	$+ 3Aeq$ $- 3Aeq$	$\|I,m\rangle : \|\frac{3}{2}\rangle \; \|-\frac{3}{2}\rangle$ $\|\frac{1}{2}\rangle \; \|-\frac{1}{2}\rangle$
Case 2 $H_z = 0$ $\eta \neq 0$	$+ 3Aeq\,(1+\frac{\eta^2}{3})^{\frac{1}{2}}$ $- 3Aeq\,(1+\frac{\eta^2}{3})^{\frac{1}{2}}$	$A_{3/2}, B_{-3/2}$ $A_{1/2}, B_{-1/2}$ A's and B's are linear combinations or $\|m\rangle$ and $\|m \pm 2\rangle$
Case 3 $H_z \neq 0$ $\eta = 0$	$E_{\pm 3/2} = 3Aeq \mp \frac{3}{2}\gamma\hbar H_0 \cos\theta$ $E_{\pm 1/2} = -3Aeq \mp \frac{1}{2}\gamma\hbar H_0 f_1(\theta)$	$\|\frac{3}{2}\rangle \; \|-\frac{3}{2}\rangle$ and linear combinations of $\|\frac{1}{2}\rangle$, $\|-\frac{1}{2}\rangle$
Case 4 $H_z \neq 0$ $\eta \neq 0$	$E_{\pm 3/2} = 3Aeq\,(1+\frac{\eta^2}{3})^{\frac{1}{2}} + f_2(\theta,\phi,\eta)$ $E_{\pm 1/2} = -3A_{eq}(1+\frac{\eta^2}{3})^{\frac{1}{2}} + f_3(\theta,\phi,\eta)$	linear combinations of $A_{3/2}, B_{-3/2}$ linear combinations of $A_{1/2}, B_{-1/2}$

TABLE 2

The 4 x 4 Matrix for a Spin $\frac{3}{2}$ System under the Quadrupolar Hamiltonian with Non-zero Asymmetry Parameter. Basis States are Labeled by the m Quantum Number.

	$\lvert\frac{3}{2}\rangle$	$\lvert-\frac{1}{2}\rangle$	$\lvert\frac{1}{2}\rangle$	$\lvert-\frac{3}{2}\rangle$
$\lvert\frac{3}{2}\rangle$	a	$\frac{\sqrt{3}}{3}a\eta$		
$\lvert-\frac{1}{2}\rangle$	$\frac{\sqrt{3}}{3}a\eta$	-a		
$\lvert\frac{1}{2}\rangle$			-a	$\frac{\sqrt{3}}{2}a\eta$
$\lvert-\frac{3}{2}\rangle$			$\frac{\sqrt{3}}{3}a\eta$	a

TABLE 3

The Matrix Elements $\langle m|H_Q+H_z|m'\rangle$ for $m,m' = \pm \frac{1}{2}$. These Matrix Elements Are General for the Case $H_Q >> H_z$, $\eta = 0$ and I = Half Integer. The Orientation of the Magnetic Field within the Principal Axis System of the Field Gradient Tensor is Specified by θ and ϕ.

	$\left\|\frac{1}{2}\right\rangle$	$\left\|-\frac{1}{2}\right\rangle$
$\left\|\frac{1}{2}\right\rangle$	$\frac{a}{3}\left[\frac{3}{4} - I(I+1)\right] - \frac{\gamma\hbar H_0}{2}\cos\theta$	$-(\gamma\hbar H_0)(\frac{1}{2})(I+\frac{1}{2})\left[\sin\theta(\cos\phi - i\sin\phi)\right]$
$\left\|-\frac{1}{2}\right\rangle$	$-\gamma\hbar H_0(\frac{1}{2})(I+\frac{1}{2})\left[\sin\theta(\cos\phi + i\sin\phi)\right]$	$\frac{a}{3}\left[\frac{3}{4} - I(I+1)\right] + \frac{\gamma\hbar H_0}{2}\cos\theta$

TABLE 4

The Matrix Elements for the Most General Case for a Spin $\frac{3}{2}$ Particle under the Hamiltonian $H_Q + H_z$, Where $H_z << H_Q$. Basis States Are Indicated, and Symbols Are Defined in the Text.

	$A_{3/2}$	$B_{-3/2}$
$A_{3/2}$	$a(1+\frac{\eta^2}{3})^{\frac{1}{2}} - \gamma\hbar H_o \cos\theta\left[\frac{3}{2}x_1^2 - \frac{1}{2}y_1^2\right]$	$-\gamma\hbar H_o \sin\theta\left[\sqrt{3}\, x_1 y_1 e^{-i\phi} + y_1^2 e^{i\phi}\right]$
$B_{-3/2}$	$-\gamma\hbar H_o \sin\theta\left[\sqrt{3}\, x_1 y_1 e^{i\phi} + y_1^2 e^{-i\phi}\right]$	$a(1+\frac{\eta^2}{3})^{\frac{1}{2}} + \gamma\hbar H_o \cos\theta\left[\frac{3}{2}x_1^2 - \frac{1}{2}y_1^2\right]$
$A_{1/2}$	$-a(1+\frac{\eta^2}{3})^{\frac{1}{2}} - \gamma\hbar H_o \cos\theta\left[-\frac{3}{2}x_2^2 + \frac{1}{2}y_2^2\right]$	$-\gamma\hbar H_o \sin\theta\,(\sqrt{3}\, x_2 y_2 e^{i\phi} + y_2^2 e^{-i\phi})$
$B_{-1/2}$	$-\gamma\hbar H_o \sin\theta\left[\sqrt{3}\, x_2 y_2 e^{-i\phi} + y_2^2 e^{i\phi}\right]$	$-a(1+\frac{\eta^2}{3})^{\frac{1}{2}} + \gamma\hbar H_o \cos\theta\left[-\frac{3}{2}x_2^2 + \frac{1}{2}y_2^2\right]$

TABLE 5

The Relationship of the Wavefunction under Various Limits of the Perturbation

$\eta \neq 0$ $H_z \neq 0$	$\eta = 0$ $H_z \neq 0$	$\eta \neq 0$ $H_z = 0$	$\eta = 0$ $H_z = 0$
$\psi_A = \psi_I^{3/2}$	$e^{-i\phi}\|\frac{3}{2}\rangle$	$A_{3/2}$	$\|\frac{3}{2}\rangle$
$\psi_B = \psi_{II}^{-3/2}$	$-\|-\frac{3}{2}\rangle$	$-B_{-3/2}$	$-\|-\frac{3}{2}\rangle$
$\psi_C = \psi_{III}^{1/2}$	ψ_+	$A_{1/2}$	$\|\frac{1}{2}\rangle$
$\psi_D = \psi_{IV}^{-1/2}$	ψ_-	$-B_{-1/2}$	$-\|-\frac{1}{2}\rangle$

Figure Captions

Figure 1. Energy level diagram indicating splittings and eigenfucntions for perturbation schemes used.

Figure 2. The principal axis frame coordinate system with orientation of the field and of the spin 3/2 - spin 1/2 internuclear vector specified.

Figure 3. The principal axis frame coordinate system with the orientation of the field and of the spin 3/2 - spin 1/2 internuclear vectors indicated.

Figure 4. The splitting of the spin 1/2 pair triplet levels by a spin 3/2 nucleus in a Zeeman perturbed quadrupolar state.

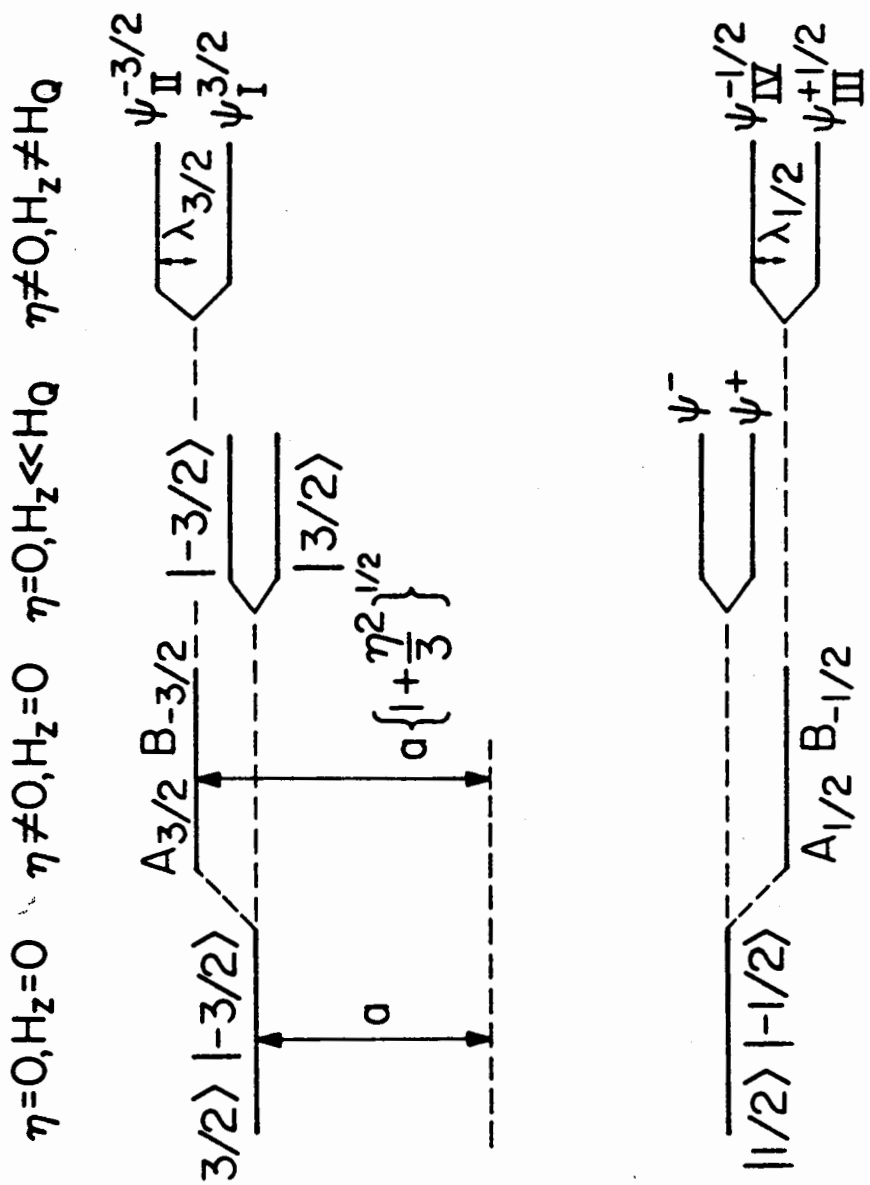
η=0,Hz=0
η≠0,Hz=0
η=0,Hz≪HQ
η≠0,Hz≠HQ
|3/2⟩ |-3/2⟩
A3/2 B-3/2
|-3/2⟩
|3/2⟩
a
a{1+η²/3}^1/2
ψII-3/2
ψI3/2
λ3/2
|1/2⟩ |-1/2⟩
A1/2 B-1/2
ψ-
ψ+
ψIV-1/2
ψIII+1/2
λ1/2

Figure 1

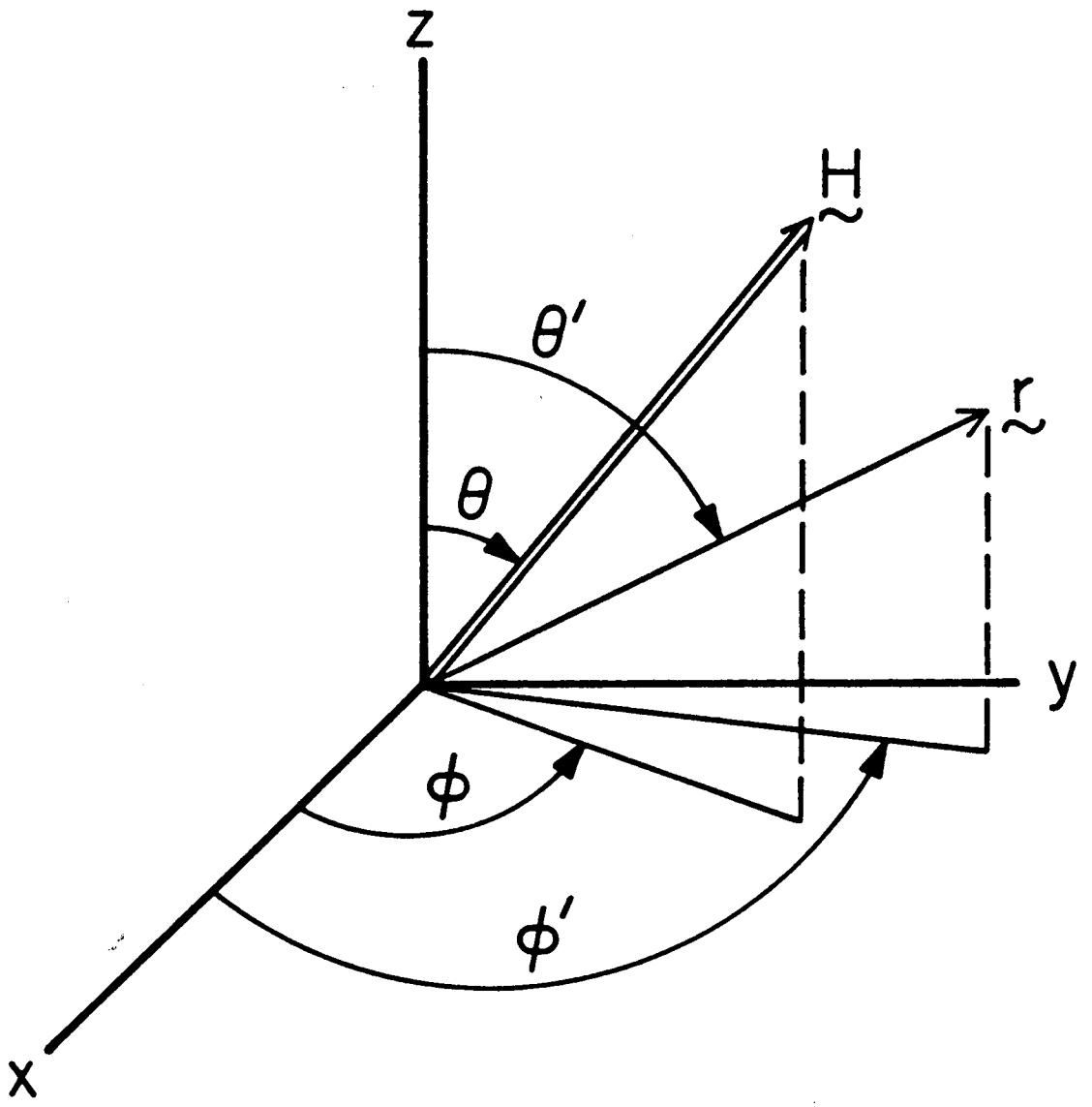

Figure 2

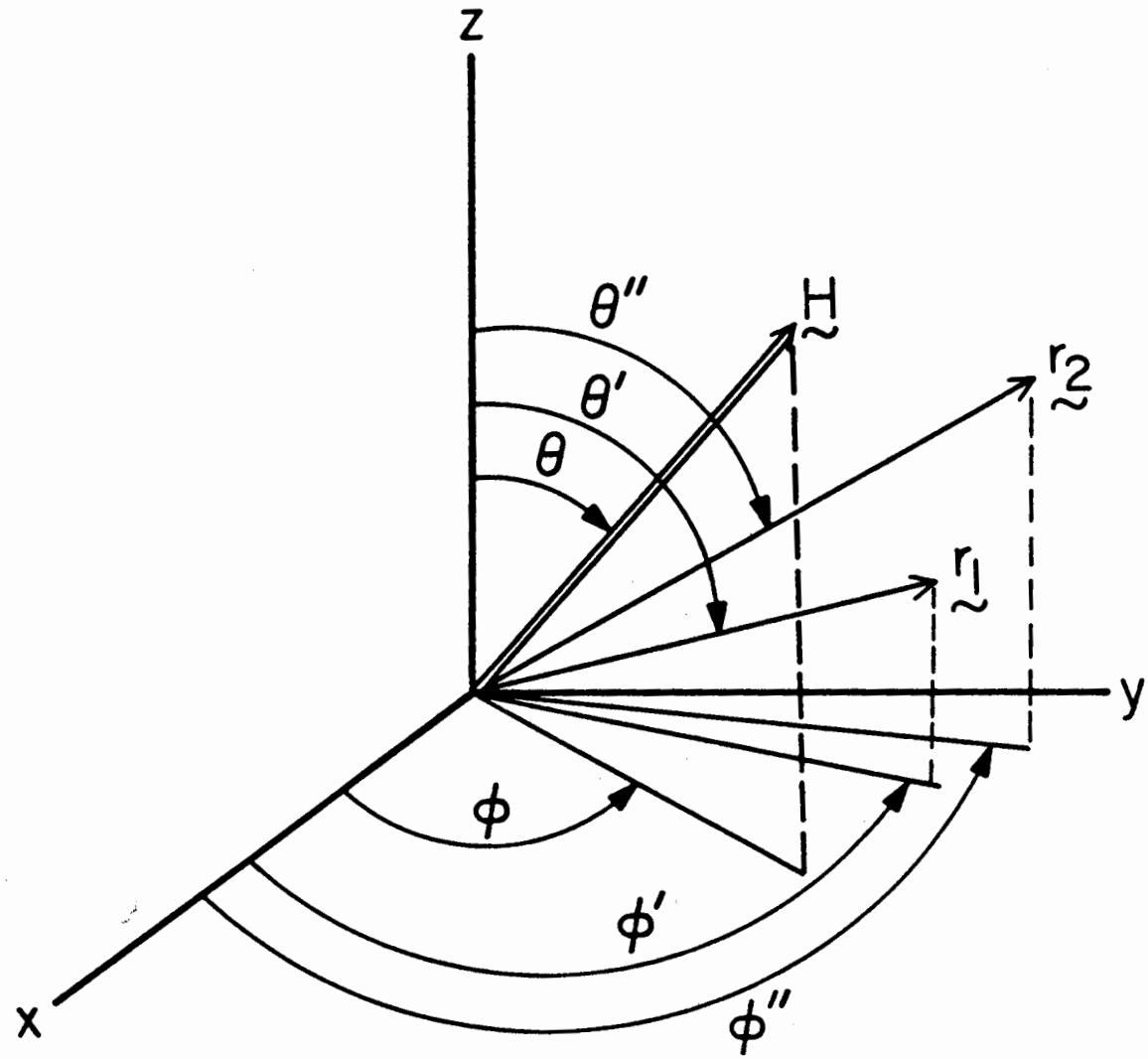

Figure 3

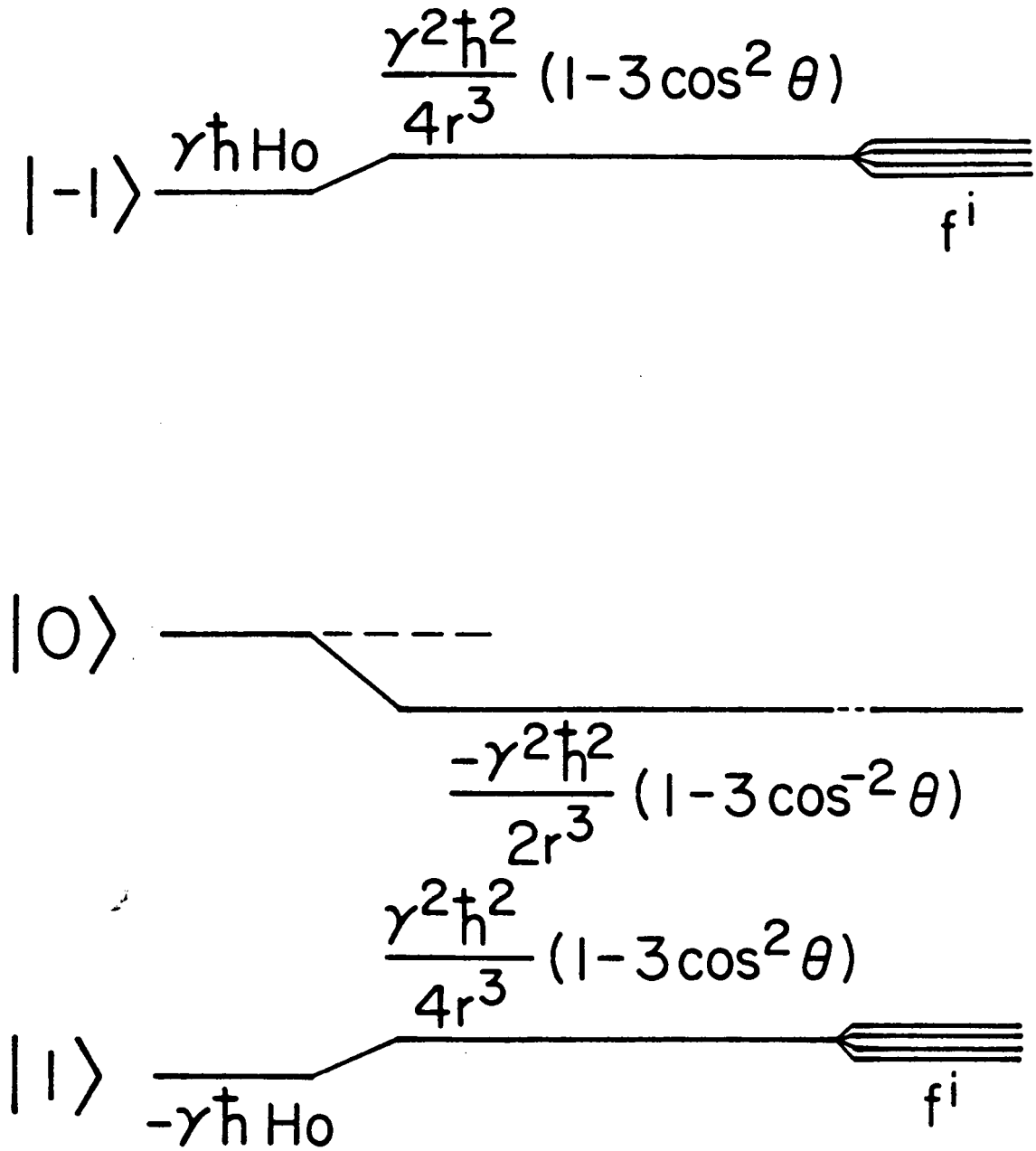
$\frac{\gamma^2\hbar^2}{4r^3}(1-3\cos^2\theta)$
$|-1\rangle$
$\gamma\hbar Ho$
f^i
$|0\rangle$
$\frac{-\gamma^2\hbar^2}{2r^3}(1-3\cos^{-2}\theta)$
$\frac{\gamma^2\hbar^2}{4r^3}(1-3\cos^2\theta)$
$|1\rangle$
$-\gamma\hbar Ho$
f^i

Figure 4

Chapter 4

Proton Dipolar Lineshapes of Metal Cluster Carbonyl Hydrides: A Comparison of Theory and Experiment

(Chapter 4 is part of a manuscript by A. T. Nicol and R. W. Vaughan which is being prepared for publication.)

I. Introduction

This paper discusses the proton NMR lineshapes observed for the compounds $H_2Os_3(CO)_{10}$, $H_4Os_4(CO)_{12}$ and $H_4Ru_4(CO)_{12}$. For these solids it is shown that the experimental results can be explained on the basis of a consideration of a parallogram configuration of dipolar coupled spin 1/2 particles.

Metal cluster hydrides have received attention recently and are of interest from the point of view of understanding catalysis. For example, they can serve as models for dispersed metals on surfaces[2] and the metal cluster compounds are of uniform and definite composition and thus more readily characterizable. Thus, there is interest in determining the structure of such compounds, including the hydrogen locations, and in characterizing the nature of hydrogen motion. Proton NMR can yield both kinds of information. In order to extract such information, however, it is necessary to consider carefully what factors may contribute to observed lineshapes. From the point of view of theoretical modeling these compounds would appear to be ideal in that, within the molecular unit, they provide systems of two or four spin 1/2 particles effectively isolated from neighboring molecules by carbonyl groups.

II. Experimental

The Fourier transformed free induction decay spectra presented in this paper were taken using a pulse spectrometer which has been described[3]. T_1s for the samples ranged from 1 to 5 minutes and the experiments were repeated as a function of pulse rate to eliminate the possibility of contributions to the lineshape from components having different relaxation times. Adamantane, which produces a symmetrical line, was used as a standard for choosing the proper phases and in some cases background spectra were run in order to correct for probe impurities.

III. Results of Discussion

$H_2Os_3(CO)_{10}$

The structure of the $H_2Os_3(CO)_{10}$ molecule taken from the work of Churchill, Hollander, and Hutchinson[4] is shown in Figure 1(a). Figure 2 shows the experimental powder lineshape at 300K for this compound with a proton pair rigid lineshape superimposed. This lineshape assumes an interproton distance of 2.44Å. As can be seen, the experimental spectrum does not correspond to a rigid lattice proton pair. For a rigid isolated pair the separation between the two inner peaks should be half the separation of the two outer peaks (shoulders); but we find that the inner peak separation is somewhat greater than this and that the shoulders show greater intensity than expected.

We discuss a number of possible explanations for the unexpected results shown in Figure 2. Explanation of the major features of the lineshape, however, will be seen to result from a consideration of four dipolar coupled spin 1/2 nuclei. Recently available neutron diffraction

data[5] indicates that, in the solid state, the molecular packing results in one short intermolecular proton-proton distance. We are presently awaiting the structural data describing the degree to which the four protons may be in a nonlinear configuration. However, we would point out that the preliminary results communicated to us by Sheldrick[5] indicates intramolecular proton-proton distances of 2.4Å and one intermolecular proton-proton distance of 2.9Å with the four protons in a nearly linear configuration.

If we consider two close proton pairs forming a planar parallelogram four spin 1/2 system with the four protons nearly in a straight line, we can make a direct comparison as we have solved the problem of a parallogram of spins analytically[6]. For the linear case where the interpair contact is $(2)^{1/3}$ times the intermolecular proton-proton distance, the theory predicts a ratio of inner peak to outer peak separation of about 0.64 in good agreement with the experimental results ($\sim$0.61).

It is necessary, however, to consider what other interactions may contribute to the lineshape shown in Figure 2. As ^{189}Os(16.1% natural abundance) has a large quadrupole moment and the osmium site symmetry is lower than cubic, it is likely that the osmium is in a Zeeman perturbed quadrupolar state; and the ability of such non-Zeeman state spins to produce anomolous effects in NMR spectra of neighboring nuclei is well documented[7,8]. Analytic calculations have been carried out in order to test the magnitude of this effect using the results presented in a previous paper[1].

The results of that calculation[1] can be specialized for the molecular geometry found for $H_2Os_3(CO)_{10}$. The notation used is the same as in the previous paper. From a consideration of Fig. 1(a) one can see that the only symmetry element for a basal osmium is the mirror plane lying in the plane of the osmium triangle. Let this plane be the x,y plane. The z axis is then perpendicular to the osmium triangle, and the interproton vector is parallel to z and is bisected by the xy plane. Otherwise, the orientation of the proton pair within the principal axis system of the field gradient tensor is unspecified. However, calling the distance from the osmium to one proton r_1 and the other oxmium proton distance r_2 provides

$$\begin{aligned} \underset{\sim}{r}_1 &= x_1\underset{\sim}{\hat{i}} + y_1\underset{\sim}{\hat{j}} + z_1\underset{\sim}{\hat{k}} \\ \underset{\sim}{r}_2 &= x_1\underset{\sim}{\hat{i}} + y_1\underset{\sim}{\hat{j}} - z_1\underset{\sim}{\hat{k}} \end{aligned} \tag{1}$$

and

$$\begin{aligned} \phi' &= \phi'' \\ \pi - \theta'' &= \theta' \end{aligned} \tag{2}$$

where θ',ϕ' specifies the orientation of r_1 within the principal axis frame of the field gradient tensor, and θ'', ϕ'' specifies the orientation of r_2.

$$\begin{aligned} \cos\gamma &= \cos\theta\cos\theta' + \sin\theta\sin\theta'\cos(\phi'-\phi) \\ \cos\gamma' &= -\cos\theta\cos\theta' + \sin\theta\sin\theta'\cos(\phi'-\phi) \\ \cos\delta &= \cos\theta \end{aligned} \tag{3}$$

and

$$\begin{aligned} \cos\gamma + \cos\gamma' &= 2\sin\theta\sin\theta'\cos(\phi'-\phi) \\ \cos\gamma - \cos\gamma' &= 2\cos\theta\cos\theta' \end{aligned}$$

where γ is the angle between the field and r_1, while γ' is the angle between the field and r_2, and δ represents the angle between the field and the interproton vector. The expression for the heteronuclear dipolar energy,[1] f^i, can then be written as

$$f^i(\eta,\theta,\phi,\theta',\phi') = \frac{\gamma_I\gamma_S\hbar^2}{r_{IS}^3} \langle S_s\rangle_i[\sin\theta][\cos\phi - 3\sin^2\theta'\cos\phi'\cos(\phi'-\phi)]$$

$$+ \langle S_y\rangle_i [\sin\theta][\sin\phi - 3\sin^2\theta'\sin\phi'\cos(\phi'-\phi)]$$

$$+ \langle S_z\rangle_i [\cos\theta][1 - 3\cos^2\theta'] \qquad (4)$$

The general form for the splitting of the proton pair is now seen to be

$$\hbar\omega(-1,0) = \gamma_I\hbar H_0 + \frac{3}{4}\frac{\gamma_I^2\hbar^2}{r_{II}^3}(1 - 3\cos^2\theta) \pm f^i(\eta,\theta,\phi,\theta',\phi')$$

$$\hbar\omega(0,1) = \gamma_I\hbar H_0 - \frac{3}{4}\frac{\gamma_I^2\hbar^2}{r_{II}^3}(1 - 3\cos^2\theta) \pm f^i(\eta,\theta,\phi,\theta',\phi') \qquad (5)$$

where $\pm$ in front of f^i indicates the symmetric nature of the splitting which arises because $\langle S_x\rangle_I = \langle - S_x\rangle_{II}$,[1] etc.

A computer program was written which simulates powder patterns using the expressions for the splittings which are given by (4), (5), and the results of the calculation of the expectation values $\langle S_i\rangle$ in the principal axis from of the field gradient tensor. The program allows for various choices of θ', ϕ', and the asymmetry parameter η as well as $r_{H\text{-}H}$ and $r_{H\text{-}Os}$. A reasonable range of values θ' and the internuclear distances was chosen, based on available structural information[4,9]; and various spectra were simulated for a range of choice of η and ϕ'. Since η was

arbitrarily chosen, it was allowed to vary from 0 to 100 (100 = ∞) and ϕ' was varied from 0^{o} to 180^{o}. The spectra were not found to vary widely for a variety of choice of parameters so long as θ' was held close to 47^{o} (a lower limit for a reasonable θ'). If θ' was increased the peaks of the power pattern were seen to broaden slightly, and the shoulders became somewhat tapered. However, in no case did the simulated spectra exhibit the features seen in the experimental results. Although the inner peaks could be broadened somewhat, no choice of angle or asymmetry parameter was seen to produce the high shoulders described previously and shown in Figure 2.

Apparently, although the perturbation of the nearby quadrupolar nucleus may contribute to the broadening of the peaks in the proton pair power spectrum in the limit where the spin 3/2 nucleus is in a Zeeman perturbed quadrupolar state, it cannot account for the unusual shoulders which are observed experimentally in $H_2Os_3(CO)_{10}$.

Another possible contribution to the experimental lineshape could arise out of indirect nuclear coupling. Using the results of the theory developed for the non-Zeeman quantized spin 3/2 nucleus it is possible to simulate the theoretical spectra expected to result from indirect nuclear coupling. Making use of the expression for $\langle \underset{\sim}{I} \cdot \underset{\sim}{S} \rangle$ obtained in the discussion of the dipole-dipole interaction of a spin 3/2 nucleus with a spin 1/2 nucleus[1], we find that it would require a ^{1}H-^{189}Os coupling constant of nearly 5 kHz in order to explain the data. ^{187}Os-^{1}H coupling constants as large as 34 Hz have been reported[10], and as ^{189}Os has a gyromagnetic ratio about 1.8 times larger than ^{187}Os one would argue that a ^{189}Os-^{1}H coupling constant might be expected to be less than 100 Hz. Furthermore, to our knowledge, the largest coupling constants for a proton

directly bonded to a transition metal are certain ^{195}Pt-^{1}H coupling constants found to be as large as 1300 Hz[11], and as ^{195}Pt has a gyromagnetic ratio about 2.8 times larger than ^{189}Os it is hard to argue that ^{189}Os-^{1}H coupling constants could be 5 KHz.

Another possibility is that the unusual features seen in the experimental spectrum for $H_2Os_3(CO)_{10}$ might result from the effect of restricted reorientational motion of the protons. However, the dipolar lineshape does not change between 300K and 140K and T_1's are long (greater than 1 minute) thus limiting the nature of possible motions. A highly restricted motional process (such as a simple flip of the proton-proton vector between two orientations[12]) in the fast motion limit could be present. One can model the effect of such fast motion on the dipolar lineship in a general fashion. That is, regardless of the physical model for the motion (e.g. three or more potential wells, unequal potential wells) one obtains the same mathematical form, namely that of a traceless symmetric second rank tensor. The general form of such a tensor would predict two sets of shoulders, one high and one low, with the high shoulders characteristic of the degree to which the tensor is non-axially symmetric. We attempted to fit the data to such a tensor as the components of the tensor could be parameterized for various specific models (such as a double minimum potential) from which one could extract inter-proton distances and flip angles. In proton pair powder spectra, there is sometimes sufficient broadening to mask the expected low shoulders[13], so we considered two cases. In one we let both sets of shoulders be present. A fit to the data under this assumption is shown in Figure 3(a). In Figure 3(b) is shown a fit where the low shoulders were "pinned" into the baseline. Neither result explains the data adequately. In Figure 3(a)

the experimentally observed features (shoulders) are completely missed by the fit. In Figure 3(b) the fitted shoulders are too broadened and the fitted peaks are too sharp.

One can conclude from this discussion that the observed proton lineshap for $H_2Os_3(CO)_{10}$ cannot be explained by either a simple two proton dipolar interaction or a two proton dipolar interaction modified by (a) a nearby nucleus in a Zeeman perturbed quadrupolar state, (b) indirect nuclear coupling, or (c) restricted reorientation of the protons.

However, a recent private communication of so far unpublished results of a neutron diffraction experiment[5] appears to indicate that a short internuclear proton-proton vector exists because of packing in the solid state. If one assumes a nearly linear arrangement of the four spins, the observed spectrum for $H_2Os_3(CO)_{10}$ can be explained, as was pointed out early in the discussion. We believe that the four proton-proton vectors deviate somewhat from a straight line, however, and are awaiting that data before attempting a fit to the experimentally observed NMR lineshape.

$H_4Ru_4(CO)_{12}$ and $H_4Os_4(CO)_{12}$

The structure of $H_4Ru_4(CO)_{12}$ as given by Wilson, Wu, Love, and Bau[14] is shown in Figure 1(b). The molecule is composed of a near tetrahedron of metal atoms with two short and four long sides. From the disposition of the carbonyls over the faces of the near tetrahedron it is inferred that the protons are edge bridging the four long sides. Thus they would be arrayed in the form of a square. There are apparently no short intermolecular proton-proton contacts for this compound[14], so we would expect that the observed dipolar spectra results from that of a square of spin 1/2 particles. From spectroscope data, Knox et al.[15] have concluded that $H_4Os_4(CO)_{12}$ has the same structure as $H_4Ru_4(CO)_{12}$.

Figures 4 and 5 show the experimental lineshapes as a function of temperature. From the detailed discussion of contributions to lineshapes in the $H_2Os_3(CO)_{10}$ case we conclude that neither indirect nuclear coupling nor the effect of nearby nuclei in Zeeman perturbed quadrupolar states will affect the lineshape greatly. On the other hand, there is evidence that $H_4Ru_4(CO)_{12}$ is undergoing reorientation at room temperature. In Figure 4 the line is seen to broaden at 220K and the central dip in the spectrum becomes more pronounced. The lineshape was not seen to change below 220K. No attempt has been made to model the apparent motion at room temperature as it may be rather complex, involving changes from square to tetrahedron to square[16]. For $H_4Os_4(CO)_{12}$, since the lineshape is not seen to change from 300K to 100K, there can be no motional process sufficient to average the dipolar Hamiltonian differently over that temperature range.

From the experimental results one calculates for $H_4Ru_4(CO)_{12}$ a second moment of 1.47 gauss^2 at 300K and 1.72 gauss^2 at 120K. Assuming that .1 gauss^2 contribution to the second moment from heteronuclear and intermolecular effects one would obtain, under the assumption of the geometry of a square, interproton distances of 2.87Å at 300K and 2.79Å at 120K. The room temperature internuclear distance is probably too long as the second moment value reflects the effects of motion. The internuclear distance of 2.79Å is in good agreement with that predicted from the structure given by Wilson, Wu, Love and Bau[14].

Similarly, for $H_4Os_4(CO)_{12}$, both at room temperature and at 100K we obtain a second moment of 1.73 gauss^2. Again adjusting that value by .1 gauss^2 an interproton distance of 2.79Å, under the assumption of the geometry of a square, is obtained.

References

1. A. T. Nicol and R. W. Vaughan, to be published
2. A. L. Robinson, Science, 194, 1150 (1976).
3. R. W. Vaughan, D. D. Elleman, L. M. Stacey, W-K. Rhim, and J. W. Lee, Rev. Sci. Instrum. 43, 1356 (1972).
4. M. R. Churchill, F. J. Hollander, and J. P. Hutchinson, Inorg. Chem. 16, 2697 (1977).
5. G. M. Sheldrick, private communication.
6. A. T. Nicol and R. W. Vaughan, to be published.
7. D. L. VaderHart, H. S. Gutowsky, and T. C. Farrar, J. Am. Chem. Soc. 89, 5056 (1967).
8. M. E. Stoll, R. W. Vaughan, R. B. Saillant, and T. Cole, J. Chem. Phys. 61, 2896 (1974).
9. R. Mason, Special Lectures XXIII IUPAC Congress, Boston, Mass. Volume 6, p. 31, 1971.
10. B. E. Mann, C. Masters, and B. L. Shaw, Chem. Comm., 1041 (1970).
11. P. W. Atkins, J. C. Green, and M. L. H. Green, J. Chem. Soc. A, 2275 (1968).
12. E. R. Andrew and J. R. Brookman, J. Mag. Res. 2, 259 (1970).
13. G. E. Pake, J. Chem. Phys. 16, 327 (1948).
14. R. D. Wilson, S. M. Wu, R. A. Love, and R. Bau, Inorg. Chem. 17, 1271 (1978).
15. S. A. Knox, J. W. Koepke, M. A. Andrews, and H. D. Kaesz, J. Am. Chem. Soc. 97, 1342 (1975).
16. J. R. Shapley, S. I. Richter, M. R. Churchill, and R. A. Lashewycz J. Am. Chem. Soc. 99, 7384 (1977).

Figure Captions

Figure 1(a) The structure of $H_2Os_3(CO)_{10}$ as given by Churchill, Hollander, and Hutchinson[4]. The shorter metal-metal distance is represented by a heavy line. Filled circles represent metal atoms and open circles represent expected hydrogen locations.

Figure 1(b) The structure of $H_4Ru_4(CO)_{12}$ as given by Wilson, Wu, Love, and Bau[14]. Again, heavy lines indicate shorter metal-metal distances and terminally directed carbonyls, directed over the face of the near tetrahedron, are indicated by straight lines. Hydrogen positions are not indicated but are believed to edge bridge the four long metal-metal bonds.

Figure 2. The proton free induction decay lineshape for $H_2Os_3(CO)_{10}$ at room temperature. The dipolar lineshape expected for a rigid proton pair is indicated.

Figure 3. The free induction decay lineshape for $H_2Os_3(CO)_{10}$ with the results of motional models indicated.

Figure 4. Proton free induction decay lineshapes for $H_4Ru_4(CO)_{12}$ near 220K and 300K.

Figure 5. Proton free induction decay lineshapes for $H_4Os_4(CO)_{12}$ near 100K and 300K.

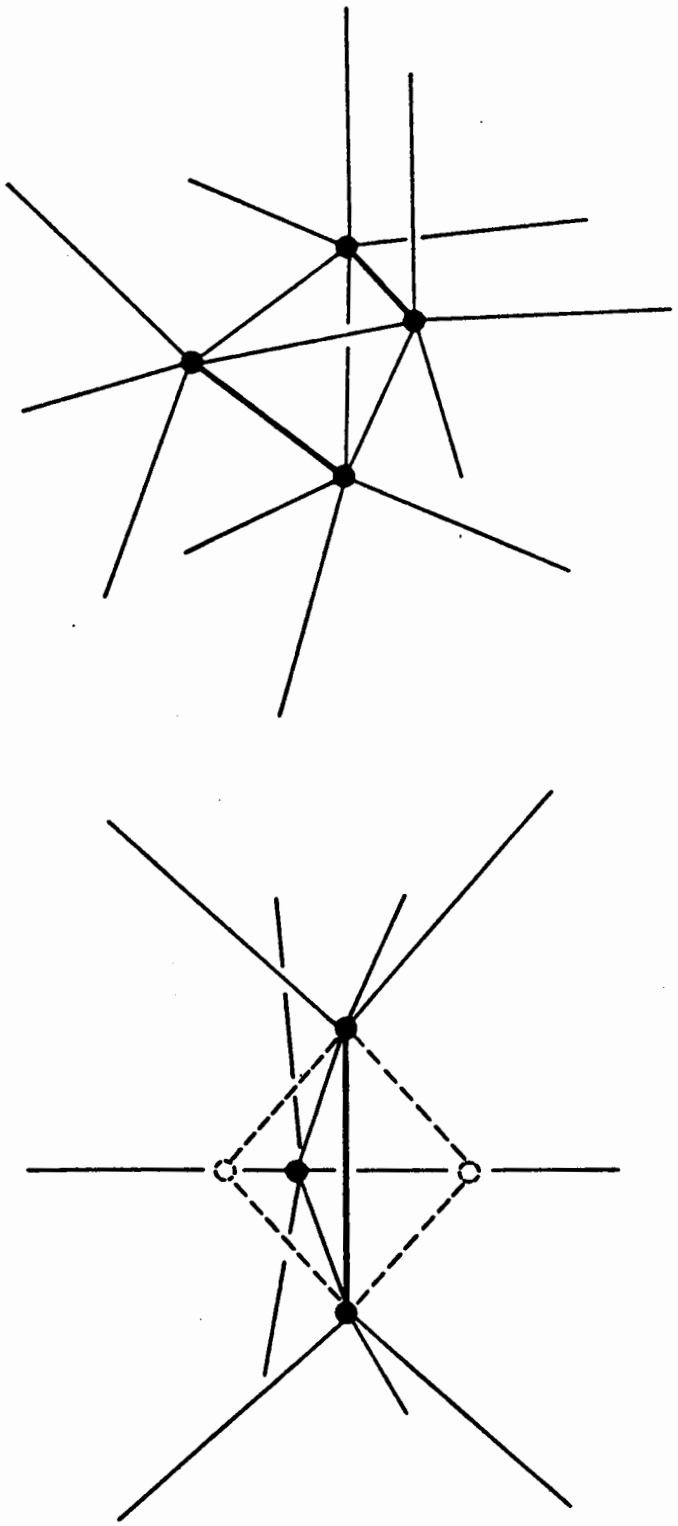

Figure 1

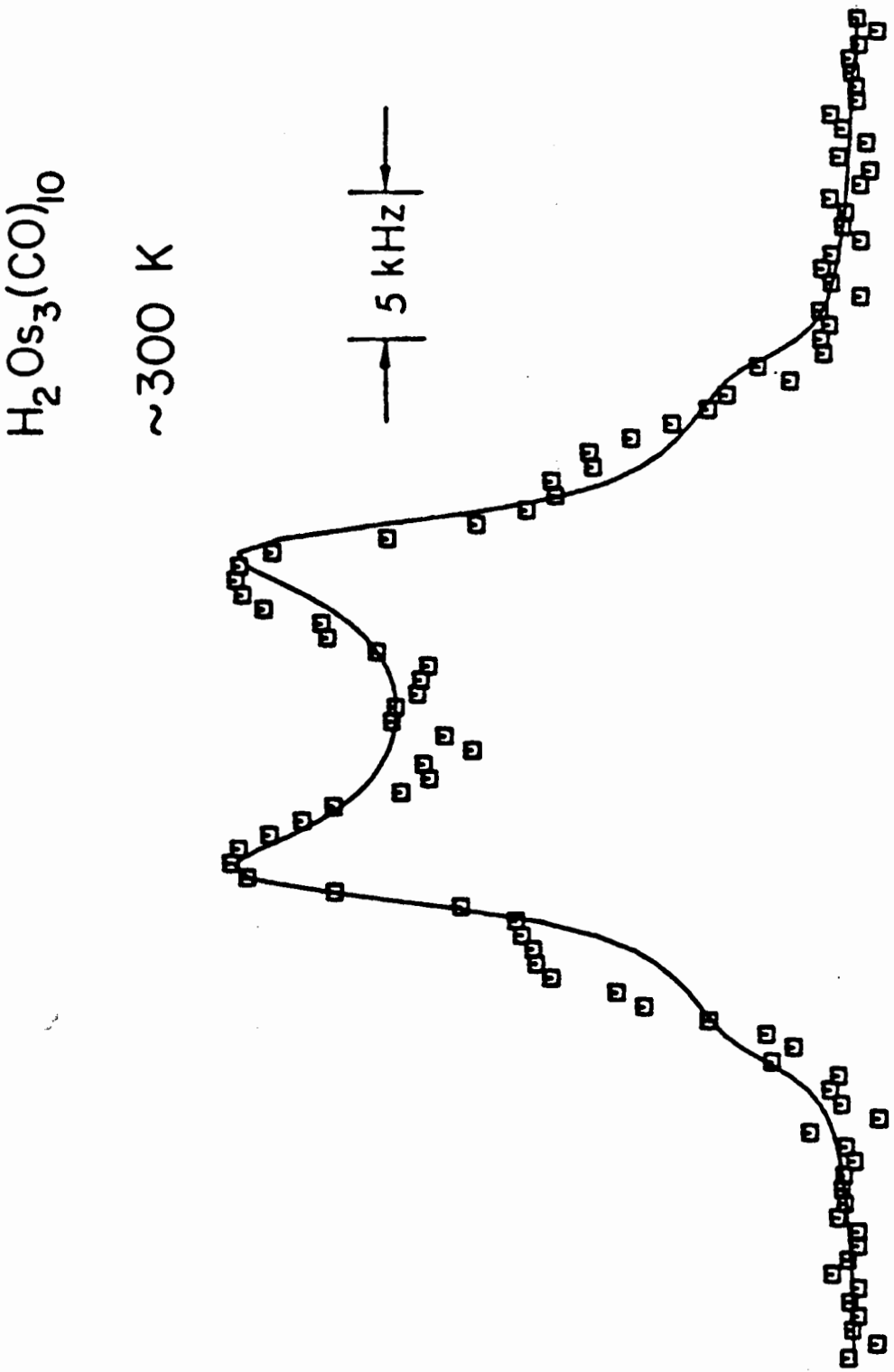

Figure 2

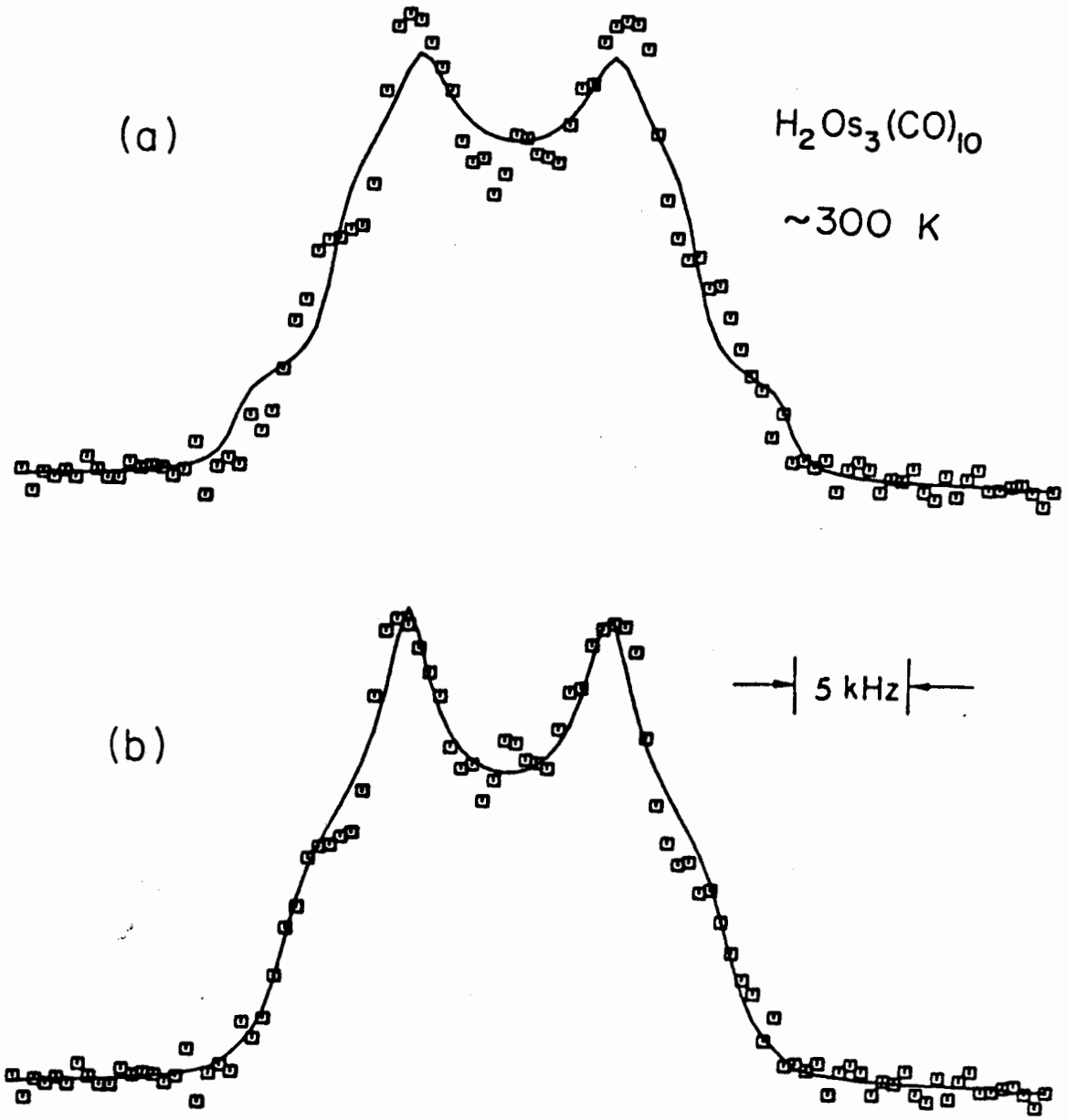

Figure 3

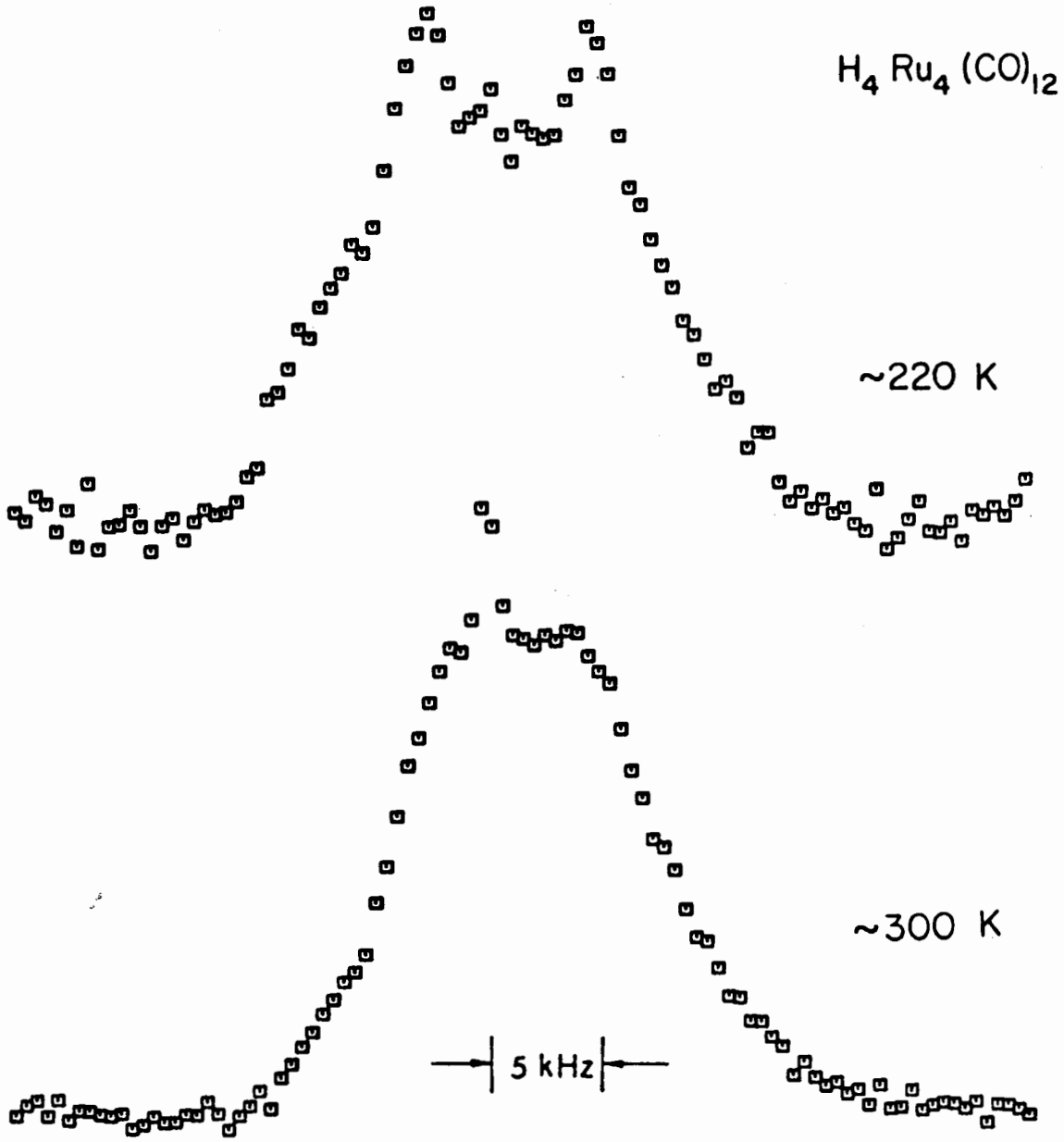

Figure 4

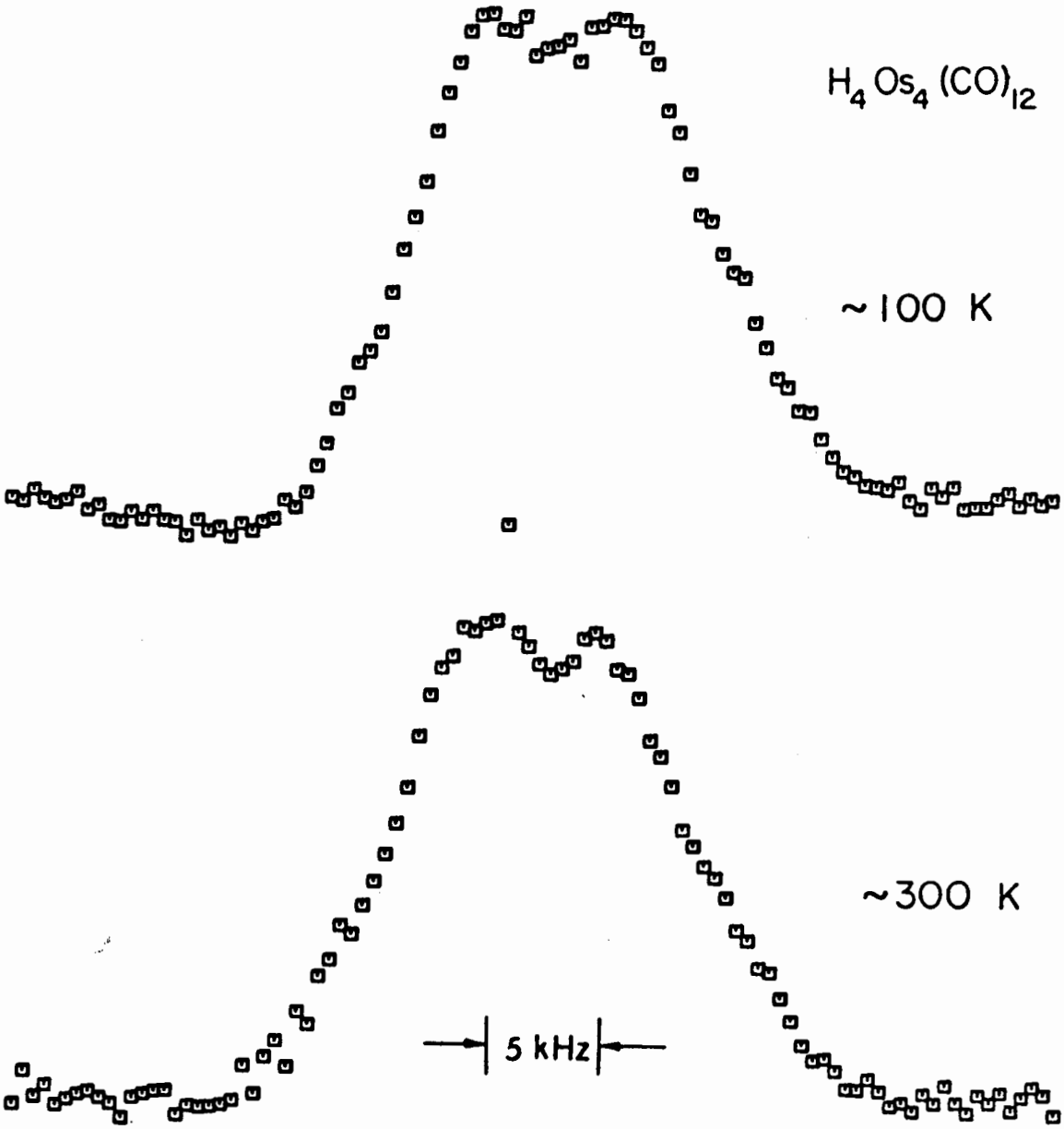

Figure 5

Chapter 5

The Proton Chemical Shift in Polycrystalline $H_2Os_3(CO)_{10}$, $H_4Ru_4(CO)_{12}$, and $H_4Os_4(CO_{12})$

(Chapter 5 is a paper by A. T. Nicol and R. W. Vaughan which is being submitted to the *Journal of Chemical Physics*.)

Introduction

In recent years it has become possible to measure proton chemical shift tensors in solids by multiple pulse techniques[1,2]. Such measurements have included studies of organic compounds[3], hydrogen-bonded crystals[4], hydrated crystals[5], or water itself[6]. This paper reports proton chemical shift spectra for protons directly bonded to transition metals via metal-hydrogen-metal bridge bonds. In solution such compounds, in contrast to other materials studied exhibit a large positive chemical shift. For example in their review Kaesz and Saillant[7] cite an isotropic chemical shift range of τ = 15 - 30 ppm (σ = 5 - 20ppm)for hydrogens directly bonded to transition metals with those hydrogens bridging metal-metal bonds typically at even higher fields. The range for proton chemical shifts for organic liquids is typically τ ~ 0-10 ppm (σ ~ -10 - 0 ppm) with similar isotropic values in the solid state[1,2]. An early theoretical prediction by Buckingham and Stephens[8] of the possibility of an unusually large chemical shift anisotropy for protons directly bonded to a transition metal (up to 500 ppm) has added speculation that such large upfield values for the isotropic values might be due to such large anisotropies.

Experimental

The spectra presented in this paper were obtained using a spectrometer[9] and an eight-pulse sequence[10] which have been discussed. A 48-μsec cycle time was used for results reported here although some 36-μsec cycle time data were taken. It was necessary to signal average, and spectra were taken on both sides of resonance and reflected in order

to determine the proper choice of phase. In some cases the resulting spectra were added to improve signal-to-noise. For $H_2Os_3(CO)_{10}$ and $H_4Ru_4(CO)_{12}$ runs were typically 1-2 hours with 3-5 min pulse rates, while for $H_4Os_4(CO)_{12}$ data were accumulated over a 24-hour period.

For temperature control a nitrogen-flow variable temperature probe was used, and the temperature was checked before and after each run and found constant to within ± 1 K. An acetyl chloride sample in a sealed spherical NMR tube was used for tuning and confirming proper operation of the spectrometer since it is liquid over the temperature range of interest (liquid range: -112^{o} C to $+50.9^{o}$ C). The chemical shift of acetylchloride relative to a spherical sample of tetramethylsilane was determined at room temperature and the result used in assigning chemical shifts relative to tetramethylsilane at other temperatures.

In addition to studying the compounds under the eight-pulse sequence, two phase-altered[11] sequences were used, the effect of which is to sort out contributions to the linewidth coming from other than static field inhomogeneity.

The samples used in this study were obtained from Professor J. R. Shapley.

Results and Discussion

$H_2Os_3(CO)_{10}$

The structure of $H_2Os_3(CO)_{10}$ taken from the paper of Churchill, Hollander and Hutchinson is shown in Figure 1(a). The molecule is composed of an isosceles triangle of osmium atoms with the proton pair bridging the base. The carbonyls in the isolated molecules are

symmetrically arranged so that the protons are equivalent, and thus the multiple pulse NMR spectrum of a polycrystalline sample would furnish a single proton chemical shift tensor. However, in the solid state the molecular packing distorts the carbonyls slightly, and there are two different kinds of protons. Since the packing distortions are small[12] and one does not expect intermolecular effects on the chemical shift tensor to be large, we have fit the spectra to a single proton chemical shift tensor. The fact that the isotropic chemical shift found ($\bar{\sigma}$ = 9 ppm at 300 K and 11 ppm at 230 K) is close to the value observed in solution $\bar{\sigma}$ = 11.7 ppm (τ = 21.7 ppm[13]) is evidence for the isolation of the molecular unit in the solid state.

Figure 2 shows the multiple pulse spectra for $H_2Os_3(CO)_{12}$ at 300 and 230 K along with the results of one of the phase-altered sequences[10]. The similarity of the 230 and 300 K spectra indicate that the protons are not involved in a motional process sufficient to average the spectrum differently at these temperatures. In addition to an anisotropy in the proton chemical shift tensor, a variety of other phenomena could be contributing to the observed linewidths of the spectra in Figure 2. An estimate of factors contributing to the linewidth other than inhomogeneity broadening was obtained by performing a phase-altered experiment[11] which has the property of suppressing inhomogeneity broadening. The suppression of inhomogeneity broadening was accomplished by establishing a vector Hamiltonian (I_y) perpendicular to the effective precession axis ($I_x + I_z$) with a phase error in the x pulses. The length of this vector Hamiltonian (the size of the phase error) was 2.5 kHz and thus sufficiently large to average out any inhomogeneity

contribution to the linewidths in Figure 2. The Fourier-transform of the decay observed in the presence of the phase error is plotted on the right side of Figure 2 for both the 300K and 230 K spectra, and it is seen to be small compared to the multiple-pulse spectra widths. Thus, the contributions to the multiple-pulse spectrum can be limited to inhomogeneity broadening from the proton chemical shift tensor and the ^{189}Os-^{1}H heteronuclear dipolar interaction (16.1% of the osmium is ^{189}Os, a spin 3/2 nuclei with a non-zero magnetic moment).

The line through the multiple-pulse spectra in Figure 2 is the result of a non-linear regressional fit of a single chemical shift tensor with a uniform Lorentzian broadening function to the experimemtal points and furnishes principal values for the proton tensor of -4.4 ppm, 9.9 ppm, and 21.6 ppm ± 1.5 ppm at 300 K[14] and 2.5 ppm, 9.8 ppm, and 21.5 ppm ± 1 ppm at 230 K. Fitting the spectra in this fashion does not rigorously account for the ^{189}Os-^{1}H heteronuclear dipolar interaction, and the principal values obtained should be considered to furnish an upper limit to the anisotropy of the proton chemical shift tensor (we attempt a more complete separation of these effects in the discussion of $H_4Os_4(CO)_{12}$ below).

$\underline{H_4Ru_4(CO)_{12}}$

The structure of $H_4Ru_4(CO)_{12}$ as given by Bau, et al.[15] is indicated in Figure 1(b). The structure is that of a distorted tetrahedron with two short and four long metal-metal bonds, and the carbonyls are directed over the faces of the near tetrahedron[15]. Within the isolated molecule, the carbonyls are symmetrically disposed, and even in the solid state

there is little distortion[15].

Figure 3 shows multiple-pulse spectra for $H_4Ru_4(CO)_{12}$ taken as a function of temperature. The center of mass for all such spectra ranged from σ = 18 to 20 ppm ± 2 ppm in close agreement with the observed chemical shift for the molecule in solution (τ = 28 ppm or σ = 18 ppm). One notes that the spectrum narrows from 230 K to room temperature and then broadens as the temperature goes higher. This same trend was observed in data taken over a slightly wider temperature range, 178 - 333 K, at a 36-μsec cycle time. ^1H dipolar spectra indicate the presence of proton motion[14] in this temperature range, and the multiple-pulse spectra are characteristic of a chemical shift powder pattern averaged by a restricted motion of the protons[1].

$\underline{H_4Os_4(CO)_{12}}$

Knox , et al.[13] have concluded that the structure of $H_4Os_4(CO)_{12}$ is similar to that of $H_4Ru_4(CO)_{12}$ from spectroscopic data. Yet, the dipolar spectra do not change from 100 K to 300 K[14], and one concludes that the reorientational motion of the protons present in the $H_4Ru_4(CO)_{12}$ is not present in $H_4Os_4(CO)_{12}$. The multiple-pulse spectrum for $H_4Os_4(CO)_{12}$ at 300 K is reproduced in Figure 4. The center of mass of the spectra furnishes an isotropic chemical shift of near 20 ppm (τ = 30 ppm) in agreement with our earlier estimate[14], and the solid line representing a nonlinear regressional fit of the spectra to that expected from chemical shift tensor with uniform Lorentzian broadening function furnishes principal values indicating an axially symmetric tensor

with an asymmetry of 26 ppm and a large Lorentzian broadening function of 11 ppm halfwidth.

As discussed above, both heteronuclear dipolar interactions with the ^{189}Os and the proton chemical shift tensor contribute to the multiple-pulse spectrum, and thus the width of the multiple-pulse spectrum furnishes an upper limit to the proton chemical shift tensor. However, one expects the heteronuclear interaction to broaden the chemical shift spectra symmetrically, and thus the asymmetric tensor obtained from the computer fit to the $H_4Os_4(CO)_{12}$ can be associated with a proton chemical shift anisotropy. That is, since ^{189}Os has a large quadrupole moment and is located in a molecular site of less than cubic symmetry, one can assume that the spin 3/2 ^{189}Os nuclei will be in a Zeeman-perturbed quadrupolar state, and we have shown by explicit calculation[16] that the heteronuclear interaction in this limit will broaden the proton spectra symmetrically.

References

1. M. Mehring, "High Resolution NMR Spectroscopy in Solids," NMR Basic Principles and Progress, P. Kiehl, E. Fluck, R. Kosfeld, eds., Vol. 11, Springer-Verlag, New York, 1976.
2. U. Haeberlen, "High Resolution NMR in Solids, Selective Averaging," Advances in Magnetic Resonance, J. S. Waugh, ed., Suppl. 1, Academic, New York, 1976.
3. L. M. Ryan, R. C. Wilson, and B. C. Gerstein, J. Chem. Phys. 67, 4310 (1977).
4. C. R. Dybowski, B. C. Gerstein, and R. W. Vaughan, J. Chem. Phys. 67, 3412 (1977).
5. C. L. McKnett, C. R. Dybowski, and R. W. Vaughan, J. Chem. Phys. 63, 4578 (1975).
6. L. M. Ryan, R. C. Wilson, and B. C. Gerstein, Chem. Phys. Lett. 52, 341 (1977).
7. H. D. Kaesz and R. B. Saillant, Chem. Revs. 72, 231 (1972).
8. A. D. Buckingham and P. J. Stephens, J. Chem. Soc., Part III, 2747 (1964).
9. R. W. Vaughan, D. D. Elleman, L. M. Stacey, W-K. Rhim, and J. W. Lee, Rev. Sci. Instrum. 43, 1356 (1972).
10. W-K. Rhim, D. D. Elleman, L. B. Schreiber, and R. W. Vaughan, J. Chem. Phys. 60, 4595 (1974); W-K. Rhim, D. D. Elleman, and R. W. Vaughan, J. Chem. Phys. 58, 1772 (1973); ibid. 59, 3740 (1973).
11. C. R. Dybowski and R. W. Vaughan, Macromolecules 8, 50 (1975).
12. M. R. Churchill, F. J. Hollander, and J. P. Hutchinson, J. Inorg. Chem. 16, 2697 (1977).

13. S. A. Knox, J. W. Koepke, M. A. Andrews, and H. D. Kaesz, J. Am. Chem. Soc. 97, 1342 (1975).

14. A. T. Nicol and R. W. Vaughan, "Solid State Nuclear Magnetic Resonance Study of Heavy Metal Hydrides," Transition Metal Hydrides, Advances in Chemistry Symposium Series, Volume 167, July 1978.

15. R. D. Wilson, S. M. Wu, R. A. Love, and R. Bau, Inorg. Chem. 17, 1271 (1978).

16. A. T. Nicol and R. W. Vaughan, to be published.

Figure Captions

Figure 1 (a) The structure of $H_2Os(CO)_{10}$ as given by Churchill, Hollander and Hutchinson[12] the shorter metal-metal distance is represented by a heavy line. Filled circles represent metal atoms and open circles represent expected hydrogen locations. Terminally bonded carbonyls are represented by straight lines.

(b) The structure of $H_4Ru_4(CO)_{12}$ as given by Wilson, Wu, Love, and Bau[15]. Again, heavy lines indicate shorter metal-metal distances and terminally bonded carbonyls, directed over the faces of the near tetrahedron, are indicated by straight lines. Hydrogen positions are not indicated but are believed to edge bridge the four long metal-metal bonds.

Figure 2 Multiple-pulse proton spectra for $H_2Os_3(CO)_{10}$ at 300 K and 230 K. Spectra on the left with the computer fit indicated were obtained using the standard 8 pulse sequence while the spectra on the right were obtained with the phase altered sequence.

Figure 3 Multiple pulse proton lineshape for $H_4Ru_4(CO)_{12}$ as a function of temperature.

Figure 4 Multiple-pulse proton lineshape for $H_4Os_4(CO)_{12}$ at 300 K where the line represents a computer fit.

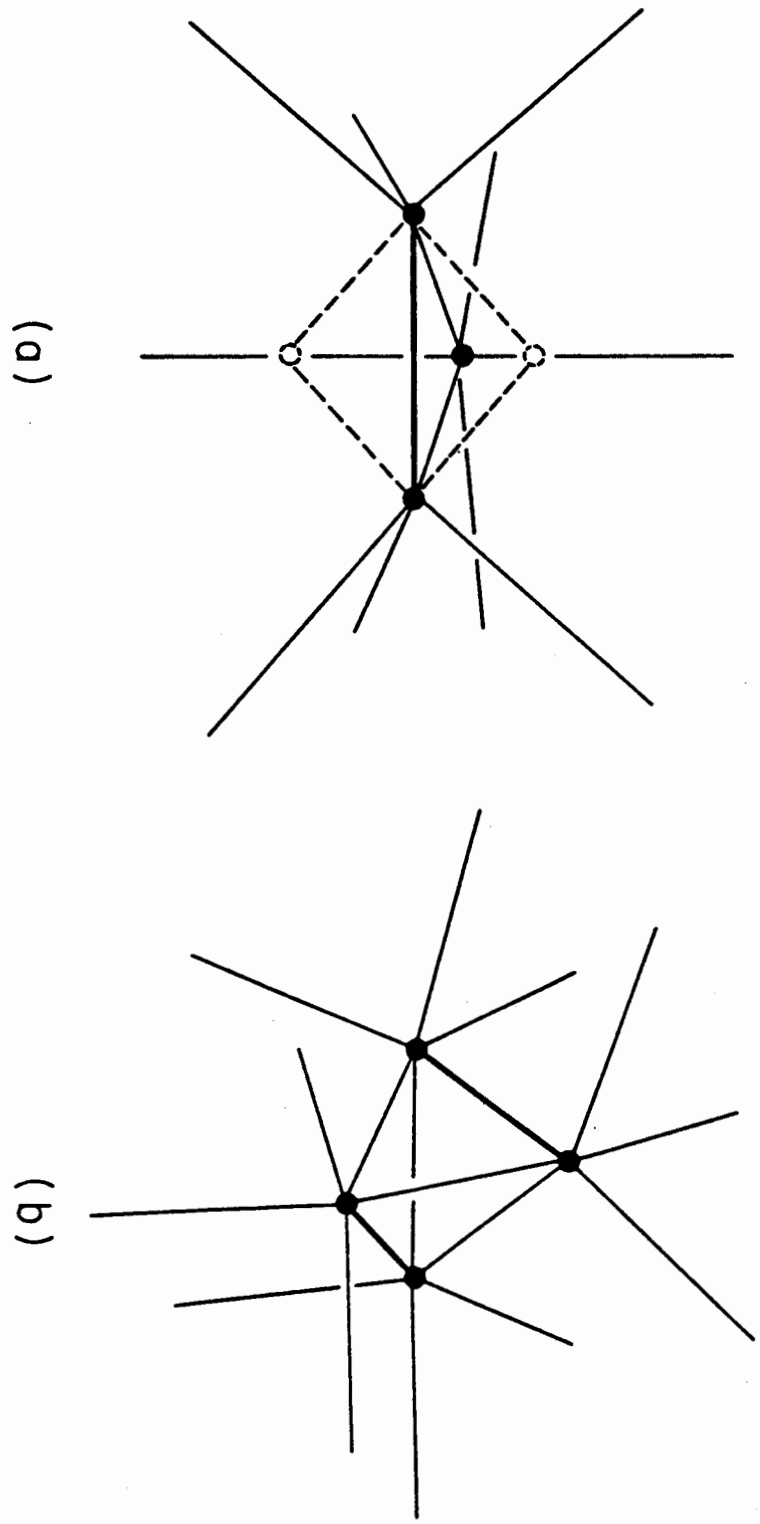

Figure 1

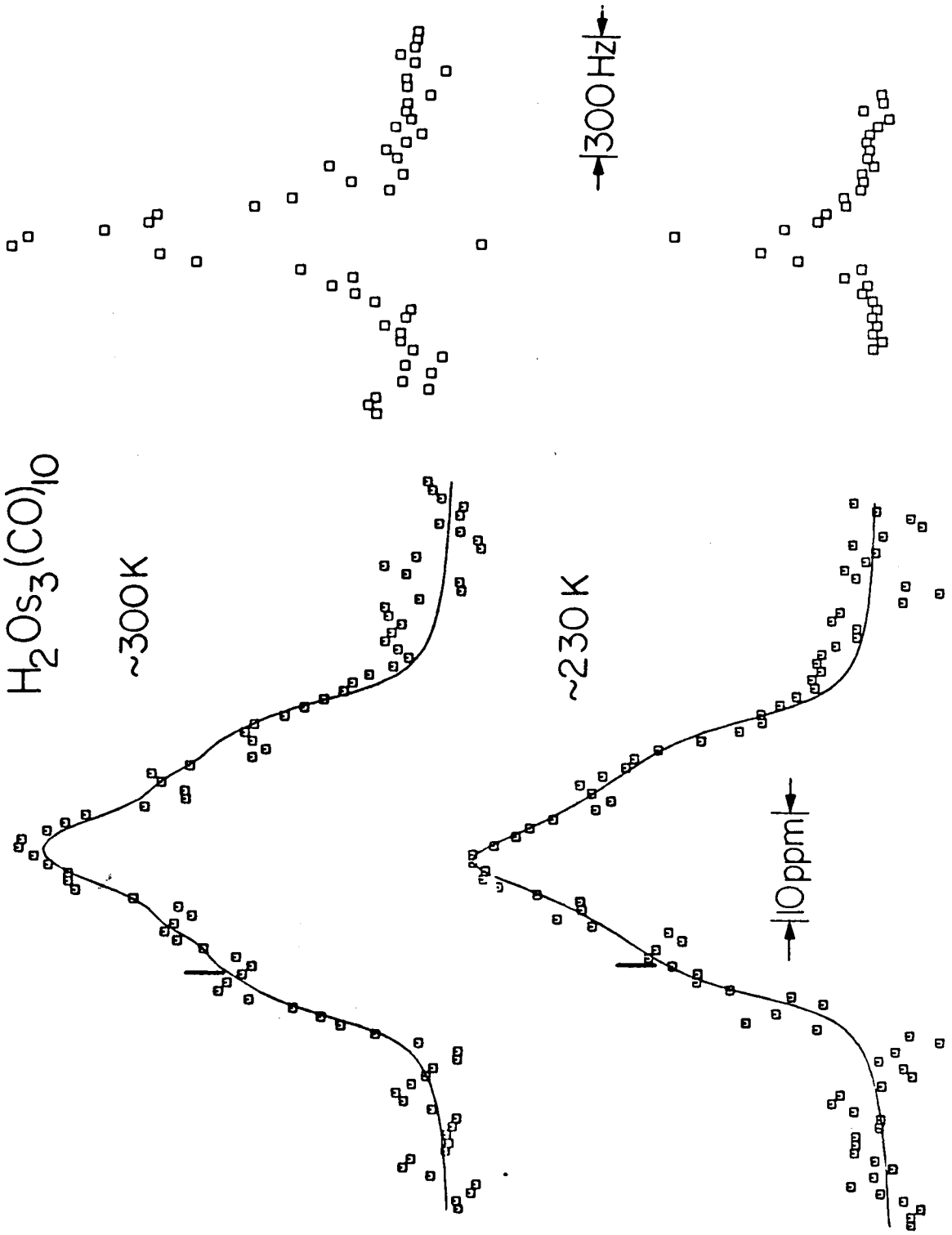

Figure 2

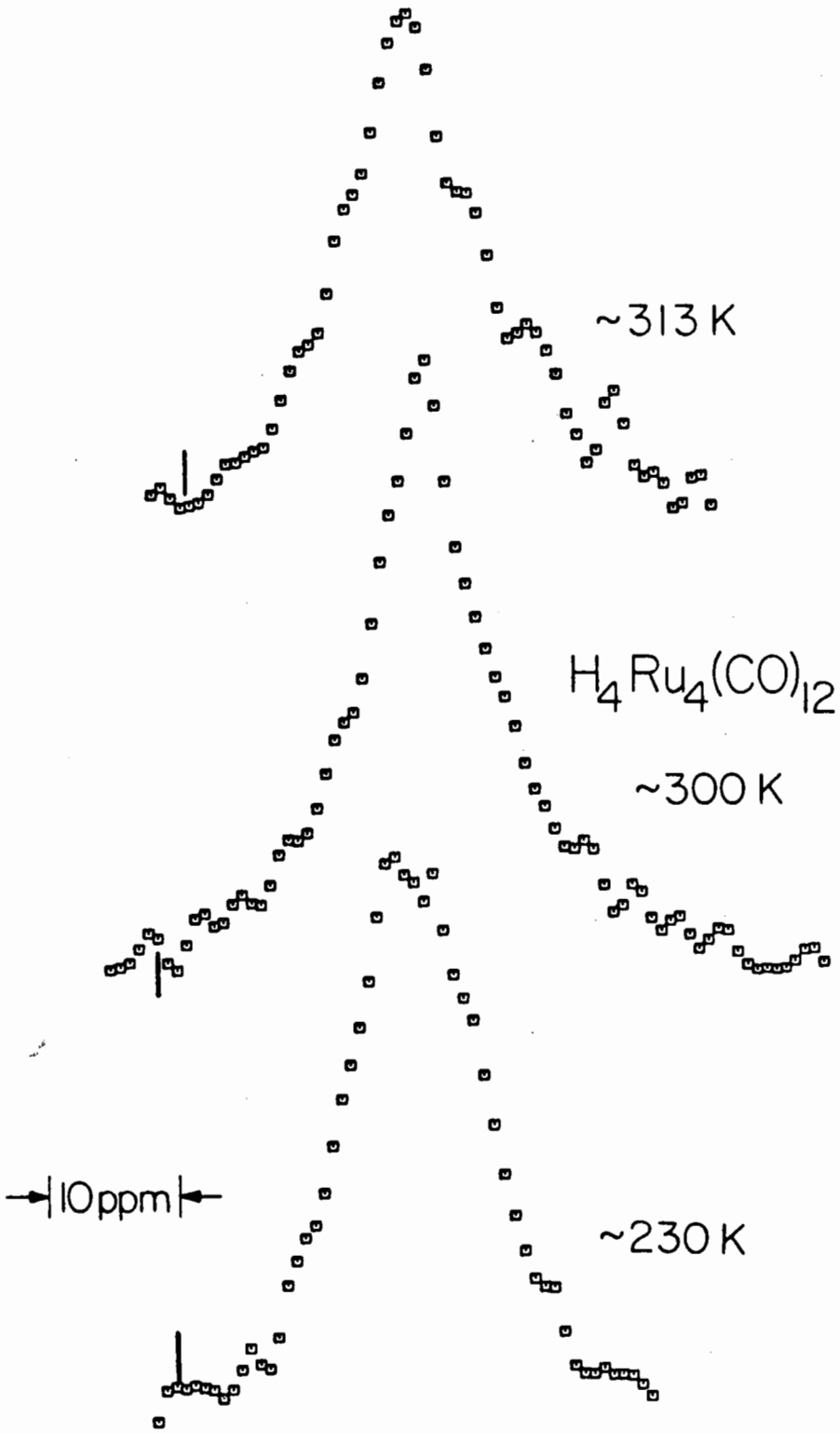

Figure 3

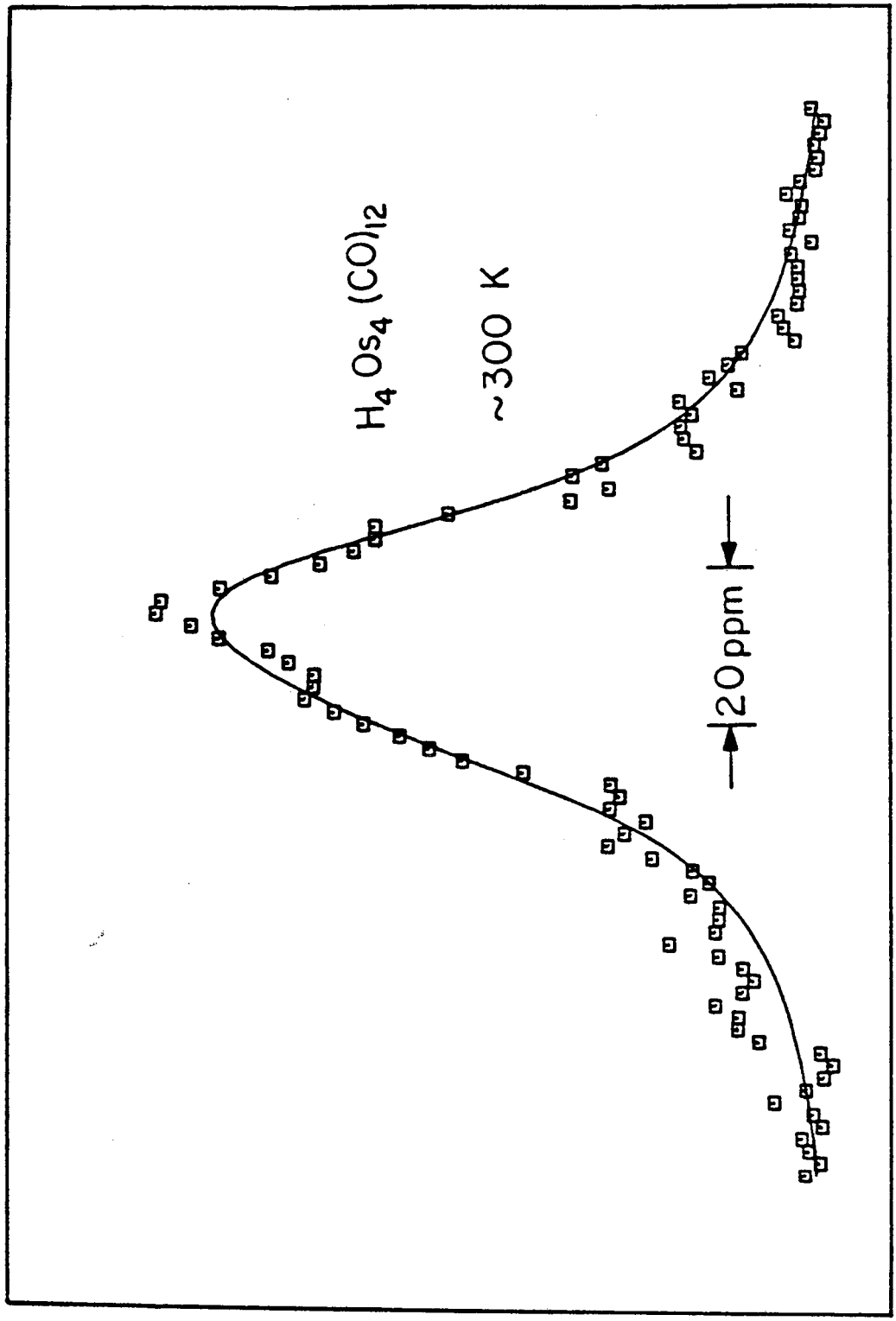

Figure 4

Chapter 6

Proton Chemical Shift Tensors of Alkaline Earth Hydrides

(Chapter 6 is a paper by A. T. Nicol and R. W. Vaughan which is being submitted to the *Journal of Chemical Physics*.)

In recent years the use of multiple pulse techniques has made possible the measurement of proton chemical-shift tensors in solids (see recent reviews[1,2]). Of the many proton-containing materials examined so far, little attention has been paid to protons in binary metal compounds, and no results have been reported for protons in the alkaline-earth hydrides. We report, in this note, the chemical shift of protons in the binary alkaline-earth hydrides: CaH_2, SrH_2, and BaH_2. These three solids have the same crystal structure[3] and, thus, would appear to be a model system for exhibiting the effects of the proximity of heavy ions on the proton chemical shift tensor.

Multiple-pulse spectra were obtained using a 56.4 MHz spectrometer[4] and an eight-pulse cycle[5] previously described. The data were taken at a cycle time of 36 microseconds, 4kHz off-resonance, and in some cases the spectra were taken on both sides of resonance and reflected to confirm the proper choice of phase. The polycrystalline samples were obtained from Research Organic/Inorganic Corporation of Sun Valley, California, and their composition confirmed by an independent analysis[6]. Conventional pulse NMR measurements characterized the compounds as rigid solids with proton free-induction decays of 15-20 microseconds and long T_1's of 4-10 minutes. The long T_1's also confirm the absence of paramagnetic impurities.

A neutron diffraction study of CaH_2 has shown it to be a distorted, orthorhombic, $PbCl_2$ structure[7]. There are four formula units per unit cell, and there are two chemically distinct types of hydrogens for which the only site symmetry is a mirror plane. Thus, the possibility of observing two chemical shift tensors exists, and in a polycrystalline sample we would expect to see a superposition of such powder patterns.

Figure 1 shows the multiple pulse results for these alkaline earth hydrides.

The line drawn through the experimental data points is a computer fit that assumes one set of principal values of the chemical shift tensor.

The center of mass of such spectra provides the average trace of the proton chemical shift tensor for each compound: -4.5 ± 3.0 ppm for CaH_2, -6.7 ± 1.0 ppm for SrH_2, and -8.7 ± 1.0 ppm for BaH_2 relative to TMS (tetramethylsilane). Bulk suspectibility corrections were estimated for the samples[8] to be less than -.7 ppm, all in the same direction, and no adjustments have been made to the reported data. The lineshapes contain possible contributions from the anisotropy in the chemical shift tensor, heteronuclear dipolar broadening, and residual homonuclear dipolar broadening. While it is not possibly to separate fully these contributions, estimates of the expected contributions from the dipolar terms can account for the observed linewidths, thus implying that any anisotropy in the proton chemical shift tensor is small. For example, one can experimentally estimate the effects of dipolar broadening in these systems by comparing the experimental proton linewidths in CaH_2(280 Hz), SrH_2 (390 Hz), and BaH_2 (640 Hz) to the corresponding fluoride linewidths in CaF_2 (200 Hz), SrF_2 (340 Hz), and BaF_2 (540 Hz)[9] where the cubic environment of the fluorine precludes any chemical shift anisotropy. Further, one can calculate from the known geometry[7] of the hydrides the contributions to the proton second moment from the nine nearest-neighbor cations, and one finds that the heteronuclear dipolar contributions to the proton second moment in SrH_2 and BaH_2 are more than sufficient to account for the excess linewidth of these samples over the CaH_2, while the width observed in CaH_2 is typical of the residual homonuclear dipolar broadening observed in tightly coupled spin systems[1].

Finally, the isotropic chemical shift observed for all three compounds lies

within the range of chemical shifts (σ = 0 to -10 with respect to TMS) observed for inorganics and non-hydrogen-bonded solids[1]. Hydrogen-bonded isotropic chemical shifts are considerably more downfield from TMS[1] and protons directly bonded to transition metals considerably more upfield[10]. Note that with increasing electronegativity of the cation, one sees a slight upfield shift. A similar, but larger, trend has been observed in the difluorides of the alkaline earths.

References

1. M. Mehring, "High Resolution NMR Sepctroscopy in Solids," Volume 11, NMR Basic Principles and Progress (ed. P. Kiehl, E. Fluck, R. Kosfeld), Springer-Verlag, New York, 1976.
2. U. Haeberlen, "High Resolution NMR in Solids, Selective Averaging," Supplement 1 to Advances in Magnetic Resonance (ed. by J. S. Waugh), Academic Press, New York, 1976.
3. G. G. Lebowitz, The Solid State Chemistry of Binary Metal Hydrides, W. A. Benjamin, Inc., New York, 1965.
4. R. W. Vaughan, D. D. Elleman, L. M. Stacey, W-K. Rhim, and L. W. Lee, Rev. Sci. Instrum. 43, 1356 (1972).
5. W-K. Rhim, D. D. Elleman, L. B. Schreiber, and R. W. Vaughan, J. Chem. Phys. 60, 4595 (1974); W-K. Rhim, D. D. Elleman, and R. W. Vaughan, J. Chem. Phys. 58, 1772 (1973); ibid. 59, 3740 (1973).
6. Pacific Spectrochemical Laboratory, Inc., Los Angeles, California.
7. J. Bergsma and B. O. Loopstra, Acta Cryst. 15, 92 (1962).
8. J. A. Osborn, Phys. Rev. 67, 351 (1945).
9. R. W. Vaughan, D. D. Elleman, W-K. Rhim, and L. M. Stacey, J. Chem. Phys. 57, 5383 (1972).
10. A. T. Nicol and R. W. Vaughan, "Solid State Nuclear Magnetic Resonance Study of Heavy Metal Hydrides," Transition Metal Hydrides, Advances in Chemistry Symposium Series, Volume 167, 1978.

Figure Caption

Multiple pulse NMR powder spectra of ^{1}H in alkaline-earth hydrides. Chemical shifts are shown relative to an arbitrary reference here, but are reported relative to a tetramethylsilane external reference in the text.

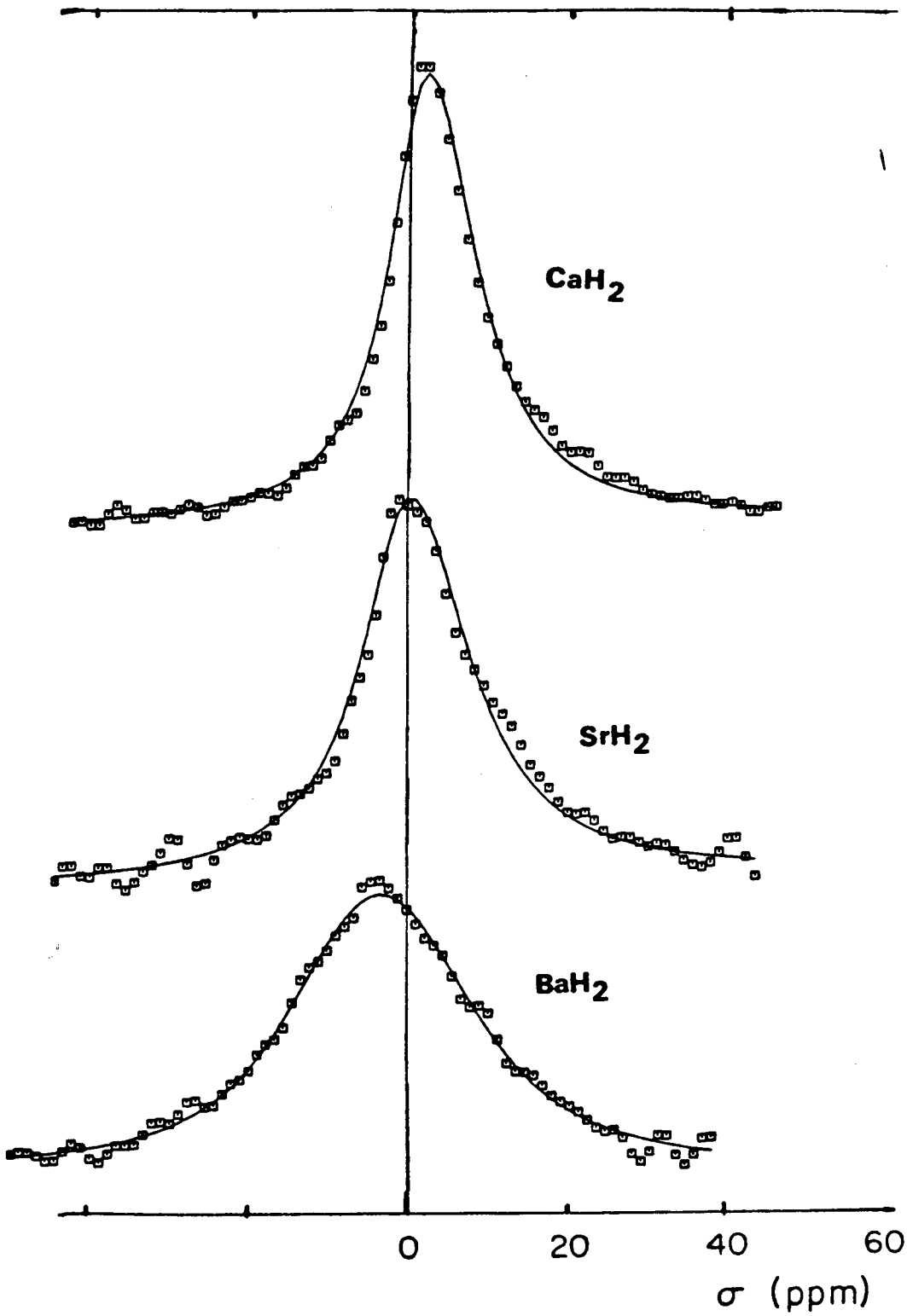
CaH2
SrH2
BaH2
0
20
40
60
σ (ppm)

APPENDIX

EXPERIMENTAL DETAILS

Experiments involving both conventional pulsed NMR and the newer techniques of high-resolution solid state NMR are presented in this thesis. Both kinds of experiments were done using a spectrometer which has been described[1]. This spectrometer is a fixed frequency unit operating at 56.4 MHz for ^1H in a 14 kG Varian magnet, and the unit can generate 1 μsec 90^o pulses. The spectrometer and detailed procedures for tuning up the pulse cycles used in the high-resolution experiments have been thoroughly described in the literature[1,2].

Prior to doing a multiple pulse experiment, it is necessary to determine approximate values of both T_1 and T_2 for the solids being studied. Pulse rates for signal averaging should be on the order of T_1, and an eight-pulse sequence, to be effective, must be run at a cycle time significantly shorter than six times T_2[2]. (A good rule of thumb is that the cycle should be at least shorter than three times T_2, and the shorter the better.) In all cases T_1 was measured using a 90^o-τ-90^o sequence as described in the book by Farrar and Becker[3]. For the alkaline earth hydrides, values of T_2 were determined by observation of the free-induction decay following a 90^o pulse. A plot of the logarithm of the amplitude vs. τ^2 (valid for the nearly Gaussian lines observed for the alkaline earth hydrides) yielded values of T_2 ranging from 16 to 24 μsec, and a cycle time of 36 μsec was chosen for the alkaline earth hydride experiments. For the metal cluster compounds a simple observation of the free-induction decay indicated values of T_2 of greater than 30 μsec, so a cycle time of 48 μsec was chosen for the multiple pulse study of those compounds. However, as an added check, some 36 μsec cycle time data were taken for $H_4Ru_4(CO)_{12}$. These

data were found to be in agreement with the 48 μsec cycle time data.

In all cases signal averaging was employed. For the alkaline earth hydrides, four averages each were taken for CaH_2 and BaH_2, both above and below resonance and the data were reflected to insure the proper choice of phase. For SrH_2 the data were taken at the same spectrometer settings as for BaH_2, so only four averages on one side of resonance were taken, and the choice of phase found for BaH_2 was used for the SrH_2 data also. Values of T_1 for the alkaline earth hydrides ranged from 4 to 10 minutes, and for these compounds data were taken every five T_1 for a total of four averages per run. The chemical shift results were referenced to an external liquid standard and the position in the spectrum of the external standard was checked before and after each run. The polycrystalline samples of alkaline earth hydrides were obtained from Research Organic/Inorganic Corporation of Sun Valley, California. The compounds were sent for an independent analysis for heavy metal impurities[4], and the long T_1's were taken as additional evidence for the absence of paramagnetic impurities.

Some initial multiple pulse studies were carried out on samples of MgH_2 obtained from two different commercial sources. However, each sample produced different results in the multiple pulse experiment, and a conventional pulsed NMR experiment carried out at 270 MHz showed a Pake doublet powder pattern characterisitic of the presence of water or methylene groups. Furthermore, atomic absorption analysis and mass spectroscopy performed by the Caltech Analytical Services facility were not able to determine unambiguously what impurities might be present to provide the unexpected NMR results. Therefore, since neither sample

investigated appeared to be pure MgH_2, the results obtained for this compound were rejected.

For the metal carbonyl hydrides the values of T_1 were found to range from 1 to 5 minutes. For these compounds, pulse rates of 3 to 5 minutes were employed both in the conventional pulsed and in the multiple pulse experiments. As previously stated, for most of the multiple pulse work, a cycle time of 48 μsec was used. As in the case of the alkaline earth hydrides, spectra were taken both above and below resonance and reflected in order to obtain the proper choice of phase. For the studies of $H_2Os_3(CO)_{10}$ and $H_4Ru_4(CO)_{12}$ the total number of averages per run ranged from four to sixteen. For $H_4Os_4(CO)_{12}$, which was studied using a probe of lower Q, up to 288 averages were taken. (The probe used in the temperature-dependent studies could produce a 1.5 to 2 μsec pulse, while the probe of lower Q can produce a 1 μsec pulse. In some cases experiments were repeated using a different probe as an added cross-check.)

As in the case of the alkaline earth hydrides referencing was to an external liquid standard. For this purpose acetyl chloride was chosen since it has chemically one kind of proton, and it is liquid over the range of temperatures used in this study. The chemical shift of the acetyl chloride sample relative to a spherical sample of TMS was determined at room temperature, and the result was used to assign shifts relative to TMS at other temperatures. A nitrogen flow variable temperature probe was used for temperature control in these experiments, and the temperature was checked before and after each run. This was done by inserting a thermocouple into an NMR tube and placing it in the

probe in the same position as the sample but with the transmitter turned off.

For the dipolar lineshape studies the experimental setup is similar to that for the multiple pulse experiments as far as temperature control and the use of standards is concerned. The use of probes designed to provide 1 to 2 μsec 90^{o} pulses for multiple pulse experiments makes it possible to observe the free-induction decay for many solids. For the initial dipolar lineshape studies of $H_2Os_3(CO)_{10}$, $H_4Ru_4(CO)_{12}$, and $H_4Os_4(CO)_{12}$ data were taken using the variable temperature probe. The data acquisition setting was 2 Msec, and data were taken 80 KHz off-resonance. For these experiments, all liquid standards yielded the same result with the reference frequency being in a single central point in the spectrum. As unexpected lineshapes were obtained, experiments were repeated as a function of pulse rate in order to check the possibility of different components of the spectrum having different T_1's, but pulse rates from seconds up to 1 ½ hour produced no changing lineshape.

For the dipolar lineshapes the proper choice of phase was made through the use of an adamantane sample. Adamantane provides a line in the NMR spectrum on the order of 15 KHz wide so one "spectrum" of adamantane was taken with three different off-resonance frequencies of 60, 80, and 100 KHz. The resulting spectrum was phase-adjusted to produce three symmetrical lines with no apparent dispersion mixed in (i.e., pure absorption lineshapes). The resulting choice of phase was then applied to the experimental data.

Additional precautions were taken to insure that the reported lineshape was correct. In order to Fourier-transform the free-induction decay

correctly, it is necessary to know the position of the center of the 1-2 μsec pulse. This was determined by attenuating to the receiver and reading out the first few lines of data points.

One other problem became apparent during the course of this study. Because of the poor signal-to-noise, it was necessary to average for long periods of time, and it was discovered that small amounts of probe impurities were contributing to the observed spectra, so in some cases background runs were made. The resulting background spectra were subtracted from the experimental data. Both the room temperature $H_2Os_3(CO)_{10}$ data and the 220 K $H_4Ru_4(CO)_{12}$ data were treated this way. No probe impurity corrections were made at lower temperatures since the background runs indicated a freeze out of the impurity contribution at lower temperatures. The room temperature results for $H_4Ru_4(CO)_{12}$ and $H_4Os_4(CO)_{12}$ were not corrected for probe impurities and the single high central point observed in these spectra coincide with the liquid line and with the main contribution from probe impurities.

Adjustments for probe impurities as well as the consideration of small changes in phase or in choice of center of the pulse or effects from the ring-down of the probe were not seen to change the form of the peaks and shoulders observed in these experiments. Also, the same form for the peaks and shoulders was observed using a probe which produces a shorter ($\sim$1 μsec) 90° pulse than the probe used in the initial studies ($\sim$1-5 μsec). On the other hand, data taken for a truly isolated spin ½ pair on the same spectrometer and under the same conditions as used in these studies show the ideal spectrum for an isolated pair.[5]

The samples of $H_2Os_3(CO)_{10}$, $H_4Ru_4(CO)_{12}$, and $H_4Os_4(CO)_{12}$ were

obtained from Professor John R. Shapley of the University of Illinois, who prepared them by the procedure of Knox, et al.[6] and purified them on silica gel.

References

1. R. W. Vaughan, D. D. Elleman, L. M. Stacey, W-K. Rhim, and L. W. Lee, Rev. Sci. Instrum. 43, 1356 (1972).
2. W-K. Rhim, D. D. Elleman, L. B. Schreiber, and R. W. Vaughan, J. Chem. Phys. 60, 4595 (1974); W-K. Rhim, D. D. Elleman, and R. W. Vaughan, J. Chem. Phys. 58, 1772 (1973); ibid. 59, 3740 (1973).
3. T. C. Farrar and E. D. Becker, Pulse and Fourier Transform NMR, Academic Press, New York, 1971.
4. Pacific Spectrochemical Laboratory, Inc., Los Angeles, California.
5. M. E. Stoll, PhD Thesis, 1977, University Microfilms, Ann Arbor, Michigan.
6. S. A. Knox, J. W. Koepke, M. A. Andrews, and H. D. Kaesz, J. Am. Chem. Soc. 97, 3942 (1975).